

## Abstract

Mohan, Abhay. Formation and Characterization of Electrospun Nonwoven Webs.  
(Under the direction of Dr. Abdelfattah M. Seyam and Dr. Tushar K. Ghosh)

It is known that not all polymers can be melted and extruded to form polymer fibers. Electrospinning process involves a direct method to produce fibers in nanometer range by dissolving the polymer in solvent(s) to form the spinning solution. In this work, the spinning solution was prepared by dissolving Poly (ethylene terephthalate) polymer in trifluoroacetic acid and methylene chloride. Charging the solution to a very high potential initiated the process to produce electrospun fibers. With increasing voltage, a critical point is reached and a charged jet of the solution is ejected. As this charged jet moves in the air, the solvent evaporates, leaving behind a charged polymer fiber that collects on a targeted source (rotating drum). Equipment to form electrospun fiberwebs on a rotating drum was designed and successfully built. The equipment for this process is relatively simple and small since this process lend itself to the production of fibers/fiberwebs from small quantity of polymer solution. An experiment was designed to investigate the influence of polymer concentration in the spinning solution and the electric field level on fiber and fiberweb response of interest.

Electrospun fibers and fiberwebs were characterized for fiber diameter and its distribution, orientation distribution function, and pore size and its distribution. The results showed that an increase in the electric field resulted in a decrease of the average diameter of the electrospun fibers. It has also been observed that there was concentration/electric field interaction effect on fiber diameter. As the electric field increased keeping polymeric concentration constant, the fibers orientation in machine direction increased. It was observed that as the electric field was increased, the average pore diameter decreased. The decrease in average pore size with increase in electric field was explained in terms of fiber diameter as well as fiberweb structural parameters (orientation and basis weight).

# Formation and Characterization of Electrospun Nonwoven webs

By

**Abhay Mohan**


A thesis submitted to the Graduate Faculty of  
North Carolina State University  
in partial fulfillment of the  
requirements for the Degree of  
Master of Science

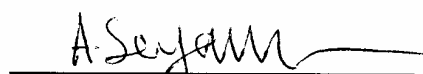
**Textile Management and Technology**

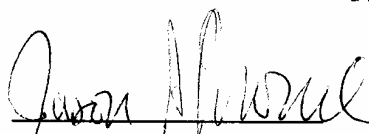
Raleigh, North Carolina

2002

**Approved By:**

  
Tushar K. Ghosh  
Co-Chair

  
Abdelfattah M. Seyam  
Co-Chair

  
Jason A. Osborne  
Member

## *Dedication*

I would like to dedicate this thesis at the Lotus Feet of “**Sai**”, to my parents, Mohan Rao and Malini, and my brother Ajay. I will always be thankful for their constant encouragement and support all along, without which I would not have reached these heights.

## Biography

Abhay Mohan was born on June 19, 1978 in Mangalore, South India. He did his schooling from Marimallappa School and Sarada Vilas College, Mysore, India in 1995 and received an undergraduate degree in Textile Technology (B.Tech) from Regional Engineering College, Jalandhar, India in 1999. He joined North Carolina State University, NC for a Masters degree in Textile Management and Technology in fall 2000.

## Acknowledgements

I am indebted to my parents who have been very understanding in allowing me to come this far to pursue my graduate studies. I thank my advisors, Dr. Abdelfattah M. Seyam and Dr. Tushar K. Ghosh for providing me with an opportunity to work under their guidance. They have been a tremendous influence on my academic and professional development over the last two years. I am also grateful to Dr. Jason A. Osborne for agreeing to serve on committee and help me out with statistical analysis. I would like to acknowledge Army Research Office (ARO), the sponsors of this research. I thank Dr. Behnam Pourdeyhimi for allowing me to use the Image analysis software. I would also like to thank the staff of College of Textiles, for all the help and suggestions during the course of my Masters curriculum. I would finally thank all my friends, who have been very instrumental to go through tough times, especially Yogeshwar Velu and Nilesh Ingle, without whom preparation of samples and analysis of data would not have been possible.

# Table of Contents

<b>LIST OF TABLES</b>	<b>VIII</b>
<b>LIST OF FIGURES</b>	<b>IX</b>
<b>1 INTRODUCTION .....</b>	<b>1</b>
<b>2 BACKGROUND.....</b>	<b>4</b>
2.1 OVERVIEW OF VARIOUS SPINNING METHODS .....	4
2.1.1 Wet Spinning.....	4
2.1.2 Dry Spinning .....	4
2.1.3 Melt Spinning .....	5
2.1.4 Gel Spinning .....	5
2.2 THE ELECTROSPINNING PROCESS .....	5
2.2.1 Governing Theory for Electrospinning.....	7
2.2.2 Principle .....	8
2.2.3 Experimental setup and procedure using various polymers.....	9
2.2.4 Bending Instabilities .....	26
2.2.4.1 Charging .....	28
2.3 ELECTROSPUN FIBER CHARACTERISTICS.....	29
2.3.1 Shapes of Electrospun fibers .....	29
2.3.2 Structure .....	30
2.3.3 Objectives of characterization .....	31
2.3.4 Fiber Diameter and its distribution .....	31
2.3.5 Pore Size Distribution.....	33
2.3.5.1 Theory of Capillary Flow .....	34
2.3.6 Fiber Orientation Distribution .....	36
2.3.6.1 Image Analysis Techniques .....	37
2.3.7 Thermal Analysis .....	38
<b>3 RESEARCH OBJECTIVE.....</b>	<b>40</b>

<b>4</b>	<b>EXPERIMENTAL</b>	<b>41</b>
4.1	ELECTROSPINNING APPARATUS	41
4.1.1	Sprayer	41
4.1.2	Collecting Device	43
4.2	MATERIAL	48
4.3	SOLUTION PREPARATION	49
4.4	EXPERIMENTAL DESIGN	49
4.4.1	Shot Formation	50
4.5	CHARACTERIZATION OF FIBER AND FIBER WEB	54
4.5.1	Fiber Diameter Distribution	54
4.5.2	Fiber Orientation Distribution	59
4.5.3	Pore Size Measurement	61
4.5.3.1	Theory and Description of the Apparatus	61
4.5.3.2	Test Procedure	63
4.5.4	Differential Scanning Calorimetry	65
4.5.5	Basis Weight of Nanofiber webs	66
4.6	STATISTICAL ANALYSIS	67
<b>5</b>	<b>RESULTS AND DISCUSSION</b>	<b>69</b>
5.1	FIBER DIAMETER AND ITS DISTRIBUTION	69
5.2	THROUGHPUT AND BASIS WEIGHT	77
5.3	FIBER ORIENTATION DISTRIBUTION	82
5.3.1	Anisotropy Ratio	86
5.4	PORE SIZE AND ITS DISTRIBUTION	88
5.4.1	Mean Flow Pore Size	88
5.4.2	Pore Size Distribution	99
5.5	THERMAL ANALYSIS BY DSC	104
<b>6</b>	<b>CONCLUSION</b>	<b>109</b>
6.1	RECOMMENDATIONS	110
<b>7</b>	<b>BIBLIOGRAPHY</b>	<b>112</b>

<b>8 APPENDICES.....</b>	<b>118</b>
8.1 SAFETY PROCEDURES FOR THE ELECTROSPINNING SET UP.....	118
8.1.1 General description of the apparatus .....	118
8.1.2 Chemical Safety.....	118
8.1.3 Electrical Safety .....	119
8.2 ANOVA MODEL FOR DIAMETER DISTRIBUTION OF ELECTROSPUN FIBERS .....	120
8.3 ANOVA MODEL FOR THROUGHPUT OF ELECTROSPUN FIBERS .....	123
8.4 ANOVA MODEL FOR ANISOTROPY RATIO OF ELECTROSPUN FIBERS .....	125
8.5 ANOVA MODEL FOR AVERAGE PORE DIAMETER OF ELECTROSPUN FIBERS .....	126
8.6 ANOVA MODEL FOR ANISOTROPY RATIO (DEPENDENT VARIABLE) ON AVERAGE PORE DIAMETER OF ELECTROSPUN FIBERS.....	127
8.7 PARTIAL CORRELATION COEFFICIENTS TO DESCRIBE LINEAR ASSOCIATIONS BETWEEN PAIR OF RESPONSE VARIABLES.....	128



## LIST OF TABLES

Table 4. 1: Independent and dependent variables of the experiment .....	50
Table 4. 2: Design of experiments .....	54

## *LIST OF FIGURES*

Figure 2. 1: Formation of Taylor Cone and subsequent splaying of fibers. ....	7
Figure 2. 2: Apparatus for electrostatic spinning used by Formhals [65].....	10
Figure 2. 3: Schematic drawing of the apparatus used by Taylor [26] [A – metal tube, B & E – metal plates, C – reservoir, D – hemispherical droplet].....	11
Figure 2. 4: Electrospinning apparatus with photographic setup used by Baumgarten [56].....	12
Figure 2. 5: Diagrammatic side view of the apparatus for continuous production of fibers used by Martin et al [67].....	13
Figure 2. 6: Apparatus for the production of fiber fleeces used by Simm et al [69] ..	14
Figure 2. 7: Apparatus for preparing tubular products used by Bornat [72, 73].....	17
Figure 2. 8: Diagrammatic illustration of electrospinning system used by How [74].	18
Figure 2. 9: Schematic drawing of the apparatus used by Doshi [60, 61] .....	20
Figure 2. 10: Schematic drawing of the apparatus used by Srinivasan [12, 64].....	21
Figure 2. 11: Schematic diagram of the apparatus for making DNA fibers [7] [1) Wire electrode in contact with the DNA solution, 2) glass pipette holding the DNA solution, 3) infra red lamp to warm the sample, 4) electrically charged polymer jet, 5) smaller jets produced by splaying of the primary jet, 6) sheet of aluminum foil, 7) box to restrict air flow] .....	22
Figure 2. 12: Theory of Capillary Flow. a) Capillary Rise ( $q < 90^\circ$ ), b) Capillary Depression ( $q > 90^\circ$ ) [43] .....	34
Figure 2. 13: Diagrammatic representation of Differential Scanning Calorimeter ....	39
Figure 4. 1: Schematic of nanofibers spraying device.....	42
Figure 4. 2: Photo of nanofibers spraying device.....	42
Figure 4. 3: Collecting Device for the electrospun fibers .....	43
Figure 4. 4: Photo of nanofibers collecting device .....	44
Figure 4. 5: Side-view of the collecting drum showing electrical connections .....	45
Figure 4. 6: Pictorial representation of the side view of the electrospinning setup...	46
Figure 4. 7: Pictorial representation of the electrospinning set-up .....	47
Figure 4. 8: Scanning Electron Micrograph showing bead formation on electrospun web produced at 15% polymer concentration, 21 kV voltage and 17 cm distance [Measurement Environment: Hitachi ESEM S 3200, 30 Pa air pressure, 10 kV voltage, 100x magnification, 16 mm working distance] .....	52
Figure 4. 9: Scanning Electron Micrograph showing bead formation on electrospun web produced at 17% polymer concentration, 19 kV voltage and 21 cm distance [Measurement Environment: Hitachi ESEM S 3200, 30 Pa air pressure, 10 kV voltage, 400x magnification, 15 mm working distance] .....	53
Figure 4. 10: Fixing the electrospun specimen .....	56
Figure 4. 11: Representation of Orientation Distribution Function [81].....	59
Figure 4. 12: Pore size of a Fabric [81] .....	61
Figure 4. 13: Principle of Capillary Flow.....	62

Figure 4. 14: Essential Parts of Automated Perm Porometer [81] .....	63
Figure 4. 15: Diagrammatic representation of Bubble point test [82] [H1 & H2 – High Flow 1 & 2, LV – low flow, FNV – fixed needle valve, R – regulator, SC – sample chamber, DV – drain valve].....	64
Figure 5. 1: Influence of electric field and polymer concentration on the measured average diameter of electrospun fibers.....	69
Figure 5. 2: SEM image of electrospun web formed at Polymer Concentration 27 %, Voltage 21 kV, Distance 19 cm. (1.105 kV/cm) [Measurement Environment: Hitachi ESEM S 3200, Air pressure 40 Pa, Magnification 3000x, Voltage 15 kV, Work distance 22 mm] .....	70
Figure 5. 3: SEM image of electrospun web formed at Polymer Concentration 27 %, Voltage 15 kV, Distance 22 cm. (0.681 kV/cm) [Measurement Environment: Hitachi ESEM S 3200, Air pressure 40 Pa, Magnification 3000x, Voltage 15 kV, Work distance 22 mm] .....	71
Figure 5. 4: Influence of electric field and polymer concentration on the measured average diameter of electrospun fibers (plotted for regression equations).....	73
Figure 5. 5: Plot showing the relationship between observed fiber diameter and predicted fiber diameter .....	74
Figure 5. 6: Effect of varying electric field on the diameter distribution of the fibers at a constant concentration of 21%.....	75
Figure 5. 7: Effect of varying electric field on the diameter distribution of the fibers at a constant concentration of 23%.....	75
Figure 5. 8: Effect of varying electric field on the diameter distribution of the fibers at a constant concentration of 25%.....	76
Figure 5. 9: Effect of varying electric field on the diameter distribution of the fibers at a constant concentration of 27%.....	76
Figure 5. 10: Effect of Concentration on the diameter distribution of fibers at an electric field of 1.0 kV/cm .....	77
Figure 5. 11: Influence of electric field on the throughput of an electrospun web produced at different polymeric concentrations.....	79
Figure 5. 12: Influence of electric field on the basis weight of an electrospun web produced at different polymeric concentrations.....	80
Figure 5. 13: Plot showing the relationship between observed throughput and predicted throughput .....	81
Figure 5. 14: Orientation distribution function of an electrospun sample at a constant concentration of 21% with varying electric fields.....	82
Figure 5. 15: Orientation distribution function of an electrospun sample at a constant concentration of 23% with varying electric fields.....	83
Figure 5. 16: Orientation distribution function of an electrospun sample at a constant concentration of 25% with varying electric fields.....	83
Figure 5. 17: Orientation distribution function of an electrospun sample at a constant concentration of 27% with varying electric fields.....	84
Figure 5. 18: SEM image of electrospun web formed at Polymer Concentration 25 %, Voltage 15 kV, Distance 21 cm. (0.714 kV/cm) [Measurement Environment: Philips 505 T, Magnification 625x, Voltage 12 kV] .....	85

Figure 5. 19: SEM image of electrospun web formed at Polymer Concentration 25 %, Voltage 17 kV, Distance 21 cm. (0.809 kV/cm) [Measurement Environment: Philips 505 T, Magnification 625x, Voltage 12 kV] .....	85
Figure 5. 20: Effect of electric field and concentration on the anisotropy ratio of an electrospun fiberweb.....	86
Figure 5. 21: Plot showing the relationship between observed anisotropy ratio and predicted anisotropy ratio.....	88
Figure 5. 22: Effect of average pore diameter and basis weight with varying electric field at constant concentration 23% .....	89
Figure 5. 23: Effect of average pore diameter and basis weight with varying electric field at constant concentration 25% .....	90
Figure 5. 24: Effect of average pore diameter and basis weight with varying electric field at constant concentration 27% .....	90
Figure 5. 25: Pictorial of fibers arranged in an electrospun web .....	91
Figure 5. 26: Effect of average pore diameter and anisotropy on a four-layered sample with varying electric field at constant concentration 23%.....	92
Figure 5. 27: Effect of average pore diameter and anisotropy on a four-layered sample with varying electric field at constant concentration 25%.....	92
Figure 5. 28: Effect of average pore diameter and anisotropy on a four-layered sample with varying electric field at constant concentration 27%.....	93
Figure 5. 29: SEM image of electrospun web formed at Polymer Concentration 23 %, Voltage 15 kV, Distance 20 cm. (0.75 kV/cm) [Measurement Environment: Philips 505 T, Magnification 625x, Voltage 12 kV] .....	93
Figure 5. 30: SEM image of electrospun web formed at Polymer Concentration 23 %, Voltage 19 kV, Distance 22 cm. (0.863 kV/cm) [Measurement Environment: Philips 505 T, Magnification 625x, Voltage 12 kV] .....	94
Figure 5. 31: Effect of average pore diameter and fiber diameter with varying electric field at constant concentration 23% .....	95
Figure 5. 32: Effect of average pore diameter and fiber diameter with varying electric field at constant concentration 25% .....	95
Figure 5. 33: Effect of average pore diameter and fiber diameter with varying electric field at constant concentration 27% .....	96
Figure 5. 34: SEM image of electrospun web formed at Polymer Concentration 27 %, Voltage 17 kV, Distance 20 cm. (0.85 kV/cm) [Measurement Environment: Hitachi ESEM S 3200, Air pressure 40 Pa, Magnification 3000x, Voltage 15 kV, Work distance 22 mm] .....	96
Figure 5. 35: SEM image of electrospun web formed at Polymer Concentration 27 %, Voltage 21 kV, Distance 19 cm. (1.105 kV/cm) [Measurement Environment: Hitachi ESEM S 3200, Air pressure 40 Pa, Magnification 3000x, Voltage 15 kV, Work distance 23 mm] .....	97
Figure 5. 36: Effect of electric field and concentration on the average pore diameter of an electrospun fiberweb.....	98
Figure 5. 37: Influence of fiberweb layers on the average pore diameter at a constant concentration of 23 % .....	100
Figure 5. 38: Effect of varying electric field on the cumulative filter flow at a constant concentration of 21% (3 layers) .....	101

Figure 5. 39: Effect of varying electric field on the cumulative filter flow at a constant concentration of 23% (3 layers) .....	102
Figure 5. 40: Effect of varying electric field on the cumulative filter flow at a constant concentration of 23% (4 layers) .....	102
Figure 5. 41: Effect of varying electric field on the cumulative filter flow at a constant concentration of 25% (4 layers) .....	103
Figure 5. 42: Effect of varying electric field on the cumulative filter flow at a constant concentration of 27% (4 layers) .....	103
Figure 5. 43: DSC Curve for Polyester.....	104
Figure 5. 44: Glass Transition Temperature of Polyester.....	105
Figure 5. 45: Crystallinity of Polyester.....	106
Figure 5. 46: Melting Point of Polyester .....	107

# 1 Introduction

Fibers have a long history and for many years, the use of fiber was restricted by the inherent qualities available in the natural world, resulting in the emergence of manufactured fibers merely a century ago. Manufactured fibers now are put to work in modern apparel, home furnishings, medicine, aeronautics, energy, industry, and more. These fibers are produced from organic polymers and inorganic materials. Fibers can be combined, modified and tailored in ways far beyond the performance limits of fiber drawn from the silkworm cocoon, grown in the fields, or spun from the fleece of animals. These manufactured fibers apart from being an alternative to natural fibers have proved to be useful and successful in the real world in terms of functionality and performance.

There have been methods to produce ultra thin fibers explained in the literature, which dates back to many years. But, the methods proved to be highly inconvenient and expensive. In recent years, a new technique called the electrospinning process was developed and understood, which could produce fibers having diameters in the nanometer range. This technique has been proved to be convenient, effective and has successfully spun many fibers.

Various industrial applications of the production of liquid jets in the presence of intense electric field have been investigated. One such application is the process of electrospinning, which is used to spin nano synthetic fibers from polymer solutions and melts. About 50 patents for electrospinning polymer melts and solutions have been filed in the past 60 years [83]. However, there is no known commercial process for electrospinning.

Electrospinning uses electrostatic forces as the driving force to spin fibers. In the electrospinning process by solution, a polymer solution held by its surface tension at the end of a capillary tube is subjected to an electric field. As the intensity of the electric field increases, the hemispherical surface of the solution at the tip of the capillary tube extends to form a cone like structure, which is also known as the Taylor cone [27]. With increasing voltage, a critical point is reached and a charged

jet of the solution is ejected from the tip of the Taylor cone. As this charged jet moves in the air, the solvent evaporate, leaving behind a charged polymer fiber, which lays itself randomly on a collecting plate. Thus, continuous fibers are laid to form a fibrous web.

Unlike conventional fiber spinning techniques, which are capable of producing fibers with diameters down to the micron size range, electrostatic spinning, or electrospinning is capable of producing fibers in the nanometer diameter size range, or "nanofibers". In electrospinning, electrostatic forces are used in addition to mechanical forces to drive the fiber forming process. The resulting nanofibers are of substantial scientific and commercial interest, as they are thought to exhibit morphologies and properties different from conventional fibers.

The electrospun nanofibers provide a very large surface area/mass due to their small diameter, hence non-woven fabrics, with small fibers can be used for filtration of sub-particles in the separation industry. These can also be used for the adsorption of biological and chemical warfare gases, protective clothing, in medical industry as artificial blood vessels, sutures, surgical facemask, fiber-reinforced materials, mono-directional composites and in agricultural field for control of pesticides. The electrospinning technique can be used in chemical and manufacturing industries for paint spraying, electrodeposition, plasma deposition, and mining minerals. In general, polymer nanofibers are used in a variety of applications, including filtration, protective clothing, biomedical applications such as wound dressing and drug delivery systems, design of solar sails, light sails and mirrors for use in space, as well as for structural elements in artificial organs and in reinforced composites. Ceramic or carbon nanofibers made from polymer precursors make it possible to expand the list of possible uses for nanofibers.

In this work, nanofibers were produced from electrospinning from solution using poly (ethylene terephthalate) as the polymer. Experiments were performed using this polymer and the electrospun web thus produced was characterized. There has been an effort to characterize the process parameters and for this a suitable experiment and equipment design was made. The process parameters investigated included concentration of the polymer solution, the voltage and the collecting

distance between the two electrodes. The electrospun web was characterized for structure by measuring fiber diameter and its distribution, fiber orientation and pore size and its distribution.



## 2 Background

This chapter explains the background and principle of electrospinning. It also elaborates on the process, various experimental setups and fiber-web structure.

### **2.1 Overview of various spinning methods**

The process of extrusion involves forcing a thick, viscous liquid through a spinneret to form continuous filaments of semi-solid polymer [77]. The fiber forming polymers being solids must be converted into a fluid state for extrusion. This can be either achieved by melting, if the polymers are thermoplastic synthetics, or by dissolving them in a suitable solvent if they are non-thermoplastic cellulose. If both of these don't work then they must be chemically treated to form soluble or thermoplastic derivatives. Conventionally, there are four methods of spinning, namely, wet spinning, dry spinning, melt spinning and gel spinning.

#### 2.1.1 Wet Spinning

This method of spinning can be used for substances that can be dissolved in a solvent. The spinnerets are completely submerged in a non-solvent coagulating chemical bath into which the filaments are extruded and as the filaments emerge they precipitate from solution and solidify. Because the solution is extruded directly into the precipitating liquid, this process for making fibers is called wet spinning [77].

#### 2.1.2 Dry Spinning

In this method of fiber formation, the solidification process of fiber forming polymers is achieved by evaporating the solvent in a stream of air or inert gas. The polymer solution is extruded through a spinneret into a heated zone where the solvent evaporates, leaving behind fiber filaments. The filaments do not come in contact with a precipitating liquid, eliminating the need for drying and easing solvent recovery [77].

### 2.1.3 Melt Spinning

This process involves heating the polymer higher than its melting temperature and then extruding it through spinneret. In this method, the fiber-forming substance is melted for extrusion and forced through the spinneret and then directly solidified by cooling [77]. Melt spun fibers can be extruded from the spinneret in different cross-sectional shapes (round, trilobal, pentagonal, octagonal, and others).

### 2.1.4 Gel Spinning

When the polymer is not in a true liquid state during extrusion this method is used and in this process, the polymer chains are bound together at various points in liquid crystal form. This produces strong inter-chain forces in the resulting filaments that can significantly increase their tensile strength [77]. Moreover, the filaments emerge with an unusually high degree of orientation relative to each other, which further enhances the strength.

## 2.2 *The Electrospinning Process*

The manufacturing process of electrospinning was first reported by Formhals [65] in 1934, the experimental setup and procedure of which has been explained in the sections to come. Since then, the process of electrospinning has caught the attention of many researchers and many reports, publications and patents in this field ascertain this. Gibson et al (79) describes electrospinning as a process in which high voltage is used to produce an interconnected membrane like web of small fibers. This method provides the capacity to lace together many types of polymers, fibers, and particles to produce ultra thin layers.

The electrospinning process is used to make fine fibers in the range of nano meters (which are also called nano fibers), by charging a polymer solution with several thousand volts. When sufficient voltage to overcome the surface tension is reached, fine jets of liquid are ejected towards a grounded object. The jet stretches and elongates as it travels and is collected as an interconnected web like structure. Various publications indicate that the voltage required to produce fibers range from 5 kV to 30kV [78]. This range of voltage is good enough to overcome the surface tension of the polymeric solution and to produce very fine charged jets of liquid

towards a grounded target. This charged jet before hitting the target undergoes splitting and drawing and forming fibers with different sizes and shapes before evaporating to form a web like structure.

The electrospinning system consists of two separate entities, a sprayer and a collecting device. The sprayer essentially consists of a glass spinneret, which holds the polymer solution. One of the metal electrodes from the high voltage supply is given to the solution, which serves as the positive terminal. A collector, which collects the fibers is given the other end of the electrode, which serves as the negative terminal. In this process, polymer solution is charged to a very high electrical potential. Because of the electric field, charge is induced on the liquid surface. The presence of potential difference between the two electrodes i.e., the mutual charge repulsion, causes a force opposite to the surface tension of the polymer solution. As the electric field increases, the hemispherical surface of the solution at the tip of the capillary tube (Figure 2.1) extends to form a cone like structure, which is also known as the Taylor cone. As the intensity of the electric field is further increased the field reaches a critical point value at which the repulsive electric force overcomes the surface tension force. At this point a charged jet of the solution is ejected from the tip of the Taylor cone. So as the force acting on the polymer solution becomes greater than the surface tension, the charged droplet becomes unstable and this instability results in the formation of a charged jet. As this charged jet moves in the air, the solvent evaporate, leaving behind a charged polymer fiber, which lays itself randomly on a collecting plate. So, fiber formation is due to the instability created by the repulsion between similar charges. Thus, continuous fibers are laid to form a web like structure. Diameters of these fibers range from 600 nanometers to 2000 nanometers. The nanofibers structured in the web show good tensile strength, excellent moisture vapor transport, extremely low air permeability, and good aerosol particle protection [79].

There are various parameters, which come into picture namely the solution, controllable and ambient parameters [61]. Solution properties include viscosity, conductivity and surface tension. Controllable parameters include electric potential at the tip, distance between the tip of the capillary and the collection plate or surface.

Ambient variables include temperature, humidity, and air velocity in the electrospinning chamber. Varying one or more of these properties can produce electrospun fibers from various polymers, which includes water-soluble polymers, biopolymers and liquid crystalline polymers. Fibers produced by this method using different polymers have been shown to have a wide variety of shapes, sizes and degree of orientation.

### 2.2.1 Governing Theory for Electrospinning

**Taylor's Theory** [26, 27]: Formation of fine threads from viscous drops in an electric field is due to maximum instability of liquid surface induced by electrical forces. At increasing voltage, it forms a spherical cap and at the critical point, the meniscus of a viscous drop becomes nearly conical before the fiber formation and just before jet formation. The contracting round top conical part had a semi-vertical angle  $\theta \sim 50$  degrees (see figure 2.1). Under the action of electrical stresses, curvature of surface of a viscous liquid change as surface tension is the only force that opposes the electrical force.

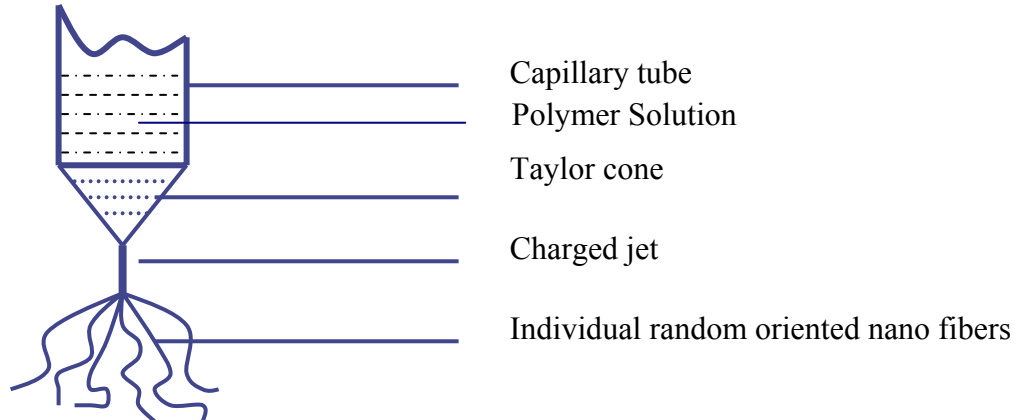


**Figure 2. 1: Formation of Taylor Cone and subsequent splaying of fibers.**

The Critical voltage  $V_c$ , at which maximum instability develops, as given by Taylor in 1969 [26]:

$$V_c^2 = 4 H^2/L^2 * (\ln (2L/R) - 1.5) * (1.3 \pi RT) * (0.09) \quad \text{Equation 2. 1}$$

for say  $\theta \sim 50$  degrees,  $H$  is the distance between electrodes,  $L$ , the length of the capillary,  $R$ , the radius of the capillary, and  $T$ , the surface tension. Flow field in the

jet will be such that velocity gradient along jet-axis has an extensional component. Extensional velocity gradient (here caused due to 2nd kind of instability i.e., repulsion of similar kind of charges) is known to be very efficient in stretching the polymer chains and forming very fine fibers. Also, width of fibers decreases as  $V$ , the voltage applied increases as it leads to electrostatic stretching.

### 2.2.2 Principle

The principle of the electrospinning process may be best understood by the reports given by Rayleigh, Zeleny and Taylor. As Taylor [26] quotes – ‘fine jets of slightly conducting viscous fluids and thicker jets or drops of less viscous ones can be drawn from conducting tubes by electrical forces. As the potential of the tube relative to a neighboring plate rises, viscous fluids become nearly conical and fine jets come from the vertices’.

Lord Rayleigh [34] in 1882 studied the condition of instability occurring in electrically charged liquid droplets. He showed that the droplet is unstable when electrical force is greater than or equal to force from surface tension i.e., when the electrostatic force overcomes the surface tension force, which is acting in the opposite direction of the electrostatic force, the unstable charged droplet breaks up into a series of charged droplets at this point and liquid is ejected in fine jets.

The electric intensity at the surface of a meniscus by measuring the length of a liquid column was determined by Zeleny [30, 31, 33]. The hydrostatic process in the column counteracts the mechanical pull exerted by an electric field on the liquid surface. The character of deformation of the meniscus was also reported. Zeleny studied the effect of the electric field on the liquid droplet hanging at the tip of the capillary. He studied the discharge from charged drops and from uncharged drops in electric fields and this showed that the surface electric intensities, when the discharge began, satisfied the theoretical relations for surface instability. He observed that the surface instability induced a cone on the liquid surface and the mode of spraying was from several sites from one cone. The liquid drop was stable at a value below the threshold for the discharge of the liquid. Using low molecular liquids, ethanol and glycerol, the spray phenomenon was reported using several

photographs [32]. Breakup of the electrified jet happened at a relatively longer distance from the droplet for glycerol than ethanol. The process of ejection of small droplets occurs because of the surface instability. As the jet from the cone surface of a liquid is ejected, it breaks down into droplets and the diameter of the drop was in the order of  $10^{-5}$  cm to  $10^{-4}$  cm. He showed that instability of liquid drop occurs when the internal pressure of droplet is same as external pressure.

### 2.2.3 Experimental setup and procedure using various polymers

Formhals [65] in 1934 reported an experimental setup for electrospinning. His method involved dispersing the spinning solution using high electric field. Solution was prepared by dissolving cellulose acetate in ethylene glycol. The spinning solution was introduced into an electric field, by giving it one end of the electrode to produce field (Figure 2.2). A collecting device, a belt was given the negative polarity. The solution is passed into this electric field formed between electrodes in a thin stream or drops in order to separate them into a plurality of threads. Potential difference of 5 to 10 kV was maintained and this difference depended on the properties of spinning solution apart from ambient conditions. The two movable bodies, spinning vessel and the collecting belt, charged with high-tension static electricity of unlike polarity, produced extremely fine threads in the direction of the collecting belt. The dried fibers were collected on the belt, but it could be observed that the fibers adhered to the surface of the moving parts of the apparatus, mainly the belt, the drum and similar parts, which made removal of fibers from these parts difficult.

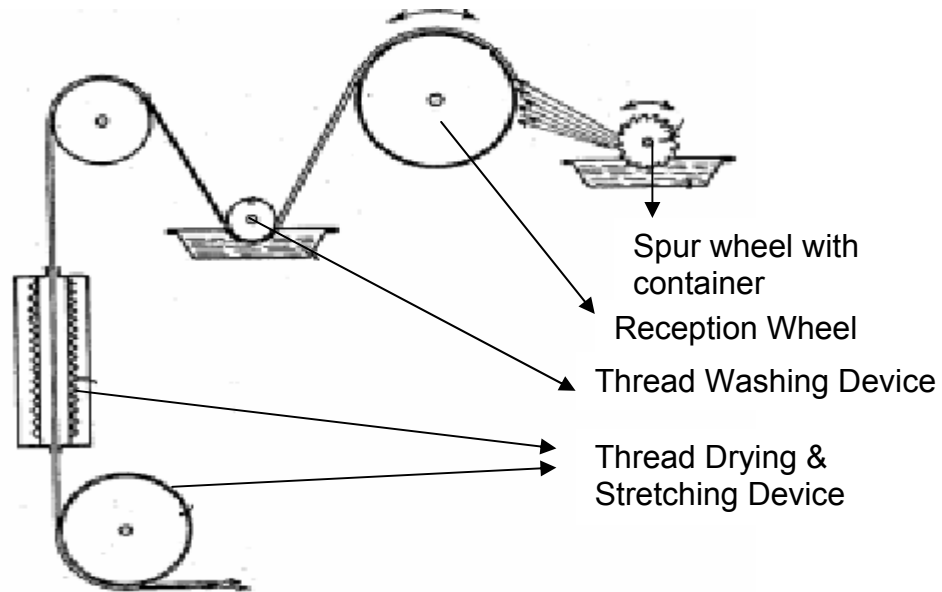


**Figure 2. 2: Apparatus for electrostatic spinning used by Formhals [65]**

Taylor showed that instability of an elongated drop would not occur unless a pressure differential exists. His papers [27, 28, 29] demonstrated that a conical interface between two fluids could exist in equilibrium in an electric field. At the onset of instability, the droplet elongates and its end develops a conical shape called the '**Taylor Cone**', which theoretically had a semi angle close to  $49.3^\circ$  at the vertex. This was even shown and proved through several photographs. At the apex of the Taylor cone, the liquid surface is usually unstable, and charged drops of liquid are emitted to give a space-charge zone in front of the cone. As the electric field approaches the breakdown field strength at this point, a corona discharge may occur. This affects the electric field at the apex, and the radius of curvature of the apex of the cone changes accordingly to sustain the field. The electric pressure due to the maximum charge that can reside on the cone surface is balanced by the surface tension of the liquid.

Taylor [26] in 1969 published theoretical and experimental work on the disintegration of pure as well as mixture of liquid drops and electrified jets. Taylor correlated his experimental observations with a theoretical model, and in this process he obtained an expression for the critical electric potential at which the droplet becomes unstable. He showed that Zeleny's mechanism of droplet disintegration was based on a false assumption that instability happens when the internal pressure is the same as that outside the droplet. In his experimental set-up

(Figure 2.3), he explains the voltage required for the fluid to be drawn from the tube. The polymer was stored in a reservoir C, and when the voltage was increased, the surface of the meniscus of the fluid, D, emerging out from the metal tube A, became convex till the critical voltage, after which it no longer can be stable. The potential difference was maintained by two parallel plates B and E. At this point, it emits a jet towards the targeted plate B. This has been explained by the equation 2.1.

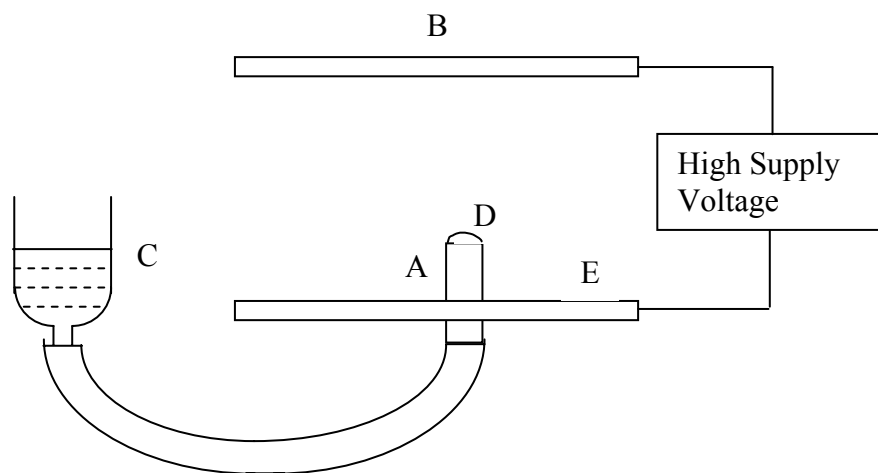


**Figure 2. 3: Schematic drawing of the apparatus used by Taylor [26]** [A – metal tube, B & E – metal plates, C – reservoir, D – hemispherical droplet]

Simons [66] in 1966 demonstrated a method for the production of patterned and textured non-woven fabrics, wherein electrically-spun filaments are aggregated into bundles defining a controlled pattern of aggregates of high filament density contrasting with controlled areas of low filament density. In his apparatus, Simons used a segmented receiver as a fiber-collecting device. A wide variety of organic polymeric materials were considered including cellulose esters and ethers, vinyl resins, acrylic resins, polystyrene, polyurethanes and polycarbonates. Solvents considered, namely chloroform, ketones such as acetone, methyl ethyl ketone, and methyl isobutyl ketone had wide range of dielectric constants. In operation, it disperses a solution into a stream of electrically spun filaments and is collected in the form of a patterned non-woven fabric. The patterned non-woven fabrics were thin and lightweight.

Baumgarten [56] in 1971 carried out experiments involving electrostatic spinning to produce acrylic micro fibers. The acrylic resin used was a commercial



copolymer of 93.6 % acrylonitrile, 6 % methyl acrylate, and 0.4 % sodium styrene sulfonate and the solution was prepared in dimethyl formamide. The experimental apparatus (Figure 2.4) consisted of a stainless steel capillary tube through which the polymer drop was suspended and to maintain constant drop, infusion pump was incorporated. Potential difference was maintained between capillary tube and a grounded metal screen. For photographic study, a camera was attached in line with the spinning fiber. The analysis showed that as the viscosity of the solution increased, the spinning drop changed its shape to conical from hemisphere and the length of the jet increased. It was also observed that the fiber diameter increased with increased viscosity and was approximately proportional to jet length. Electron photomicrographs obtained showed that the fiber had the appearance of smooth, straight cylinders. As the solution flow rate increased, the jet length almost doubled but there was not much change in the diameter of the fibers.

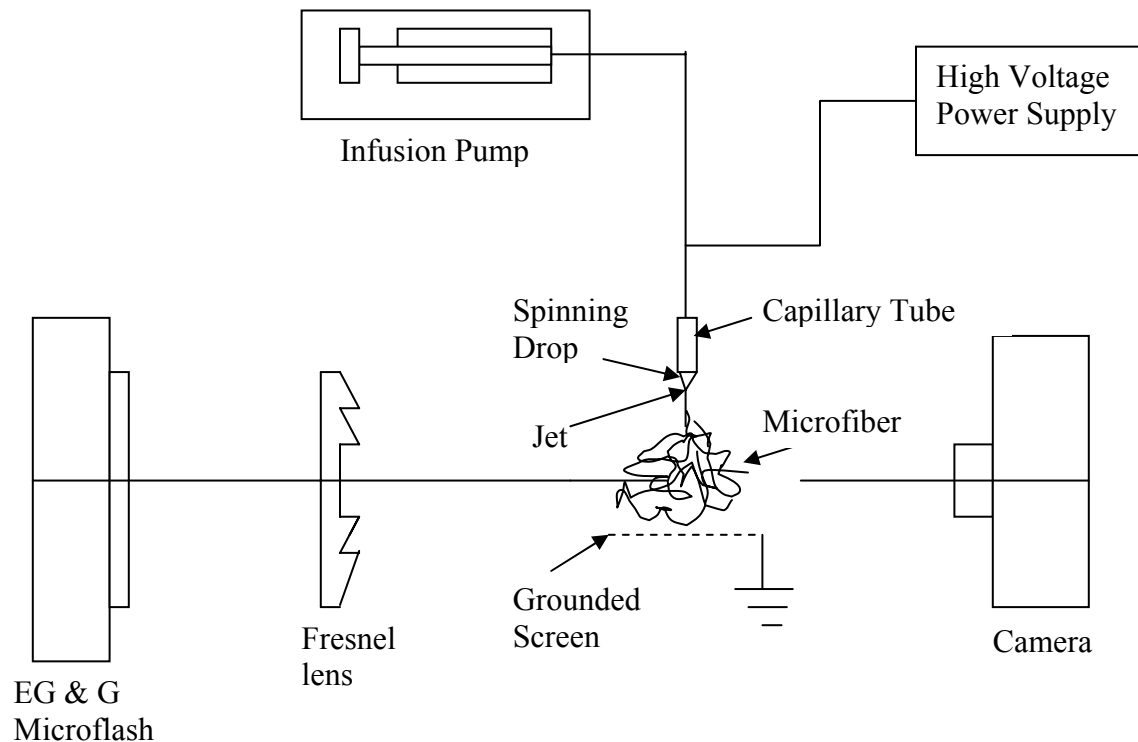


**Figure 2. 4: Electrospinning apparatus with photographic setup used by Baumgarten [56]**

Martin, Cockshott, and Fildes [67] invented fibrillar mat, with two and three-dimensional articles for prosthetic device comprising a plurality of fibers of organic

material, wherein the fibers were produced by electrostatic spinning. Materials involved included suspension of PTFE, polyurethanes and aqueous solutions of polyvinyl alcohol, polyvinyl pyrrolidone and polyethylene oxide. The spinning material is fed into an electrostatic field from a syringe reservoir to the tip of an earthed syringe needle (Figure 2.5). An electrostatically charged surface was placed at an appropriate distance. Fiber is formed between the tip of the syringe needle and the charged surface. Potential maintained was around 20 kV at a distance of 5–35 cm between syringe needle and collecting surface. Mats collected on a rotating non-conducting belt had a few microns to a few centimeters thick, highly porous, low diameter, and high surface area. These fiber mats were supposedly made for medical purposes, especially wound dressing.

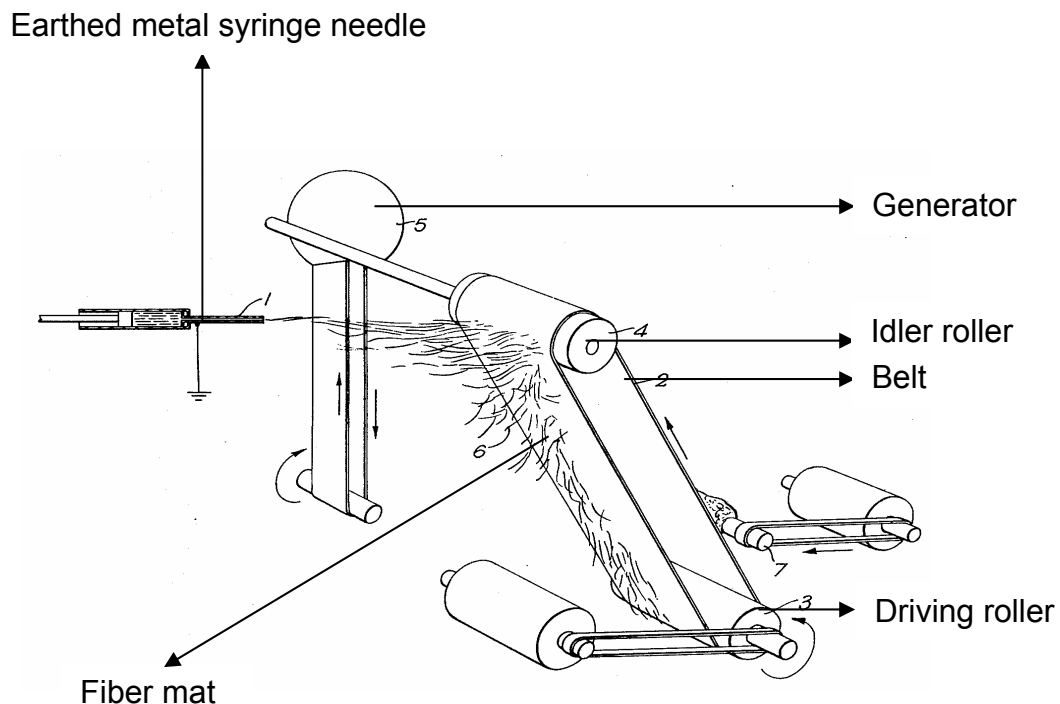


**Figure 2. 5: Diagrammatic side view of the apparatus for continuous production of fibers used by Martin et al [67]**

It has been known that advantageous directional properties may be obtained by the directional orientation of small pieces of cellulose material. Talbott and Logan [68] described a process for forming a composite mat of directionally oriented lignocellulosic material. Here the elongated small pieces of the material are caused to descend individually as separate and discrete objects through an electric field

orienting zone. An electric field is passed through the composite mat to produce a directional electric field above the mat in which the electric field is directed in the direction of movement of the mat and parallel with the mat. This is done to exert forces on the elongated small pieces to cause the pieces to orient their long dimensions in the direction of the electric field as the pieces descend through the orienting zone in the formation of the mat. By contacting the mat with electrodes and by applying a voltage between the electrodes produces the electric current to flow through the mat. This method can be considered as one of the economical and reliable methods for forming a continuous mat of oriented small pieces of lignocellulosic material.

Simm et al. [69] in 1978 described a process of producing filters made of electrostatically spun fibers from polystyrene. The spraying of the spinning solution placed in storage tank was from a rotating annular electrode, overcoming the problem of blockage of spray edge by the drying up of liquid (Figure 2.6). Spinning takes place in the spray chamber and movable electrodes, like conveyor belts, carry the collected fibers. Apart from the air temperature and relative humidity for producing thin, dry filaments, it was observed that electrical conductivity of the spinning solution affects the thickness of the fibers formed.

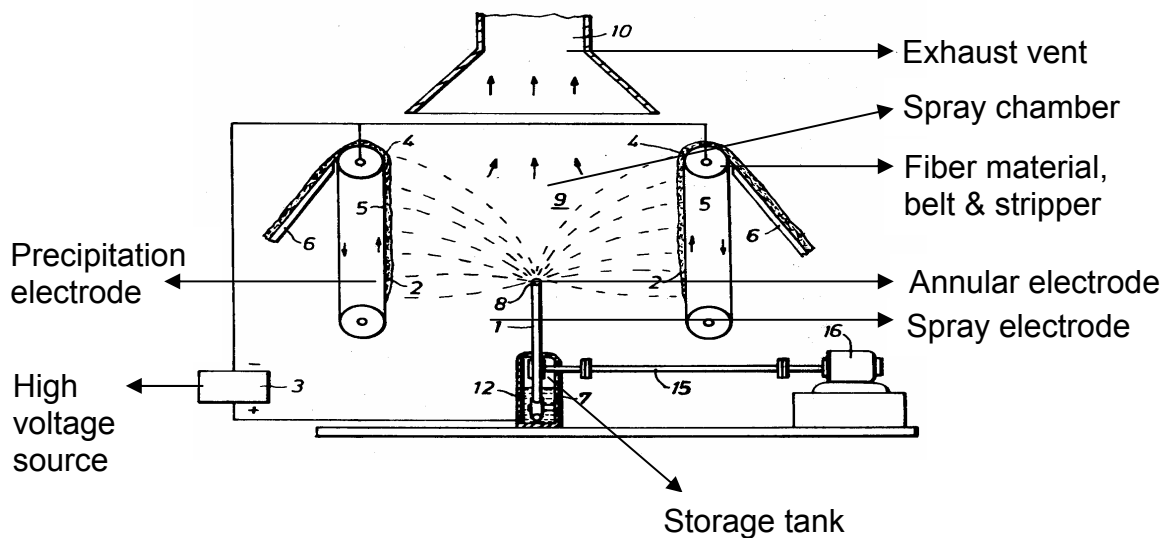


**Figure 2. 6: Apparatus for the production of fiber fleeces used by Simm et al [69]**

Simm et al [70] obtained very thin, relatively short and highly charged fiber fleece in large numbers for filtering purposes, when the fiber material was sprayed electrostatically. The polymers used were polystyrene, cellulose esters or polycarbonates. Non-combustible solvents considered were methylene chloride, chloroform and carbon tetrachloride. The solution was sprayed and they dried along their way to the precipitation electrodes, the collecting device that was placed at equidistant from the ring electrode. The fiber filters produced by this process thus consist of a fiber fleece, which has been electrostatically sprayed from the liquid state on to a conductive support. The resultant fiber fleece covered with permeable cellulose fleece was thick, dry, and porous and was used as an air filter.

Fine and Tora [71] considered a liquid solution of a thermoplastic elastomeric polyurethane in a volatile solvent (like tetrahydrofuran) contained in a cup supplied to a surface rotating about an axis to form a film which is whirled by centrifugal force. By charging the cup to a high electric potential, an electric field is created on the surface of the solution. The electrostatic potential is maintained between this film and the collecting surface, an aluminum foil in the form of a belt and the fibers are attracted and collected in this surface. So, the filaments are formed by the combined action of centrifugal force and the electrostatic force.

Larrondo and Manley [57] demonstrated the formation of continuous electrospun fibers from rapidly crystallizing polymers, polyethylene and polypropylene. Conventionally, high pressures were involved to extrude polymer melt from the spinneret, but in this process, the pressures applied were as little as to form a hemispherical drop of molten polymer at the end of the capillary orifice. A potential difference is established at this stage and as the voltage is gradually increased a critical point is reached where static equilibrium can no longer be maintained. The drop results in a fine, continuous, stable jet of molten polymer, which ultimately solidifies, and a continuous fiber is formed. The interaction between the electric field and the charges induced on the surface of the polymer melt is the probable reason for the drawing of fibers through electrostatic force.

The electrospun fibers formed by this method were unoriented and spherulitic in structure. Properties of these fibers were comparable to the fibers obtained from

conventional spinning processes. Electric field intensity and temperature or melt viscosity affected fiber diameters. Generally speaking, fiber diameter decreased with an increase of electric field intensity. Increasing the temperature of the molten polymer formed smaller diameter fibers. The diameter of the orifice was of little importance. The flow field of an electrified jet, nature of the streamlines and magnitude of the stream velocities were analyzed by using tracer particle photography in a model fluid [58]. It was observed that the velocity field had both extensional and rotational components. It was found that the region about the symmetry axis is void of rotational components and the extensional flow along this axis depended on the electric field intensity at which the jet was operated. Experiments were carried out on nylon 12 and polyethylene to study the electrostatic deformation of a pendant drop [59]. Theoretical and experimental observations show that the deformation was proportional to the dielectric constant of the polymer melt and inversely proportional to the surface tension of the polymer melt.

Bornat [72] in 1982 described the electrostatic spinning process for the production of tubular products, used in medical field. In this process biologically acceptable polymeric substances were used such as PTFE, polyurethanes, dispersions of polytetrafluoroethylene, thermoplastics such as polyamides, polyacrylonitrile, water-soluble polymers such as polyvinyl alcohol, polyvinyl pyrrolidone and polyethylene oxide. The spinning solution is fed to an electrostatic field from a syringe reservoir to the tip of an earthed syringe needle (Figure 2.7). An electrostatically charged surface is kept at a distance and the fibers were formed between the needle tip and the charged surface. This system also involved several capillaries for higher production rate and spinning solution was filled in these capillaries. The potential was maintained between these capillaries and the collecting surface. The collecting device is a rotating mandrel or a rod so as to impart a core-sheath structure to the collected fibers so as to obtain a tubular product. The core may be conductive or non-conductive whereas the sheath is a non-electrically conducting material made of sheet metal or metal foil and is collapsible. The collected composite fibers in tubular form have low diameter and thickness, and are porous.

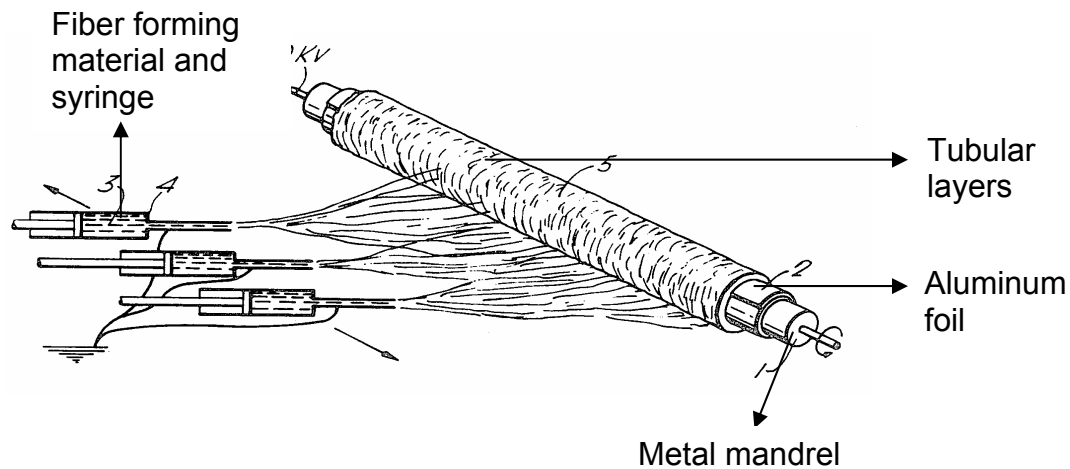


**Figure 2. 7: Apparatus for preparing tubular products used by Bornat [72, 73]**

Bornat [73] also explained that the composite fibers obtained display a pattern of fiber deposition, which tends to be longitudinal i.e., parallel to the long axis of the tube rather than circumferential and is conjectured that the force field generated by the charge on the collector is such that this deposition is resulted. This invention modifies the apparatus explained earlier, by introducing an auxiliary electrode so that higher proportions of the fibers are circumferential rather than longitudinal.

How [74] described a process for the production of synthetic vascular grafts from polyurethane. The polymer solution was ejected through a stainless steel nozzle from a syringe, wherein the nozzle is earthed (Figure 2.8). Flow of the polymer solution through nozzle is maintained by the syringe piston, which is subjected to a constant hydraulic force. Fluid from the nozzle is fed to an electrostatic field surrounding a charged mandrel which is charged to around  $-12$  kV. Because of the high electric potential, filaments are drawn and collected here. This invention essentially relies on the controlling the speed of rotation of the mandrel (between 2000 to 20000 rpm) such that a desired degree of anisotropy is present in the graft. This is because, the purpose for which these grafts are produced, the natural arteries are generally anisotropic.

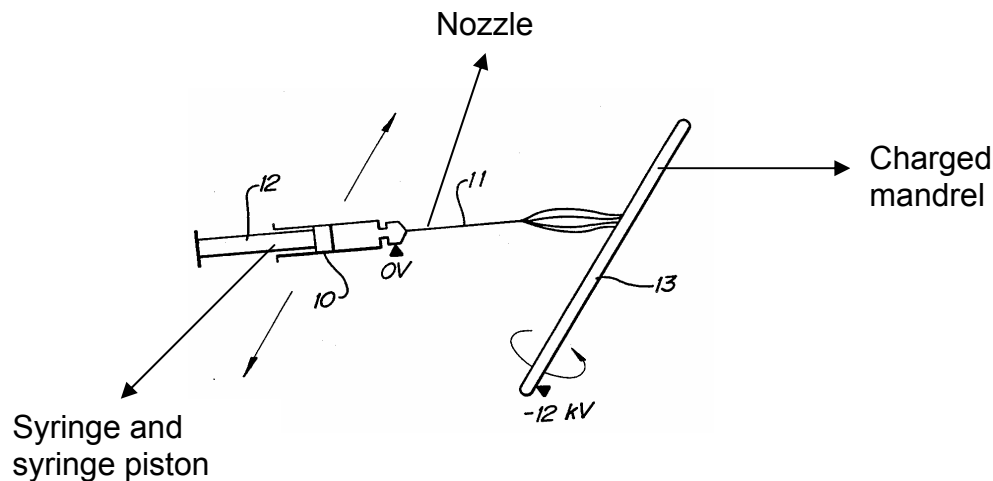


**Figure 2. 8: Diagrammatic illustration of electrospinning system used by How [74]**

The electrostatically spun products for medical use may be made of any biocompatible, non-absorbable or absorbable fiberizable material. A fiberizable material is one, which is capable of forming a solution or melt, which can be electrostatically spun to form fibers. Some of the fiberizable materials include polyethylene terephthalate, polytetrafluoroethylene, silicones, nylons, polyacrylonitrile, and urea/formaldehyde resins. Middleton and Paprotny [75] described a process for producing a medical prosthesis. It consists of forming the prosthesis from uncross-linked polyurethane and then at least partially cross-linking the polyurethane with a cross-linking agent. Here the medical prosthesis is formed by electrostatically spinning a melt or solution of the polyurethane material. The production of tubular products by electrostatic spinning, which describes a tubular fibrous structure comprising randomly oriented smaller diameter fibers in the fibrous structure and substantially circumferentially oriented large diameter fibers embedded in a matrix of small diameter fibers, has wide range of end uses. They may be used as artificial urinary or bile ducts, artificial heart components, artificial trachea, components of auxiliary medical equipment, and as reinforcements for weakened tissue areas.

Berry [76] invented a method for producing electrostatically tubular fibrous spun products using polyurethanes. The spinning solution is fed into the electrostatic field through capillary needles. The emerging droplets were attracted towards

electrostatically charged mandrel kept at a distance. The mandrel consisted of two charged grids and a potential of 6 to 12 kV is maintained. Because of the two charged grids the tubular fibrous structure produced had fibers of different diameters and varying fiber orientations along their length, as the needles traversed. These low diameter fibers were oriented circumferentially around the tube, offered little resistance to bending and assumed a very tight loop without kinking. Also, it had greater axial compliance and when compressed along its axis, it shortened with a minimal tendency to buckle.

Doshi [60, 61] carried out experiments on aqueous solutions of poly (ethylene oxide), and tried to characterize the process parameters. Fibers were also successfully electrospun from water-soluble polymers, biopolymers, and liquid crystalline polymers. The experimental set-up used is shown in Figure 2.9. The operational parameters were divided into the solution properties (surface tension, viscosity, electrical conductivity of the polymer solution), the controlled variables (pressure in the capillary, potential at the tip, collecting distance, jet diameter, jet velocity), and the ambient parameters (temperature, humidity, air velocity in the spinning chamber). The electrospinning process characterization involved measurements of electric potential to start and stop the spinning process, current and jet length, jet diameter and flow rate. The size and geometry of the Taylor cone was carefully investigated in terms of vibrations and instabilities of the cone and the jet. Simulation and computer modeling were used to understand the process. Efforts were made to investigate structure and morphology of the electrospun fiber using scanning electron and atomic force microscopes. It was observed that a wide variety of shapes and sizes could be produced from various types of polymers.



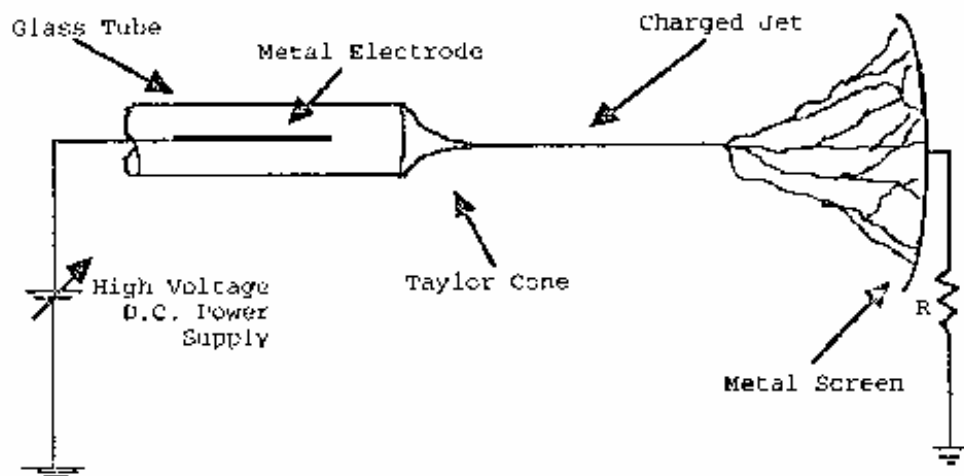


**Figure 2. 9: Schematic drawing of the apparatus used by Doshi [60, 61]**

Srinivasan [12, 64] spun poly (p-phenylene terephthalamide) {PPTA} by the electrospinning process. PPTA fibers (Kevlar 49®) were dissolved in sulphuric acid to form an isotropic solution. The fibers collected in the bath (Figure 2.10) were formed by coagulation and these fibers were washed in fresh water and dried in vacuum. Fibers were coated with carbon before viewing under transmission electron microscope. Single fiber seen under crossed polars was birefringent, with no perceivable banding. Electron diffraction experiments were carried out for the as-spun and annealed fibers. The results showed meridional and equatorial reflections showing the orderliness in the material. Bright and dark field electron microscopy revealed aspects of the morphology and arrangement of crystallites in the fiber. Atomic force microscope images were used to extract roughness parameters. The produced fibers were in the order of a few hundred nanometers in diameter and were thermally stable.

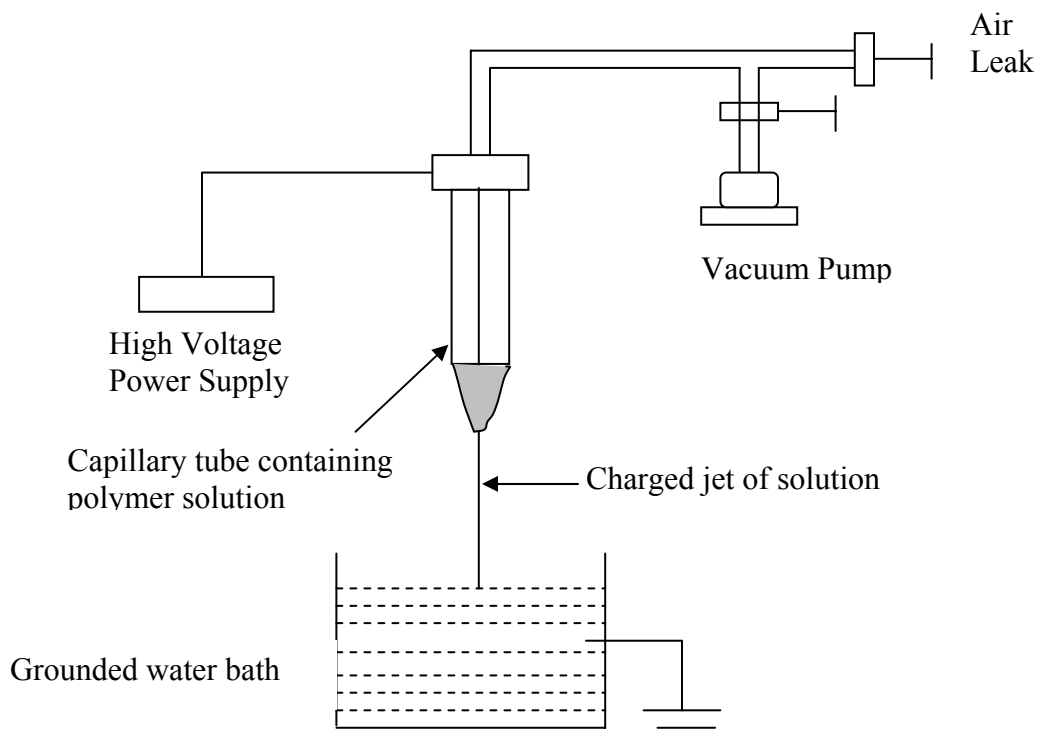


**Figure 2. 10: Schematic drawing of the apparatus used by Srinivasan [12, 64]**

Chun [62, 63] developed a new process model to describe the electrospinning process, which showed the relationship between applied voltage, electrical charge, fiber geometry, fiber velocity, mass flow rate, and electrical current. He conducted experiments on solutions of poly (ethylene terephthalate), poly (amic acid), and poly (acrylonitrile). The obtained fibers had diameters less than 1 micron. Characterization of these fibers involved studying the effects of applied potentials, flow rate and the spinning velocity. Structural and morphological studies included analysis of electrospun fibers with the aid of optical, scanning electron, transmission electron and atomic force microscopes. Experiments were carried out on poly (ethylene terephthalate) and poly (ethylene) melts using the electrospinning process in air and Poly (ethylene terephthalate) melts in vacuum. The fibers were successfully electrospun under these conditions and the fibers were around 15 microns in diameter.

Fang [7] produced DNA fibers by electrospinning (Figure 2.11). Spinning solution was prepared by dissolving fibrous calf thymus Na-DNA in water and ethanol. The process was carried out in a closed chamber. The produced electrospun DNA fibers (30 to 80 nanometers) were 1000 times smaller in diameter

than usual DNA fibers and these fibers were transparent when looked under transmission electron microscopy.

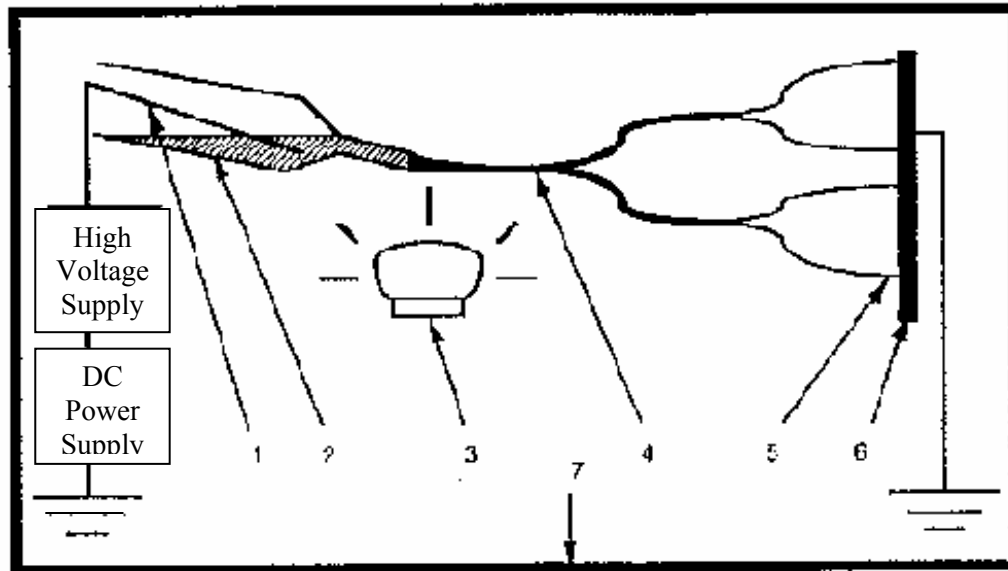


**Figure 2. 11: Schematic diagram of the apparatus for making DNA fibers [7]** [1) Wire electrode in contact with the DNA solution, 2) glass pipette holding the DNA solution, 3) infra red lamp to warm the sample, 4) electrically charged polymer jet, 5) smaller jets produced by splaying of the primary jet, 6) sheet of aluminum foil, 7) box to restrict air flow]

Jaeger et al [3] carried out electrospinning processes using poly (ethylene oxide) and water, poly (vinyl alcohol) and water, poly (ethylene oxide) and chloroform, cellulose acetate and acetone. They used two different experimental layouts, a one-electrode set-up and a two-electrode set-up. The two-electrode set-up had an additional ring electrode which helped to create a field-free space at the tip of the capillary (needed to avoid corona discharge at the tip of the Taylor cone), and the occurrence of a more stable field between the ring electrode and the collecting electrode. Fibers produced were seen under atomic force microscope, which showed that the diameters range between 16 nanometers to 2 microns.

Zarkoob et al [11] produced and investigated electrospun silk fibers. Spinning solutions were produced by dissolving *Nephila clavipes* dragline silk in Hexafluoro-2-propanol and *Bombyx mori* silk in Hexafluoro-2-propanol. The fibers were coated with a layer of evaporated carbon to avoid electrical charging before viewing under transmission electron and scanning electron microscopes. The diameters ranged from 8 to 200 nanometers, were round and smooth, and showed birefringence when

observed between crossed polars. Electron diffraction was performed on unannealed fibers and it showed no signs of crystalline diffraction pattern.

Fong [16] spun electrospun fibers using poly (ethylene oxide). The apparatus consisted of a metal spoon as the positive terminal whereas an aluminum foil collected the fibers. Jet initiation, surface shape of the jet, single jet diameter, the growth of bending instability, jet splaying, jet traveling velocity jet length, solution flow rate, jet current and spinning voltage were studied and measured. Variation of jet diameter was investigated for different jet traveling distance, electric field, solution viscosity and solution surface tension coefficient. Fiber diameter was calculated using scanning electron microscope. SEM images showed bead formation and this was also investigated and reported that the beads are formed because of variation in solution viscosity, net charge density, charges on the fiber and the surface tension.

In another experiment, elastomeric nanofibers of Styrene-Butadiene-Styrene tri-block copolymer were produced using electrospinning process. Solution was prepared by dissolving SBS in tetrahydrofuran and dimethylformamide. The fibers were collected either as a nonwoven elastomeric fabric, or on a layer of graphite that was evaporated onto a glass microscope slide. A bundle of aligned fibers, which were birefringent, were examined by X-ray diffraction, which showed a weak indication of molecular orientation along the fiber axis. Observation under polarized optical and transmission electron microscopes showed the three-dimensional morphology of the SBS fiber and diameters of the fibers were in the range of 100 nm. In a further extension, carbon fibers were spun using polyacrylonitrile, mesophase pitch and poly (vinyl alcohol). The physical properties range from highly crystalline, strong fibers to very porous, large surface area and poorly crystallized fibers. The fibers observed under scanning electron microscope showed diameters in the range of 100 nm.

Bergshoef et al. [8] carried out experiments on solutions of nylon-4, 6 in formic acid to produce ultra thin fibers of nylon-4, 6 with a semi finite length. The produced fibers had diameters in the range of 30 to 200 nm when observed under scanning electron and transmission electron microscopes. The fibers were assessed for mechanical performance and also investigated for pattern of the structure by

wide-angle X-ray scattering and degree of crystallinity by differential scanning calorimetry.

Kim [9] spun electrospun fibers of aromatic heterocyclic polybenzimidazole (PBI). Solution was prepared by dissolving PBI with a little lithium chloride in N, N-dimethylacetamide under nitrogen gas. The obtained non-woven sheet was washed with dilute sulphuric acid, dried and was then heated above the glass transition temperature of PBI so as to impart stabilization against shrinkage and to increase the strength of the fabric. The fibers having diameters of around 300 nm observed under scanning electron, transmission electron and atomic force microscopes showed that the fibers were round and smooth. The sheet under polarizing microscope showed that the fibers are birefringent, indicating the molecules are aligned.

Composite specimens were prepared from 8 to 32 plies of the non-woven PBI fabric sheets produced by electrospinning process [13]. A resin rich layer between each of the sheets was prepared using epoxy resin. In another experiment, PBI fibers were chopped and a rubber composite was prepared using styrene-butadiene rubber. The composites were prepared to measure mechanical properties, wherein three-point bend and double torsion tests were done to fiber-reinforced epoxy composite and tensile and tear tests for the fiber-reinforced styrene-butadiene rubber composite. The SEM micrographs and data results revealed that the fracture toughness and the fracture energy of the composites depend on the direction of the fabric and the crack. Young's modulus was ten times and tear strength was twice as large as for the normal composite.

Norris et al. [10] produced a non-woven mat using electrospinning process by blending the conducting polymer polyaniline and poly (ethylene oxide) in chloroform. Polyaniline was doped with camphorsulfonic acid. The conductivity of the fibers was measured and compared with cast film on a microscope glass slide. The polymer conformation of the fibers was determined using UV-visible spectroscopy. The morphology showed that these blended fibers had diameters less than 2 microns.

Buer et al [15] carried out electrospinning processes using solutions of Poly (acrylonitrile) and Poly (ethylene oxide). The solution was fed through an inclined

pipette wherein the flow rate was maintained by a syringe pump. Laser Doppler velocimetry experiments revealed information about the velocity of the jet at various distances from the apex. Mechanical testing and morphological studies indicate that the process partially orients the molecules in the fibers. The strength of the fibers was calculated and the fiber diameter was analyzed with the help of SEM micrographs.

Deitzel et al [25] carried out electrospinning experiments on poly (ethylene oxide). In a newly designed apparatus, a series of charged rings was used as an electrostatic lens element that changes the shape of the macroscopic electric field from the point of jet initiation to the collection target. Also, the collection target had a potential bias whose polarity was opposite to that of the lens element and syringe needle. This allowed for a continuous increase in the electric field strength and a corresponding increase in downward force on the jet as it approached the collection target. By these two improvements, control of the deposition of fibers was possible. The application of secondary external field helped to control the bending instability. The samples were analyzed using wide-angle X-ray technique and it showed the presence of some molecular orientation and a poorly developed crystalline microstructure in the fibers.

Koombhongse [17] carried out electrospinning experiments using aqueous solutions of poly (ethylene oxide). Studies on jet initiation, corona discharge on jet initiation, flow of the jet, electrically driven bending instabilities, motion of the jet, and jet path was carried out. A mathematical model for a charged jet was designed to calculate the three-dimensional path of the charged jet, wherein electrical force from external field, repulsive force between charge carried by jet, viscoelastic force, force from surface tension and gravitational force were calculated. Measurements of the trajectory and velocity of a particular segment of a jet was also carried out. Investigations were made on the effects on spinning behavior in terms of shape of the envelope, increase of perimeter of each loop and movement of the charged jet. Also the effects of charge density and solution concentration were looked upon the fiber diameter. To understand the behavior of the jet in the electric field, some of the

conditions looked into were quasi-stable jet, multiple jets, jet oscillation, jet translation, and dying jet on the hemispherical droplet.

#### 2.2.4 Bending Instabilities

The foremost part of the electrospinning process is a fluid instability or in other words the rapidly whipping liquid and this is the cause for the bending and stretching of the liquid. At high electric fields, the jet becomes unstable and has an appearance of inverted cone, which is a single, rapidly whipping jet [18, 19]. At higher field strength and flow rate, there is a transition from a stable jet to a whipping jet. The dependence of transitions on the electric field and the flow rate is reproduced by a model proposed by Shin et al [19], wherein the electrospinning process is based on the observation that the instabilities occur with wavelengths much longer than the jet radius. The whipping instability can occur through either small lateral fluctuations in the centerline of the jet or mutual repulsion of surface charges carried by the jet. The whipping instability is the cause for the large decrease of jet diameter, by increasing the path length over which the fluid is accelerated and stretched before solidification of the liquid.

An analogy between electrically driven and the aerodynamically bending instabilities using a localized approximation was developed, which calculated the bending electric force acting on an electrified jet [20]. Continuous, quasi-one-dimensional, partial differential equations were derived and used to predict the growth rate of small electrically driven bending perturbations of a liquid column. Discretized equations were used to calculate the jet paths during the course of nonlinear bending instability that accounts for solvent evaporation and polymer solidification.

A theoretical framework, consisting of two components, a stability analysis of a cylinder of fluid with a static charge density in an external electric field, and a theory for how these properties vary along the jet as it thins away from the nozzle has been developed for understanding the physical mechanisms of electrospinning [21]. It was shown that by analyzing various instabilities of the jet, it was possible to make predictions for the onset of electrospinning.

Using the stability theory, a quantitative method was developed to predict when the electrospinning occurred [22]. The dominant instability strongly depends on the fluid parameters of the jet, namely, the viscosity, dielectric constant, conductivity and the static charge density on the jet. A method for calculating the shape and charge density of a steady jet as it thins from the nozzle was reported. It was shown that stability theory could be related to electrospinning in terms of determining the jet paths, jet shape and surface charge density. The theory reports that the charge density on the jet interacts with the external field to produce instability in the jet.

An experimental investigation of the electrically forced jet and its instabilities was presented by Shin et al [23]. Stability jets, jet currents and whipping instabilities were reported for solutions of glycerol and poly (ethylene oxide). The experimental observations were compared with theoretical analysis such as electrohydrodynamic equations. It was reported that the current is a measure of the charge density carried by the jet and depends on the charge induced in the fluid. That means, apart from the whipping jet, equipment configuration plays an important role in the formation of fibers during the electrospinning process.

Considering inertial, hydrostatic, viscous, electric, and surface tension forces, an electrohydrodynamic model was developed of a weakly conductive viscous jet accelerated by an external electric field [24]. Nonlinear rheologic constitutive equation was used to describe polymer fluid and one-dimensional differential equation for the jet radius was derived and analyzed. The model could be used for better control and optimization of the electrospinning process.

In electrospinning, the energy required to spray the liquid from the spinneret is mechanical or in other terms the centrifugal force. But mostly it is the electrostatic field that exerts enough force on the liquid and disrupt into highly charged sprays. Atomization may be defined as the residue remaining after the evaporation of droplets that have been produced in the atomization that forms the required deposit [35]. The first break-up of the liquid during the atomization process is mainly due to mechanical forces wherein the polymer solution is drawn out of the spinneret into filaments, which subsequently break-up into droplets. The second break-up in the



process is due to electrical forces. As the break-up of the liquid takes place there is emission of droplets. At this junction, knowing the physical local conditions is necessary. Before the break-up, a drop becomes elongated, or if the meniscus is flat, the emission of the droplet takes place from the apex of a conical projection, which appears in all cases before the break-up. Liquid filaments or jets can be seen originating from the apex of the conical projection and these jet filaments then break-up into small droplets and these droplets are highly charged. Some of the physical properties that determine the atomization process are [35],

1. Surface tension of the liquid
2. Conductivity of the liquid
3. Dielectric constant of the liquid
4. Electrical and physical properties of the surrounding medium
5. Hydrodynamic flow and hence the viscosity and applied pressure of the liquid

#### 2.2.4.1 Charging

Drop charging may be considered by two distinct factors, natural and induction. Considerable work has been done in both fields since the beginning of 19<sup>th</sup> century [36]. Blanchard in 1963 measured the charge produced from jets when the bulk liquid surface was subjected to an electrostatic field (induction charging). When induction charging occurs, drop charge levels are generally higher than in the absence of an external field. Here the earth is negative with respect to the upper atmosphere and any induction charging due to this field should thus result in drops that are negatively charged as opposed to the positively charged small drops [36]. Blanchard studied induction charging using water samples of different conductivities and his results indicated that induction charging might be considered as independent of the natural charging processes.

The electrostatic principles are similar to those used for electrostatic spraying of fluid [37]. When the surface of a liquid drop or film is electrically charged, the charge opposes the cohesive surface tension forces. An electric field is produced between a spray electrode, which is supplied with the solution to be sprayed, and a counter-electrode consisting of a rotating roller over which a web carrier for continuous

deposition and the removal of fine fibers is passed. The solvent evaporates as the nascent fiber travels between the electrodes, so that the fibrous form is retained on the web carrier. The length of the fiber depends on many factors but mainly upon the viscosity of the sprayed liquid. The roller passes through a series of spray stations so that several layers of fiber are deposited. Thus fiber production and web formation take place at the same time.

There may be a few problems caused due to electrostatic charge on fibers and fabrics [37]. These problems are more evident with fibers having low moisture regain and at low relative humidities. The charge may accumulate during handling of the material and this can pass on to isolated conductors. They continue during use, and problems arise from charge on fibers or on bodies in contact with, or in the neighborhood of, textile materials.

### **2.3 *Electrospun Fiber Characteristics***

The process of electrospinning results in submicrometer size fibers, which are laid as a extremely fine, randomly oriented, average pore size membrane. This explains the need to study the fiber characteristics of electrospun fiber web. The property of having large surface area of the web enhances the interest. This section tries to explain about the techniques of fiber characterization, namely, fiber diameter distribution, fiber orientation distribution function and pore size distribution.

#### **2.3.1 Shapes of Electrospun fibers**

It has been observed under scanning electron microscope that electrospinning a polymer solution can yield in addition to round nanofibers, a wide variety of cross-sectional shapes, which includes branched fibers, flat ribbons, ribbons with other shapes, and fibers that were split longitudinally from larger fibers [1]. As Koombhongse says, 'this may be due to many reasons including, the ejection of smaller jet from the surface of primary jet, separation of primary jet into smaller jets, and electrically driven bending instability of the jet. The elongation of the jet and the evaporation of the solvent change the shape and the charge per unit area carried by the jet'. These shapes can be used as guides for the extension of existent models for the electrospinning process. Bergshoeff et al [8] observed split fibers

while producing ultra thin fibers of nylon-4, 6, which is probably due to splaying during the process.

Jaeger et al. [2, 3] observed beaded electrospun fibers obtained from aqueous solution of Poly (ethylene oxide) and they reported that the bead diameter and spacing depended on the fiber diameter i.e., thinner the fiber, shorter the distance between the beads and smaller the diameter of the beads. They explained that the formation of beads is the draw resonance phenomenon, which occurs if fibers are drawn to high draw ratio. Yarin [4] and Entov et al. [5] developed a mathematical model for the break-up of jets of polymer solutions and they reported that the beaded electrospun fibers are related to the instability of the jet. Fong et al [6] carried out experiments on aqueous PEO and reported that the formation of the beaded structures can be considered as the capillary breakup of the jets by surface tension altered by the presence of electrical forces. They observed four reasons for the bead formation, viscosity, net charge density, surface tension, charges on the jets and gave probable solutions namely, as the viscosity is increased, beads become bigger, the average distance between beads longer, and the shape of the beads changes from spherical to spindle-like. The beads become smaller and more spindle-like when the net charge density is increased. Decreasing the surface tension results in bead disappearance and neutralization of the charge affects the formation of beads. Fang [7] reported bead formation during electrospinning of DNA fibers. This suggests that some of the DNA retracted into droplets at intervals along the fiber.

### 2.3.2 Structure

Depending on the process and material variables the diameter of the fibers produced by electrospinning vary and it ranges from a couple of hundred of nanometers to a couple of micrometer fibers. The arrangement of fibers collected is usually random, with a slight bias to the machine direction. This is probably due to two main reasons, namely the movement of the collector and the air drag/suction. The variation in the length of the fibers has still not been quantified, but for sure

there is lot of variation in the length because of high speed splaying of fibers, charged jet and air current.

During the electrospinning process, the polymer in the spinneret is subjected to various external conditions/variables. These variables can be broadly classified into control and process variables. The control variables mainly include the temperature and pressure of the polymer, both of which were not studied in detail in my work. But it has been observed that there have been changes in splaying of fibers under different temperatures and pressures.

The process variables and material used to produce the electrospun web effects the structure and properties of the web. The processing variables are classified into online variables and offline variables [38]. The online variables have been defined as those that can be altered during the production of the web, and offline variables are those, which cannot be altered during the operation of the process. The online processing variables in general include electric voltage, the distance between the spinneret and the collector, the polymer concentration. The offline processing variables in general includes the diameter of the spinneret and design parameters.

Although the concept the electrospinning dates back to many years now, not much of characterization has been done in this field. The demand of these electrospun fibers in wide variety applications has influenced to develop the characterization and testing techniques for the webs produced.

### 2.3.3 Objectives of characterization

Analyzing the electrospun webs yield results and information, which will help researchers in improving the quality and predicting the overall performance of the electrospun web. Some of the reasons for characterization may be process control, process development and product or quality control [81].

### 2.3.4 Fiber Diameter and its distribution

One of the foremost roles of the electrospinning process is to produce thin fibers. Almost everybody who have done electrospinning experiments have reported that the fibers spun through this process have fiber diameters in the range of a few

nanometers to a couple of microns. Fibers spun through different polymer solutions did not make much of a difference in the fiber diameter.

The measurement of fiber diameter in the electrospun webs that have been reported in the literature is based using various techniques. The instruments for measuring the fiber diameter and the analysis have been done using various instruments, mainly scanning electron microscope, transmission electron microscope and atomic force microscopes. The analyses have been done by capturing of images through these devices called the micrographs.

Fiber diameter distribution in nonwovens was done by Pourdeyhimi and Dent [53] through Image analysis techniques. The method uses a binary image to create a distance map of the image, which records the distance from each pixel to the background, and from the distance map, the fiber diameter at any pixel location could be determined. The distance transform applied to a binary image is accomplished by scanning the image twice in opposite directions. The image capturing and segmentation is done as explained by Pourdeyhimi and Dent [52]. The algorithm for determining fiber diameter uses the skeleton and a distance transformed image and the skeleton acts as a guide for tracking the distance-transformed image by recording the intensities to compute the diameter at all points along the skeleton. But, both the distance-transform and the skeletonizing procedures result in slight deviations at the corners. Since the measurements do not distinguish between true variations in diameter and variations caused by multiple fibers being joined together, this causes the skewing of the distribution.

There is no standard technique to measure the fiber diameter and analyze its distribution. To eliminate all possible errors, the ideal case of measuring the fiber diameter of electrospun webs would be to produce a good image of the web at a suitable magnification using the electron microscopy techniques and then analyze the image manually using suitable calibration scale. The manual analysis usually consists of the following steps, determining the length of a pixel of the image, identifying the edges of the fibers in the image and counting the number of pixels between two edges of the fiber.

### 2.3.5 Pore Size Distribution

A pore can be defined as a portion of space bounded by solid surfaces and by planes erected where the hydraulic radius of the space exhibits a minima [39]. The local minima define an arbitrary pore size. The hydraulic radius of a capillary of uniform cross-section is the ratio of volume of the capillary to the surface area of a capillary.

Pore characteristic is one of the main tools for evaluating the performance of any nonwoven fabric and it applies to electrospun web too. The size and shape of the pore can influence permeability and filtration properties [40]. Pore orientation reflects fiber orientation and pore placement indicates the structure uniformity and hence both have effects on fabric mechanical properties such as strength and elongation. The increasing success and demand for nonwoven webs in various areas and applications have led to the development of more effective and accurate methods for measurement of pore size, shape and other pore characteristics.

Porosity, ' $\phi$ ' is the fraction of the bulk volume of the porous media ( $U_b$ ) that is occupied by void or pore space ( $U_p$ ). The void volumes include the blind pores, the closed pores and the through pores [41]. The porosity for a solid material like metals will be close to zero while that of the highly porous medium like filters will be high. Depending on the type of porous medium the porosity of the material will vary from zero to almost unity. The porosity of a material depends on the mode of packing and compaction of solid particles in a consolidated material, whereas on the other hand it depends on the packing of the particles, their shape, size and arrangement in an unconsolidated material [42].

The measurement of porosity is dependent on the measurement of two of the three volumes of porous material, namely, the bulk volume, the volume of the solid matrix, and the volume of the pore space. There are various methods for the measurement of porosity and some of them are mercury injection method, imbibition method, optical method, gas expansion method, and density method.

The pore size and its distribution are determined by two main techniques, namely intrusion and extrusion types. Mercury porosimetry is an example of intrusion type while the bubble point method is of extrusion type [43]. Both types are

based on the principle of capillary flow, which states that a porous material will allow a fluid to pass when the pressure applied on the system exceeds the capillary force of attraction of the fluid in the largest pore [44].

### 2.3.5.1 Theory of Capillary Flow

The capillary flow in the porous structure is based on the capillary rise phenomenon, where an excess pressure is required to cause a non-wetting liquid to climb up a narrow capillary. The pressure difference across the interface is given by the equation given below, and its sign is such that the pressure is less in the liquid than in the gas phase if the contact angle  $\theta$ , is greater than  $90^\circ$  and more if it is less than  $90^\circ$  (Figure 2.12).

$$\Delta P = \sigma \left[ \frac{1}{r_1} + \frac{1}{r_2} \right] \cos \theta \quad \text{Equation 2. 2}$$

where,  $\sigma$  is the surface tension

$r_1$  and  $r_2$  are mutually perpendicular radii

$\theta$  is the contact angle between the capillary walls and liquid.

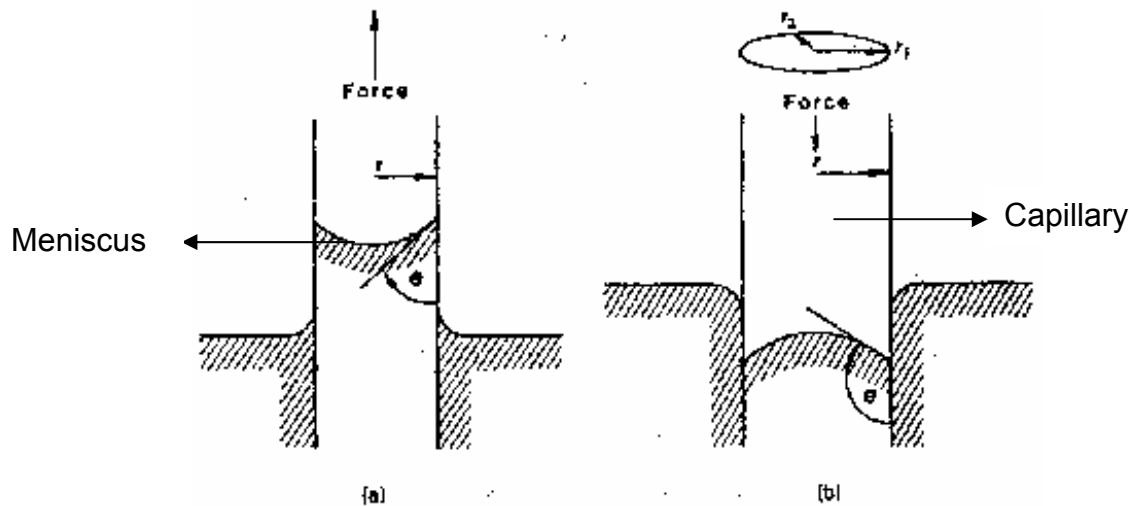


**Figure 2. 12: Theory of Capillary Flow. a) Capillary Rise ( $\theta < 90^\circ$ ), b) Capillary Depression ( $\theta > 90^\circ$ ) [43]**

The disadvantage in the capillary flow techniques is that they assume the cross section of the pore, hence the values are only comparative in nature. Also, the

presence of constricted neck pores and blind pores affect the flow of the liquid through the porous material.

In the bubble point test, which is a dynamic test, a porous material is allowed to saturate by a liquid, so that the contact angle between the liquid and the porous material is equal to zero. When the gas pressure is increased gradually at the upstream face, at a critical pressure, the first air bubble comes through the largest pore. By continually increasing the pressure and allowing progressively smaller and smaller pores to be emptied of the liquid, complete measurement of pore size distribution can be made [44]. This test gives information on the number and sizes of the smallest effective through-flow pore channels in a sample. The bubble point test is based on the following two factors [44],

1. A dry specimen will pass air through all of its pores when any amount of air pressure is applied to one side of the specimen
2. A saturated specimen will only pass air through pores when the air pressure exceeds the capillary attraction of the fluid.

In the mercury intrusion porosimetry, which is a static test, a porous material is completely surrounded with mercury and pressure is applied to force the mercury into pores. With incremental increase in pressure, a given pore volume in the porous material is measured [44]. The number of pores of a particular size is evaluated by considering the percentage of the total volume of mercury intruded into the sample for each pore size range. Thus, this method gives information on the sizes of all pores found within a sample and a pore size distribution based on total pore volume.

Because of its convenience to detect individual pores in a non-woven image, it seemed to be advantageous to use Image analysis techniques for pore measurement. Xu [40] presented the use of image analysis techniques for the comprehensive and accurate measurements of pore characteristics such as pore boundary locations, size, pore shape, pore orientation and pore placement. In pore size measurement, pore area, hydrodynamic diameter and opening diameter could be chosen according to different end use requirements. Bilobal, trilobal are some of the shapes observed for these pores. Pore orientation was illustrated by the



dispersion curve. The pore placement could be quantified with the help of index of uniformity, and structure uniformity, and was classified into different spatial patterns.

Image analysis techniques showed that it is quick and accurate to analyze pore structure in thin nonwoven webs explained by Huang and Bresee [45]. They investigated the feasibility of this technique to characterize pore number, size, shape, total area of pores, fiber orientation, web uniformity, fiber diameter and defects. An optimum procedure was identified for each step beginning with illumination of webs prior to image acquisition and ending with data presentation.

The utility of image analysis in assessing pore shape of nonwoven materials was reported by Pourdeyhimi and Xu [46]. It was characterized using Fourier series of a pore boundary function. The results were presented for a set of simulated images with varying density and fiber orientation.

Gibson et al [78, 79] carried out extensive research on the transport properties of electrospun web, explaining largely the water vapor, liquid, solid transport and breathability of the web. They determined water vapor diffusion and gas convection properties with automated dynamic moisture permeation cell and showed that the convective flow resistance of electrospun fiber mats is quite large compared with normal clothing. Cross-linking the fibers of the electrospun membrane significantly decreases liquid transport through the fibrous membrane [78]. Studies also showed that fiber mats produced by electrospinning to be extremely good at trapping aerosol particles [79].

#### 2.3.6 Fiber Orientation Distribution

One of the aims of the production of fibers is to produce webs that have the same properties in all directions. Usually, the webs have a preferential direction for the arrangement of fibers due to the movement of the collector in a particular direction. The spatial distribution of the fibers in the webs is an important structural feature that significantly influences many physical and mechanical properties of the web and this was carried out by Image analysis technique [47]. This distribution of fibers in the web causes variation of the properties in different directions of the web and influences other properties as well.

#### 2.3.6.1 Image Analysis Techniques

This technique uses the intensity of the gray levels of the different pixels to determine the presence of the fibers and the orientation of the fibers. The image that is obtained of the web is analyzed using different algorithms to determine the Orientation Distribution Function (ODF) of the fibers in the web. These techniques are used both on-line to measure the orientation at rapid rates and impart quality control over the web, and offline to research the structure-property relationships of the web. The results obtained from these tests are independent of the mechanical characteristics of the fiber. The various image analysis algorithms for characterizing the fiber orientation are simulation [48], direct tracking [49], Fourier Transform [50], Flow field analysis [51], and Hough Transform [54]

##### □ Fourier Transform [50]:

This method coded in C language is composed of an image of spatial details in the form of brightness transitions cycling from light to dark and from dark to light and these spatial frequencies are related to the orientation of the fibers. In this technique, the intensity spectra of the pixels in the image are decomposed into a frequency domain with appropriate magnitude and phase values. The discrete Fourier Transform helps to determine the rate at which intensity transition occurs in a given direction in the image. So, if the fibers are oriented in a given direction in a nonwoven fabric, the spatial frequencies in that direction will be low and the spatial frequencies in the perpendicular direction will be high and this is used to determine the fiber orientation distribution. The Fourier method provides the mean orientation, models its frequency representation of the original image on the assumption that the image is periodic, and is significantly affected by the thickness. Although this method is fairly accurate and reliable, it slightly overestimates the standard deviation of the distribution.

A new image-segmentation algorithm, the line operator was found out, which gave better results than the edge-enhancement algorithms for images containing thin fibers was reported by Gong and Newton [55].

It has been observed that the entire image analyses techniques described in the literature in determining the orientation distribution function of the fibers are for

thin webs. In principle, all of these techniques can be used to determine the distribution function of nonwoven webs, as there are no standard methods that have been developed by any organization to measure the same.

### 2.3.7 Thermal Analysis

Fiber web characterization can also be done by Thermal Analysis. It is based upon the detection of changes in the heat content (enthalpy) or the specific heat of a sample with temperature [87]. As thermal energy is supplied to the sample its enthalpy increases and its temperature rises by an amount determined, for a given energy input, by the specific heat of the sample. The specific heat of a material changes slowly with temperature in a particular physical state, but alters discontinuously at a change of state. As well as increasing the sample temperature, the supply of thermal energy may induce physical or chemical processes in the sample. Such enthalpy changes may be detected by thermal analysis and related to the processes occurring in the sample. Thermal analysis can be done by different methods such as the measurement of heating curves, dynamic adiabatic calorimetry, differential thermal analysis (DTA), differential scanning calorimetry (DSC), thermogravimetry (TG), thermal mechanical analysis (TMA), dynamic mechanical thermal analysis (DMTA).

Differential Scanning Calorimetry, a material characterization technique, measures the amount of energy (heat) absorbed or released by a sample as it is heated, cooled or held at constant temperature [87]. Differential Scanning Calorimeter also performs precise temperature measurements. In DSC, the sample and reference are both maintained at the temperature predetermined by the program even during a thermal event in the sample. The amount of energy which has to be supplied to or withdrawn from the sample to maintain zero temperature differential between the sample and the reference is the experimental parameter displayed as the ordinate of the thermal analysis curve. The measuring principle in DSC is to compare the rate of heat flow to the sample and to an inert material, which are heated or cooled at the same rate.

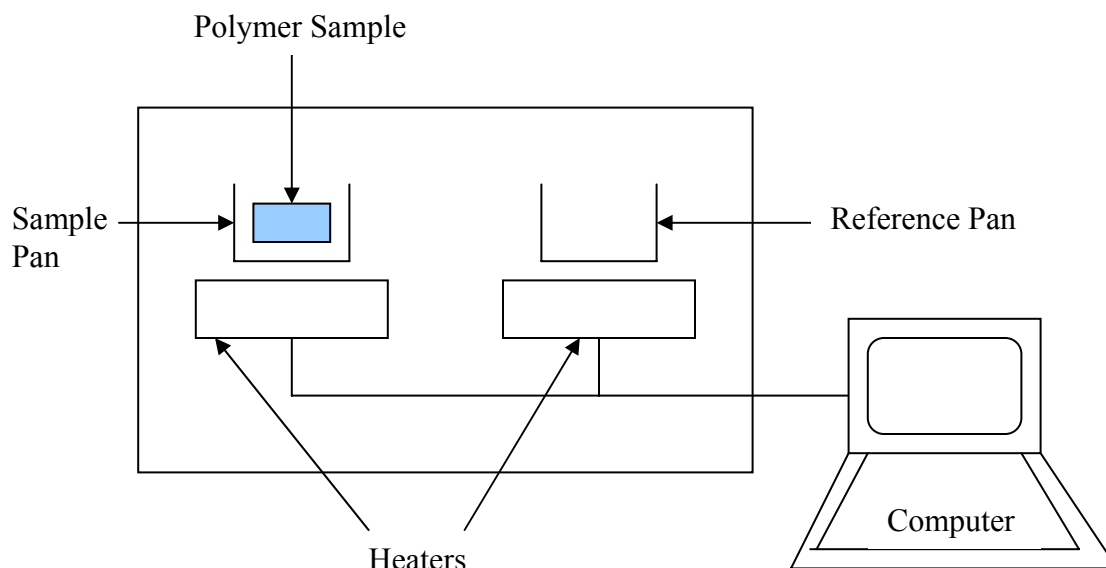


**Figure 2. 13: Diagrammatic representation of Differential Scanning Calorimeter**

Kim and Lee [14] spun electrospun fibers from Poly (ethylene terephthalate), Poly (ethylene naphthalate) and Poly (ethylene terephthalate)/Poly (ethylene naphthalate) blend. Differential scanning calorimeter and thermogravimetric analyzer helped in understanding the thermal properties of these polymers before and after electrospinning process. All the polyesters showed decrease of specific heats due to glass transition of amorphous phase and exotherms and endotherms due to crystallization and melting of crystalline phase. This thermal property change is due to a decrease in molecular weight because of thermal degradation. Electrospinning in general resulted in increase in crystallinity and henceforth decrease in temperatures of glass transition and crystallization of PET and PEN. Exchange reaction in blends causes these thermal changes in PET/PEN blends.

### **3 Research Objective**

The objectives of this research were to produce very fine fibers, develop a simple electrospinning device, influence of process control parameters and characterizing the structure of the electrospun web. A process model was developed to explain the electrospinning process and this process was carried out by using poly (ethylene terephthalate) polymer solution. Characterizing the process parameters included identifying the parameters, the working range of the parameters, and controlling the process. The investigated process parameters were the concentration of the polymer solution, the voltage and the collecting distance between the two electrodes i.e., the sprayer and the collector. The characterizations of fibers were based on three main distributions, namely, the fiber diameter distribution, the pore size distribution, and the fiber orientation distribution function. The analyses were done for the distributions using different equipment and techniques.

Characterizing nonwoven structure from electrospun fibers was carried out using scanning electron microscopy (SEM), pore measuring instrument and image analysis. The fiber diameter of the poly (ethylene terephthalate) electrospun nanofibers was measured and analyzed using scanning electron micrographs. These micrographs/images were obtained from scanning electron microscope. The pore measurement of the electrospun web was carried out using an equipment involving bubble point method (PMI instrument) for measuring the pore size and its distribution. The fiber orientation distribution function was determined using image analysis technique.

Many organic polymers and inorganic materials have been successfully used to spin fibers with diameters in nanometer range using electrospinning technique. This research work was carried out using poly (ethylene terephthalate) as the polymer solution.

## 4 Experimental

This chapter explains about the apparatus used for the electrospinning process, a complete picture of equipment design and experimental design of the process.

### **4.1 *Electrospinning apparatus***

To achieve the research objectives an electrospinning apparatus was designed and constructed. The apparatus consists of two main devices, the sprayer and the collecting device.

#### 4.1.1 Sprayer

The spraying setup (Figures 4.1 and 4.2) has a glass spinneret of 0.3 mm inner diameter filled with polymer solution. The solution is filled to almost half of the glass spinneret, so that however viscous the solution is, it can be passed through the spinneret because of its own weight/pressure. The polymer solution is given a positive field with the help of a high voltage power supply. The terminal wire (metal electrode) from the high voltage power supply is held to the glass spinneret with the help of a rubber holder. The glass spinneret is held at a height from the ground with the help of a garolite stand and is at an inclined angle to the ground so as to facilitate fiber spraying on the drum surface. The high voltage power supply has a capacity ranging from 0 to 40 kV and the voltage can be increased at 1/10<sup>th</sup> of a kilo volt. An aluminum foil is placed just below the spinneret to collect waste polymer solution and stray charged fibers.

As has been explained in the principle of electrospinning process (2.1), when the charge of the polymer at increasing voltage exceeds the surface tension at the tip of the spinneret, the polymer gets ejected. The charged jet comes out of the spinneret, first in the form of Taylor cone and then is splayed randomly as fibers.

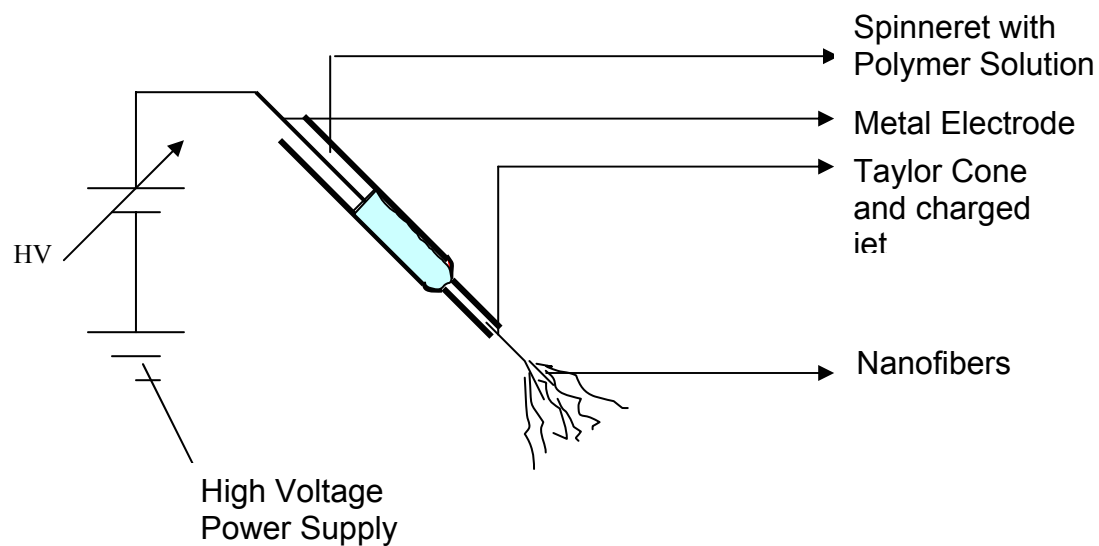


**Figure 4. 1: Schematic of nanofibers spraying device**

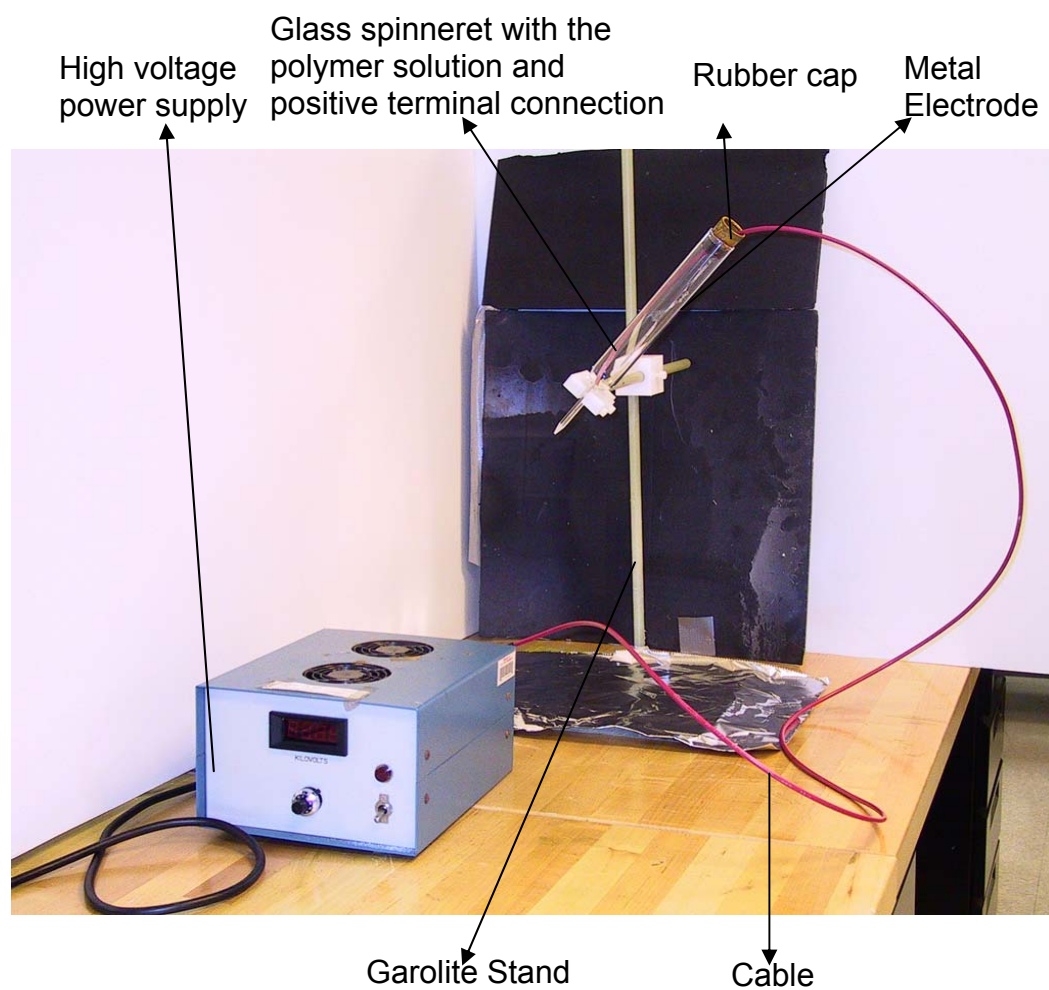


**Figure 4. 2: Photo of nanofibers spraying device**

#### 4.1.2 Collecting Device

The system of collection of fibers (Figure 4.3 and Figure 4.4) includes a cylindrical drum with an external drive. The collector is a cylindrical drum (8" in diameter and 14" in length), made of poly vinyl chloride (PVC) pipe. The drum is held by a central shaft and is fixed to a wooden frame. A rotating drum for collection of fibers has been reported earlier [88]. The PVC pipe and the wooden frame were used during the construction of the equipment to maintain the metal free system. The wooden frame is built in such way that there are slots in the frame. This facilitates the movement of the drum either upward or downward. This is done so that the vertical position of the cylinder can be adjusted to change the distance from the spinneret as per requirements. The drum is attached with a metal plate, a bush so as to complete the electrical connection (this has been explained in succeeding paragraphs with the help of suitable figures). The electrical connection is used as the negative terminal from the high voltage equipment. Hence the cylindrical drum serves as the negative terminal and thus aids in the collection of fibers.

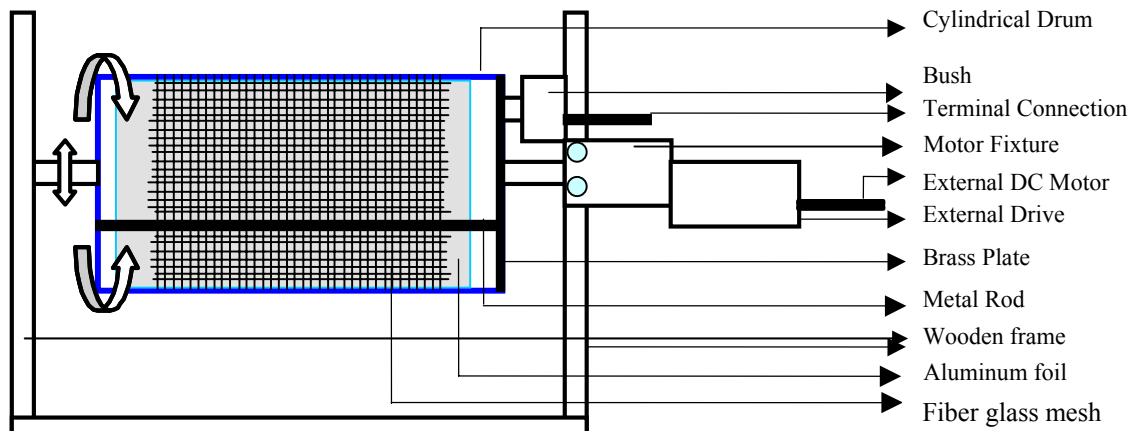


**Figure 4. 3: Collecting Device for the electrospun fibers**

One side of the pipe (right side on the Figures 4.3 and 4.4) is covered with a brass plate throughout its circumference. A metal rod is placed on a groove in the drum throughout its length fixed at one end by the brass plate and the other end is free. The metal rod carries the electric field given by the brass plate. An aluminum foil is wound over the drum, covering the metal rod. This is done to maintain the



same electric field over the entire drum surface. The negative end for the system is derived from the high voltage power supply to the brass plate with the help of a connection wire and a bush, which is attached to the brass plate.

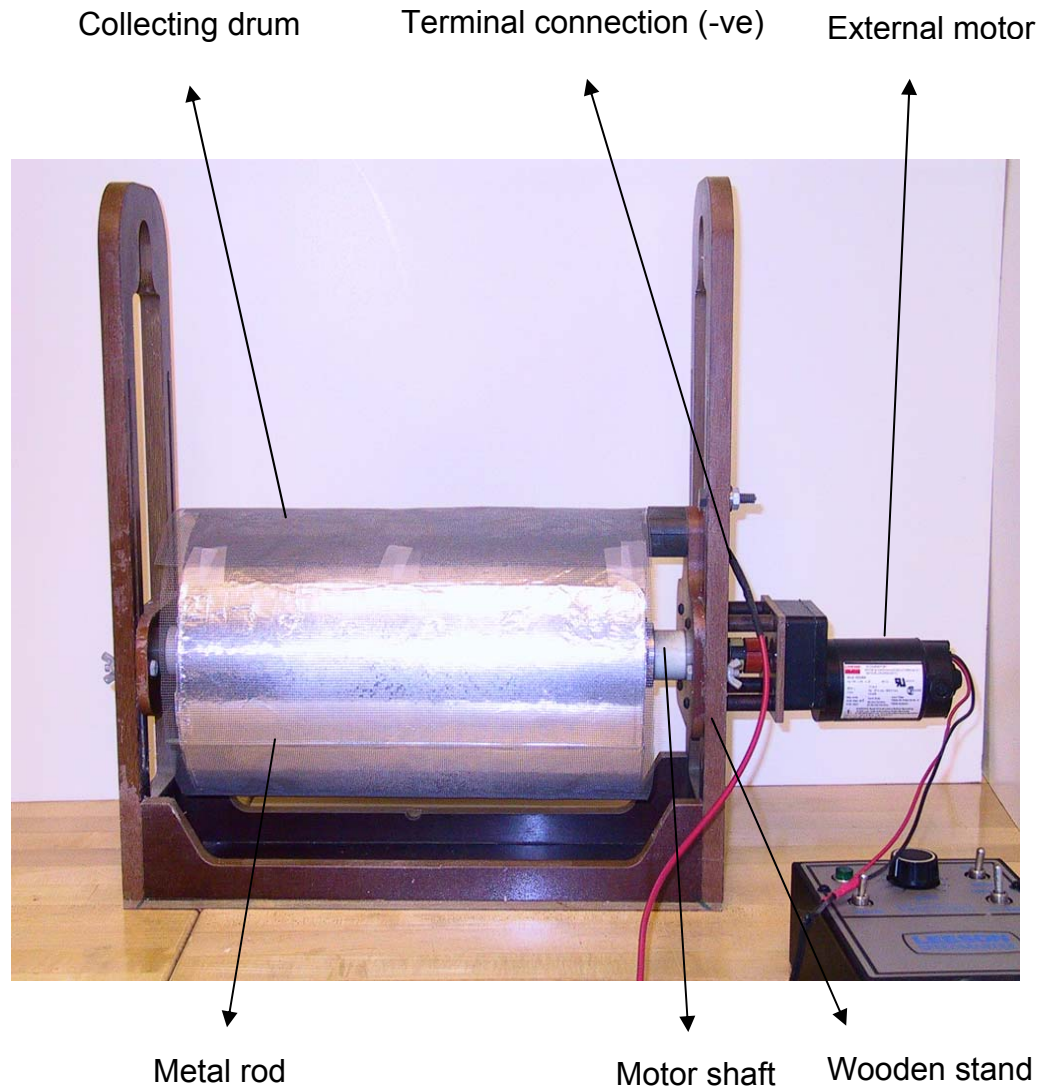


**Figure 4. 4: Photo of nanofibers collecting device**

A pictorial representation of the side view of the collecting drum is shown in Figure 4.5. The figure shows that the negative terminal from the high voltage power supply is given to the brass plate through the bush. The central shaft carrying the drum is given movement with the help of an external motor, which can rotate in either direction.

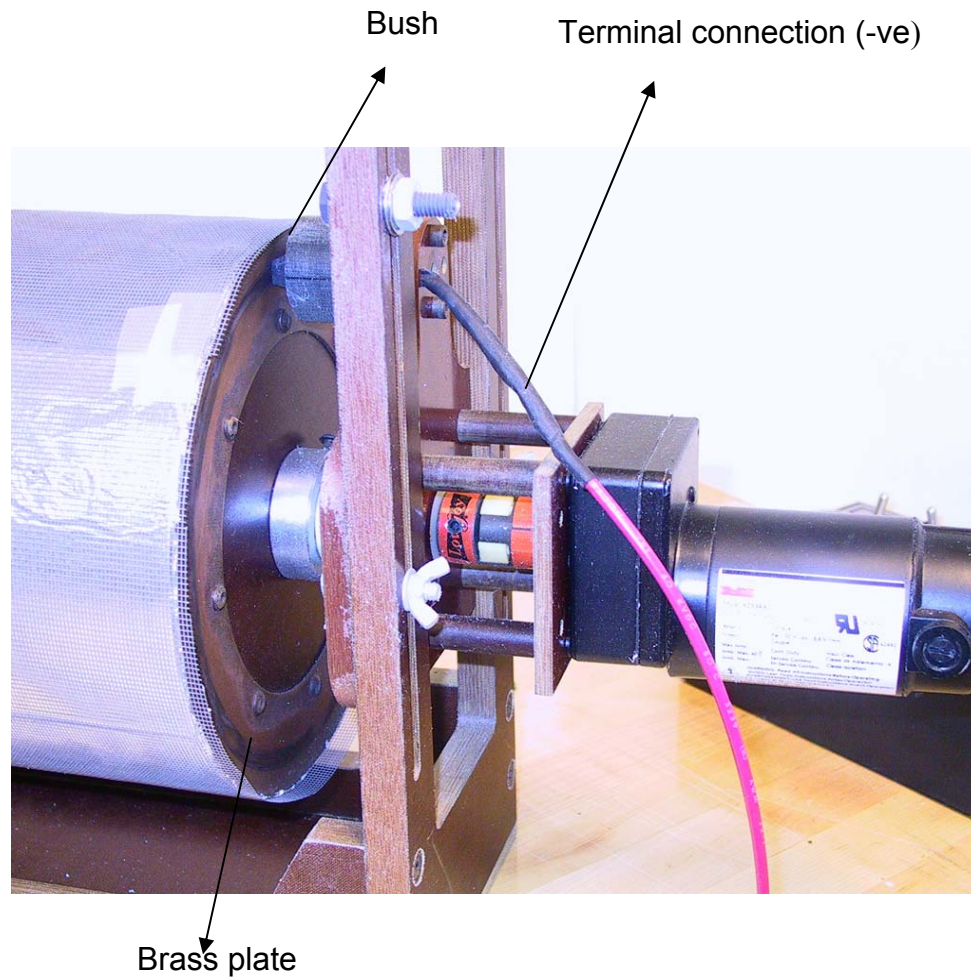


**Figure 4. 5: Side-view of the collecting drum showing electrical connections**

The electrospinning apparatus consisting of fiber splaying system, collecting device, high voltage power supply and an external device to drive the collecting drum on the whole can be seen in Figures 4.6 and 4.7. The operation process of this system can be carried out by switching on the power of the high voltage system and slowly increasing the voltage through regulator, which starts from 0. The range being used for the electrospinning process is 15 to 25 kilovolts. The fibers are splayed towards the targeted source i.e., the rotating collecting drum as explained in earlier chapters. The speed of the collecting drum was around 12 rpm and a minimum of three layers of fibers was laid to form the nonwoven web. In this work, webs were

produced having three and four layers, because less than three layers was too thin to handle. To turn down the system, slowly decrease the voltage, turn the power switch off and then take out the power supply plug. Turn the system down when the polymer level is near the ending stage and polymer is near the vicinity of the submerged wire or when the polymer is still around 5 ml in the glass pipette.

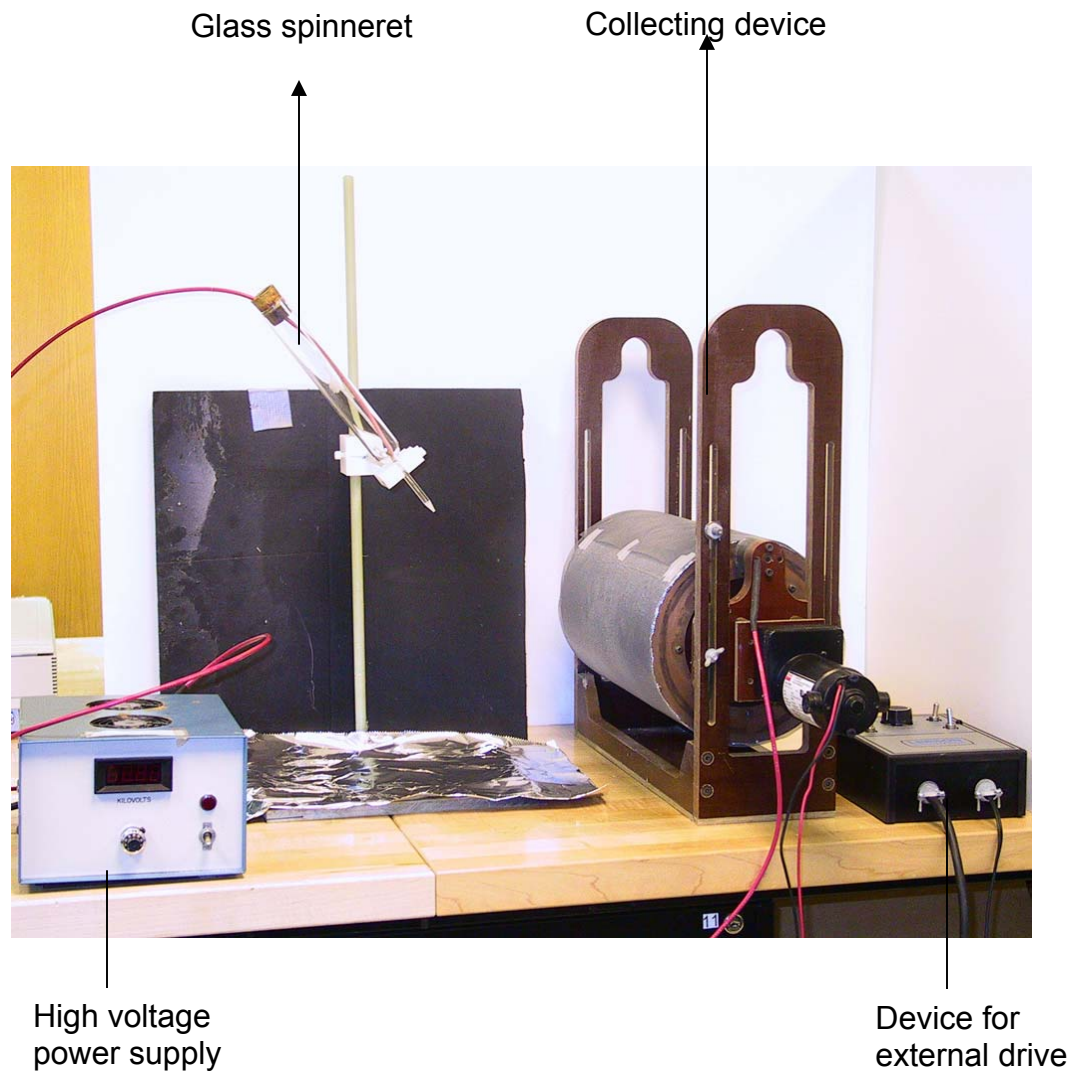


**Figure 4. 6: Pictorial representation of the side view of the electrospinning setup**



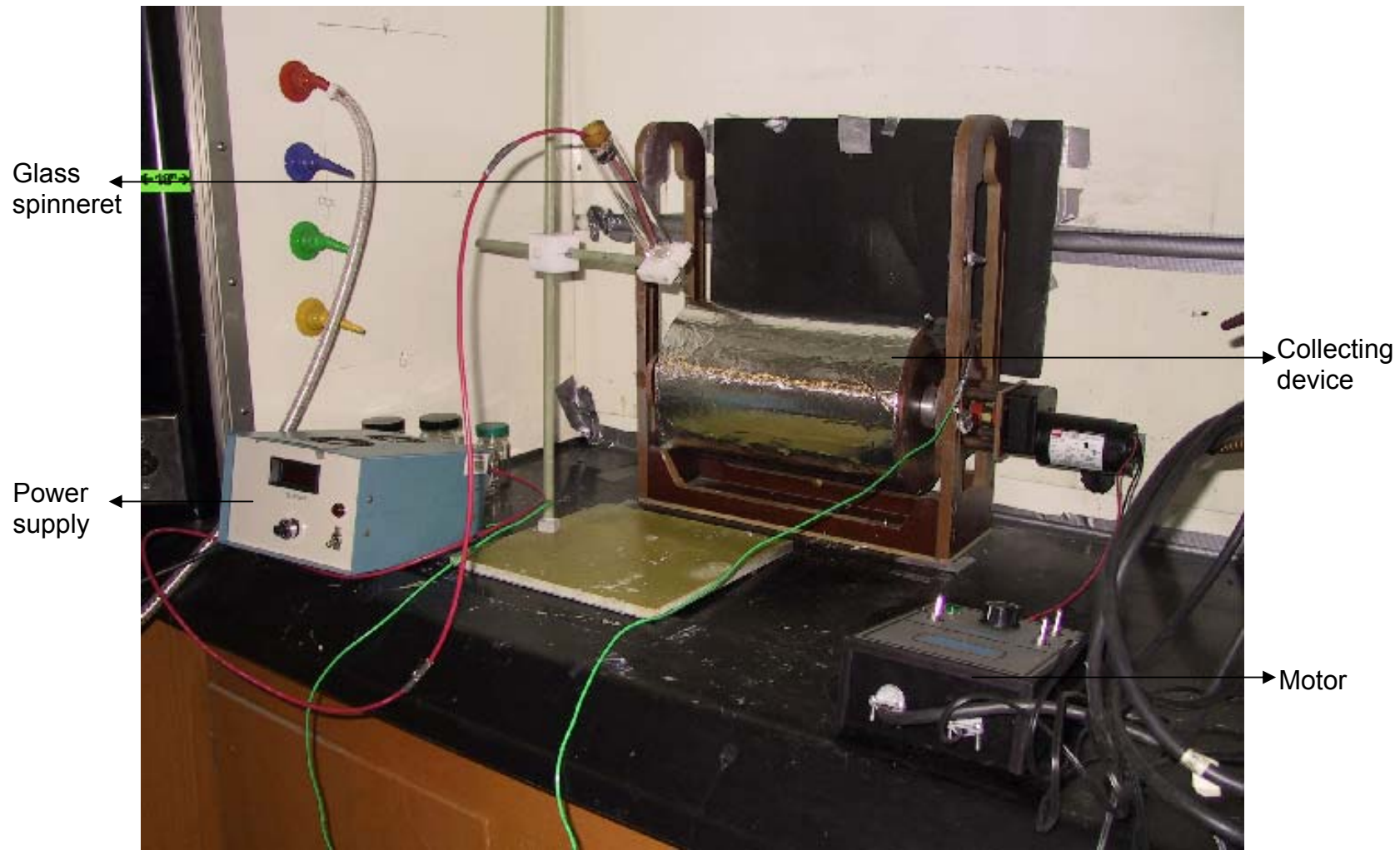


**Figure 4. 7: Pictorial representation of the electrospinning set-up**

As the polyester is dissolved in the solvent mixture described in the experiment, their rigid structure becomes amorphous & flexible and they transform to a rubbery state and this deformation progress more & more near its heat deflection temperature. The viscosity of the solution also enhances the softening. Because of this rubbery state softening and high surface area, the fibers cling to the aluminum foil and it is very difficult to remove the sample from the foil. The problem of taking out the sample from the aluminum foil was successfully fixed with the help of the fiberglass screen. This screen is an insulating material and is wound over the cylindrical drum, which already has the aluminum foil. By this the electrical potential difference could be maintained and the nanofibers were collected on the fiberglass mesh. After forming nanofiber web of a particular run, the fiberglass mesh with the nanofiber web were taken off the drum. The integrity of the fiber web was thus maintained and protected from distortion due to handling.

The electrospinning apparatus has been constructed in such a way as to keep as little metal parts as possible. All the support system, stands have been constructed either by PVC pipe or Garolite, which is a woven glass fabric coated with epoxy resin. Also the metal parts near the vicinity of the equipment have to be essentially grounded. Electrical sparks has been observed if a small metal part was around the system. As the process needs voltage of very high order, proper care must be taken in understanding the electrical connections of the system. Grounding of wires and feed-return paths of electricity should be checked regularly. The chemicals required for the process should be handled with care. A detailed version of the chemical and electrical safety factors has been listed in the appendix.

## **4.2 Material**

Electrospinning experiments were carried out using Poly (ethylene terephthalate) pellets as the polymer having density 1.385 g/cc, refractive index 1.575, and inherent viscosity 0.58. The solvent used to dissolve the PET was a mixture of trifluoroacetic acid and dichloromethane. Poly (ethylene terephthalate) or polyester has placed itself as one of the foremost players in the fiber manufacturing industry and is one of the most sustainable polymers. This can be attributed to its

many fiber characteristics, some of which include, strong, resistant to stretching and shrinking, resistant to most chemicals, quick drying, crisp and resilient when wet or dry, wrinkle resistant, mildew resistant, abrasion resistant, retains heat-set pleats and crease, and easily washed.

#### **4.3 Solution Preparation**

The solutions of PET were prepared in glassware using the following technique. Glassware was cleaned using an initial rinsing with tap water. The desired amount of PET, according to the concentration required was weighed. These polymer chips were poured into a glass bottle containing a 50:50 mixture by volume of trifluoroacetic acid and methylene chloride (dichloro methane). The glass bottle has to be closed by an air-tight lid to maintain the concentration throughout. A homogeneous solution was achieved by slow agitation. This was either by keeping the solution for sometime or by using a magnetic stirrer. The agitation was slow to avoid mechanical degradation of the polymer chains [61]. All solutions were prepared at room temperature.

#### **4.4 Experimental design**

The two variables considered for this work were the concentration of the polymer in the solution, and the electric field. The electric field is defined as the ratio of electric voltage and the collecting distance, wherein electric voltage is the applied voltage to the polymer solution and collecting distance is the shortest distance from the tip of the spinneret to the surface of the cylindrical drum.

Initial experiments were conducted to identify the optimum levels of the parameters, concentration, voltage and the collecting distance. Independent and dependent variables of the experiment identified are listed in table 4.1. The range reported from literature [63] for poly (ethylene terephthalate), poly (amic acid), and poly (acrylonitrile) led to the initial experiments using poly (ethylene terephthalate) as the polymer, which have also been listed in the table.

**Table 4. 1: Independent and dependent variables of the experiment**

Independent Variable	Levels (range)
<b>Concentration (<math>x_1</math>)</b>	<b>15 % - 27 %</b>
<b>Electric Field (<math>x_2</math>)</b>	<b>0.5 kV/cm - 1.4 kV/cm</b>
voltage	15 kV - 25 kV
collecting distance	17 cm - 30 cm

↓

Dependent Variable
<b>Fiber diameter (<math>y_1</math>), Orientation of fibers (<math>y_2</math>), Pore size (<math>y_3</math>)</b>

To determine the lower limit of polymer concentration, several runs were conducted. It was found that, no significant fibers were produced at 13% polymer concentration. This could be due to the lack of continuity of the polymer molecules in the solution, and hence the lower limit on the concentration of the solution should be 13%. Another series of runs were conducted to determine the upper limit of the polymer concentration. At 28% there was no formation of fibers. The solution was dropping off as droplets (discontinuous flow), the reasons could be too low electric field (ratio of voltage to collecting distance) and higher viscosity of the solution. From these experiments, it was decided that the polymer concentration in the solution should vary from 15% to 27%.

The collecting drum speed was also one of the factors considered in the design and the speed was kept constant for all experiments. The speed of the collecting drum was 12 revolutions per hour or 0.2 revolutions per minute or 0.128 m/min surface speed.

#### 4.4.1 Shot Formation

Fibers formed by electrospinning process from polymer solution, observed under scanning electron microscope showed that it had a wide variety of cross-sectional shapes than the usual round, smooth fibers, which has also been shown in the literature [1, 2, 3, 6, 7, 8]. Apart from these shapes, which are formed due to the differences in ejecting the polymer solution, there are other problems too, which

happen during the process, which is mainly the formation of shots or beads (polymer particles that did not form fibers).

As mentioned in literature [63], the electric field should be in the range of 0.7 to 0.9 kV/cm. Experiments were conducted to verify this range. Samples produced below or above this range had a variety of defects. Although the fiber splaying was random, innumerable shots were produced. Shots on electrospun web have been observed when a small web sample was placed under scanning electron microscopy. Our experiments revealed that viscosity of the solution, the speed of the external drum, the collecting distance, surface tension of the solution, net charge density [6] and the electric field play an important role in the formation of shots. Considerable steps have been undertaken in the design of equipment and the experimental procedure to prevent the formation of shots and have been successful in doing so. For example, when the electric field reaches a critical value at which the repulsive force overcomes the surface tension force, charged jet of the solution is ejected from the tip of the Taylor cone. Since this jet is charged, its trajectory can be controlled by the electric field. Higher viscosity favors formation of fibers without shots, higher net charge density not only favors formation of fibers without shots, but also favors the formation of thinner fibers. Reduced surface tension favors formation of fibers without shots. Henceforth, smooth beveling has been done to the spinneret and the inner and outer diameter of the pipette has been reduced to about 0.3 mm near the tip. Changing the polymer concentration, designing the collecting device are some of the other steps undertaken. Hence, for experimental setup, it was concluded that the voltage should be in the range of 15 to 25kV and the collecting distance should be in the range of 17 to 30 cm to produce an electric field in the range of 0.65 to 1.15 kV / cm.

The other factors for the formation of shots or beads may be due to the lack of enough time and air drag to evaporate the solvent before it reaches the collecting surface, the speed of the drum/collecting surface, and the collecting distance. To avoid shot formation, experiments were conducted to identify the optimum conditions of the three parameters namely the concentration of the polymer solution (which constitutes the viscosity of the solution), the voltage and collecting distance (which



comprises the net charge density, and charge on the jet).

It was observed that when the polymer concentration in the solution was less than 21 %, these beads were formed (Figures 4.8 and 4.9). It was observed that the shots were formed from solutions having concentrations less than 21 % and greater than 15 %. Also, if the electric field fell below 0.65 kV/cm or went above 1.1 kV/cm, the web showed shots. Successful attempts have been undertaken in the design and the experimental procedure to prevent the formation of shots. Controlling the three parameters, polymer concentration, voltage and distance helped to form fibers without beads.

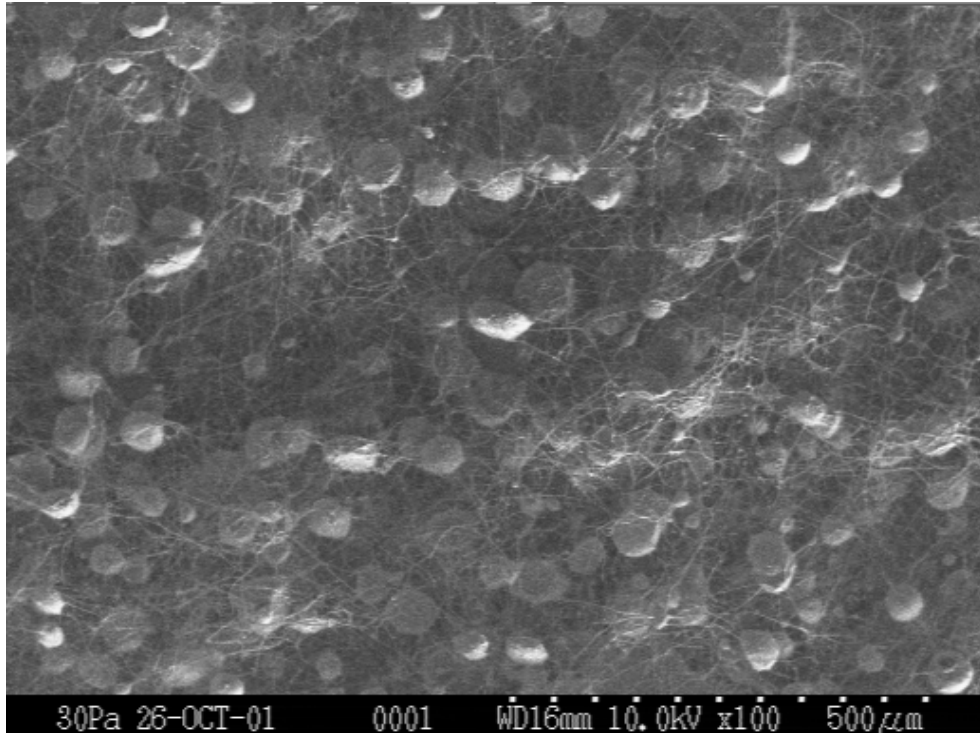


**Figure 4. 8: Scanning Electron Micrograph showing bead formation on electrospun web produced at 15% polymer concentration, 21 kV voltage and 17 cm distance** [Measurement Environment: Hitachi ESEM S 3200, 30 Pa air pressure, 10 kV voltage, 100x magnification, 16 mm working distance]

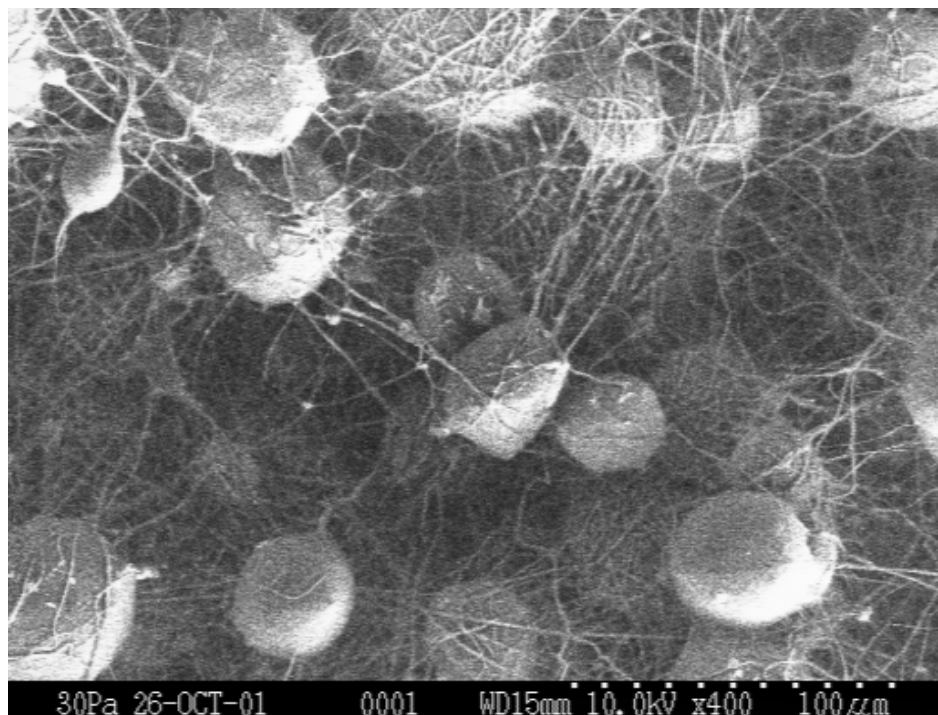


**Figure 4. 9: Scanning Electron Micrograph showing bead formation on electrospun web produced at 17% polymer concentration, 19 kV voltage and 21 cm distance** [Measurement Environment: Hitachi ESEM S 3200, 30 Pa air pressure, 10 kV voltage, 400x magnification, 15 mm working distance]

Because of various limitations and constraints of the set-up and the environment, narrower values of the parameters have been used. The solvents used to dissolve the polymer, methylene chloride and trifluoroacetic acid was corrosive, so the entire experimental apparatus was to be setup in a fume hood (See appendix for the usage of fume hood and safety procedures for the electrospinning process). The fume hood was air controlled with regulated air blowing and air suction/exhaust. The air drag inside the fume hood was a major constraint for the process as it hindered the formation of fibers, splaying of fibers and deposition of fibers on the drum. The entire setup being inside the fume hood, there was a space limitation to carry out the experiments and hence higher collecting distances was not possible. The concentration of the solution was in the range of 21-27%, voltage in the range of 15-21 kV, and the collecting distance between 19-22 cm. Based on these parameters an experimental design was setup (Table 4.2) having four values of each parameter. A completely randomized design was conducted for carrying out the experimental runs.

**Table 4. 2: Design of experiments**

Polymer Concentration (%)	Electric Field								
	kV	cm	kV/cm	kV	cm	kV/cm	kV	cm	kV/cm
21	17	20	0.850	19	21	0.905	21	22	0.955
23	15	20	0.750	15	19	0.789	17	21	0.809
25	15	21	0.714	17	22	0.773	17	21	0.809
27	15	22	0.682	17	21	0.809	17	20	0.850

#### **4.5 Characterization of fiber and fiber web**

Structural parameters of nanofiber webs (such as fiber diameter and distribution, fiber orientation, and pore size and distribution) and material properties (such as melting temperature, glass transition temperature and setting temperature) determine the physical and mechanical properties of the fiber web. As explained in the experimental design and device development sections, two processing parameters were identified, namely electrical field and polymer concentration. The influence of these two parameters on the structural parameters and material properties of the produced nanofiber web need to be revealed in order to produce webs of predetermined properties for certain end use. The following sections describe the methods implemented to measure the structural parameters and material properties of the nanofiber webs produced for this study.

##### **4.5.1 Fiber Diameter Distribution**

Electrospinning process produces very fine fibers and this is one of the very few methods from which fibers of sub-micron size can be produced. So it becomes immensely important to understand the behavior of fiber diameter and fiber diameter distribution in the electrospun web as impacted by the independent variables (processing parameters). Understanding how fiber diameter and distribution are affected by the processing parameters is essential to produce webs with desired fiber diameter and distribution. Moreover, fiber diameter determines pore size.

Images of nanofiber webs were captured by scanning electron microscopy (SEM) as a first step to determine fiber diameter and distribution.

The Scanning Electron Microscope is a microscope that uses electrons rather than light to form an image. There are many advantages to using the scanning electron microscopy over using the traditional light microscope. The scanning electron microscope has a large depth of field (enabling 3-dimensional observation), that allows several layers of the sample to be in focus at one time thus enable measurements of large number of fibers in an image. The SEM also produces images of high resolution, which means that closely spaced features can be examined at a high magnification. Preparation of the samples is relatively easy since most scanning electron microscopes only require the sample to be electrically conductive, which surely applies to the electrospun sample. The combination of higher magnification, larger depth of focus, greater resolution, and ease of sample observation makes the SEM the best choice for the study of electrospun fiber web structures.

The operating principle of the scanning electron microscope can be illustrated as a finely focused electron probe made to scan the specimen surface [86]. As a result of this secondary electrons and backscattered electrons are emitted from the specimen surface, which are detected and fed to a synchronously scanned cathode ray tube as an intensity-modulating signal. The signal thus received displays the specimen image on the cathode ray tube screen. [Secondary electrons are low-energy electrons emitted from the vicinity of the surface of specimen. Backscattered electrons are the electrons backscattered by specimen and having almost the same energy as that of incident electrons. These electrons contain two types of information: one on specimen composition and the other on specimen topography].

The analyses of the electrospun webs were done with the help of two scanning electron microscopes, namely Hitachi ESEM S 3200 and Philips 505 T. Measurements were made in environmental mode in case of Hitachi ESEM S 3200 and the electrospun web samples used in this method were not coated. In case of Philips 505 T, the electrospun web samples were coated.

Since the scanning electron microscope uses a high voltage for its operation and the electron beam is so sharp and intense that a small speck of dust in the system or in the sample may ruin the measurement of the whole sample. The conceivable residual gases in the specimen chamber, which cause contamination are gas caused from the instrument itself and gas that specimens brings into the instrument [86]. The other common contaminants are oil (hydrocarbons), air and specimen itself.

So proper care must be taken while preparing the sample and mounting the sample on the microscope. The samples for the scanning electron microscope can be prepared first of all by cleansing the sample holders (stubs). Cleaning the holders was done using a sonicator and acetone was used as the cleansing agent. Couple of runs was carried out so as to make sure, it is completely cleaned. It is then dried and a layer of sticky pad (double sticky tapes) is pasted to the stubs.

Proper fixing of the specimen is very important because the sample is entirely dry and it will not conduct electrons. So as to prevent charging of the sample, the sample should be properly grounded so that the excessive charges can dissipate (Figure 4.10). To ground the sample, conductive coating has to be applied between the sample and the stub [86]. Proper mounting must be ensured so as to have good interface between the sample specimen and the stub. A layer of silver paint was coated on the sides of the stub, which were hard to coat by the adhesive tapes. This is to ensure that there is proper electrical contact from the stub to the specimen and thus to prevent charging-up of samples.

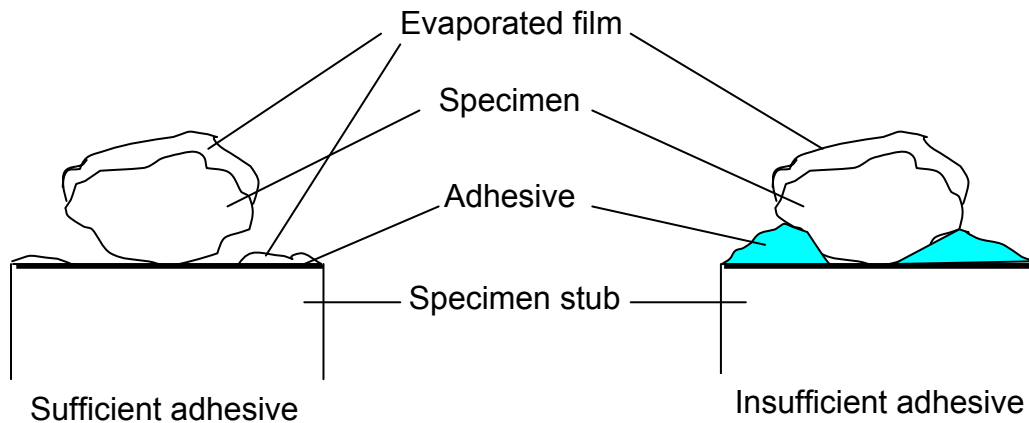


**Figure 4. 10: Fixing the electrospun specimen**

The samples were prepared by cutting them from the electrospun web with dimensions of around 4mm x 4mm. The stub has an area of around 120 square millimeters, so the specimen samples are cut in such a way that 4 to 5 could fit into the stub.

The specimen samples at this point are dry and non-conductive. To obtain SEM images the samples have to be made conductive and this can be done by applying a thin coat of a metal and this is done using sputter coating [86]. Coating in SEM analysis is aimed mainly to prevent the charge-up on the specimen under observation by covering the nonconductive specimen surface with a conductive material, and increasing the secondary electron emission by covering the specimen surface with a metal coating. Samples without proper coating will charge up during image capturing in scanning electron microscope and the image looks very hazy and measurements are not accurate. Coating of electrospun samples were done by Hummer V sputter coater. The substance used for coating was gold-palladium alloy (Au-Pd). It has to be made sure that proper coating takes place, since too thick of a coating may bury the structures of interest in the specimen. If the samples are not coated enough, they can be recoated again without causing other problems with respect to getting a good image. The electrospun samples were given 20-25 nanometers of coating in all directions. While the coating increases fiber diameter, the increase is not significant as it will be seen from the results of fiber diameter and distribution reported later.

The specimen fixed stubs were then mounted on the microscope chamber. To begin with the image capturing, proper spot size and accelerating voltage should be selected. Improper settings may cause image disturbances, some of them being, unstable images, images lacking sharpness and contrast, poor quality and noisy images, images showing jagged edges, unusual contrast images, and distorted or deformed images [86]. Although the resolution and surface detail are increased with increasing spot size, it also increases noise, and decreases contrast and signal strength. A spot size of 20 nanometers was fixed to analyze the electrospun samples.

Higher accelerating voltage will increase resolution, but also increases specimen damage, contamination, and charging, and decreases surface detail [86]. In SEM, finer surface structure images can generally be obtained with lower accelerating voltages. At higher accelerating voltages, the beam penetration and diffusion area becomes larger, resulting in unnecessary signals, which reduce the image contrast and buries fine surface structures. Also, the loss of electron beam energy in the specimen occurs mostly in the form of heat generation at the irradiated point, which can be rectified by using lower accelerating voltage, decreased electron beam intensity, to control thickness of coated material and shorten exposure time. Taking all factors into consideration 12 kV was set for all the electrospun samples.

The other two factors to be considered are magnification and working distance. Increased magnification means increased specimen contamination. The magnifications at which images of electrospun samples were taken ranged from 1000x to 3000x, depending on the structure parameter study. Higher working distance will result in decreased resolution, signal, charging, but increased depth of field. The working distance used in Hitachi ESEM S 3200 was 22 mm, whereas the working distance in Philips 505 T was 12 mm.

When an image was obtained at a suitable magnification, it was set for proper black level and gain level for clarity and was digitally scanned and stored in a computer attached to the microscope. Philips 505 T was interfaced with the computer having 'JEOL Digital Scan Generator V2.00' software. This system had preset scan controls of integrated acquisition mode, a gain factor of 4, resolution of 1280 x 960 and a scan time of 160 seconds. The images obtained could be stored with TIFF format in a zip disk.

The obtained images are analyzed by measuring the fiber diameters. The measurement of fiber diameter was done by commercially available NIH image software (Java version). The fibers were analyzed manually, by measuring the diameter of every fiber, from an individual image. Five photographs from each sample were analyzed. There were around 10-15 randomly laid fibers in each photograph. The analysis was done by first setting the scale (as nanometers) and then measuring manually. The measurements were made by dragging the cursor

towards the entire width of the diameter, i.e., perpendicular to the direction of the fiber-axis. The data obtained can be directly converted to a Microsoft excel sheet, from which the analyses for fiber diameter distribution can be made.

#### 4.5.2 Fiber Orientation Distribution

The orientation of fibers in a nanofiber web plays an important role in the overall property of the web. There is no literature available about the orientation of electrospun fibers and in this work, the orientation distribution was measured and analyzed. The splaying of fibers during the electrospinning process produces fiber web with unknown fiber orientation. Say for example, while testing the tensile property of a nonwoven fabric, the fabric whose fibers are oriented in the machine direction shows more strength if the applied force is in the machine direction. For such a fabric, if the force is applied in the cross machine direction, the fabric will show the least strength. In this study the fiber orientation is impacted by the electric field and polymer concentration since the speed of the collecting surface was kept constant.

Orientation distribution function,  $\psi$ , is a function of the angle  $\theta$ , from the images analyzed. The integral of the function  $\psi$  from an angle  $\theta_1$  to  $\theta_2$  is equal to the property that the fiber has an orientation between  $\theta_1$  and  $\theta_2$  (Figure 4.11).

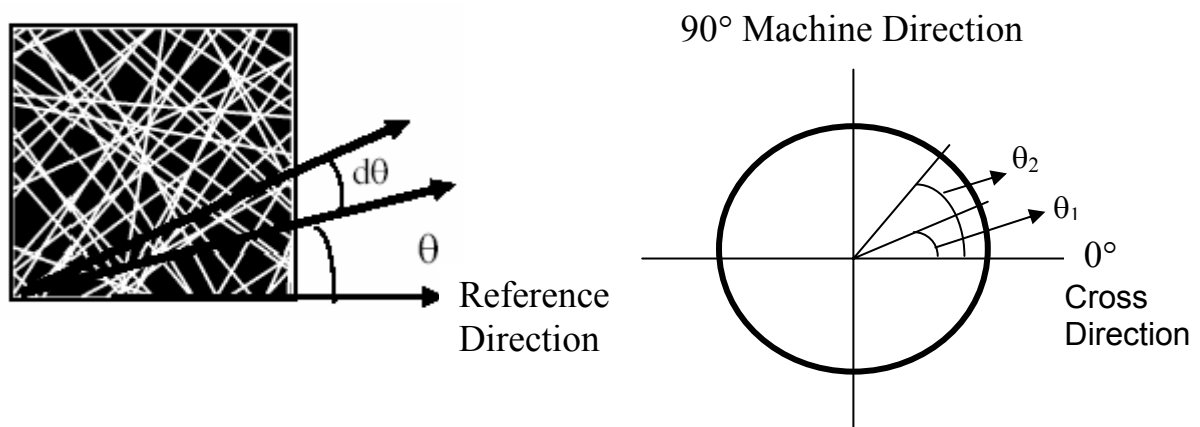


**Figure 4. 11: Representation of Orientation Distribution Function [81]**



Orientation distribution function or otherwise termed as ODF can be defined as the distribution function of fibers with respect to angle between the fiber and a reference direction in a  $15^\circ$  interval [80]. In all cases in this work, the orientation distribution function data was calculated for individual bin ranges of  $18^\circ$  or ten intervals in  $180^\circ$ . The ODF was computed by the Fourier transform method on the gray images. All the images were captured at 625x magnification and at 12 kV beam voltage on the scanning electron microscopy. The method used to measure the fiber orientation in electrospun web was Fourier transform, developed by Pourdeyhimi et al [50]. This is an indirect method of measuring the orientation, wherein the orientation information is obtained by transforming an intensity image into a frequency image. Although this method overestimates the standard deviation of the distribution, this is fairly good in terms of dealing with noisy images and dealing with varying basis weight. Fourier method requires a gray image as input and it provides the mean orientation, and an approximate value of orientation distribution function, standard deviation or standard error.

Image capturing was done using scanning electron microscopy. Images were obtained by the same procedure as explained in the previous section. All the images were obtained from Philips 505 T scanning electron microscope and were in digital format. It has to be made sure that the images are well focused throughout the depth of the sample and should have proper black and gain level. The brightness and contrast can be changed with the help of the image gamma correction. These images were composed of spatial details in the form of brightness transitions and these spatial frequencies, which form the complex details of the image, are related to the orientation of fibers. Fourier transform actually decomposes an image from its spatial domain of intensities into a frequency domain and it determines the rate at which intensity transition occurs in a given direction in the image. Fourier transform has its reference in the center and orientations may be directly computed from the transform image [50].

The digital images, which were in tiff format, were converted to bitmap files to be fed to the image analysis software. The software invariable of the specimen image position captures the image of the picture from its center. The software

automatically calculates the orientation of fibers within that formed circle. The results are obtained in two tables. One of them, which give the statistical data, provides the following parameters, namely, dominating angle, standard deviation, machine cosine squared anisotropy and cosine squared anisotropy. The other table gives the bin range, which is from 0 to 180 and provides the frequency of fibers in that particular range. From this table the orientation distribution function can be analyzed.

#### 4.5.3 Pore Size Measurement

The Pore size is obtained by experimental technique and is usually defined in conjunction with pore size distribution. The pore size of a fabric is defined as the diameter of the right cylinder that will pass through the fabric (Figure 4.12).

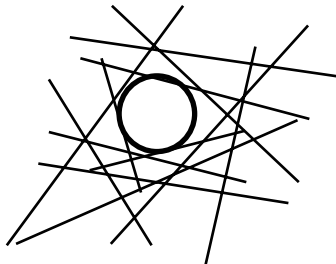


**Figure 4. 12: Pore size of a Fabric [81]**

The control of the pore of electrospun web or for that matter any nonwoven fabric is of prime importance in the fabrics that are being produced for the purposes of filtration and fluid flow. There is no literature available about the pore size and its distribution of electrospun fibers and in this work, the pore size and its distribution was measured and analyzed. The Automated Perm Porometer is an instrument being used to characterize the pore and its distribution of nonwoven fabrics.

##### 4.5.3.1 Theory and Description of the Apparatus

The Automated Perm Porometer works on the principle of capillary flow. The fabric sample is saturated with a solution, which wets the fabric. The relative magnitude of the liquid-liquid interaction versus the liquid-solid interaction determines the degree to which a liquid can “wet” the solid. If the magnitude of the liquid-liquid interaction force is greater than the liquid-solid interaction then the liquid will not completely wet the surface of the solid. If the surface tension of the liquid is sufficiently low then the solid is readily “wetted”. In such a situation the contact

angle  $\theta$  is equal to zero and the liquid meniscus is hemispherical. When a gas pressure is applied to the saturated surface, the liquid will be forced out from the cylinders in the solid when the applied pressure is greater than the liquid-solid interaction. The relationship between the applied pressure and the diameter of the cylinder is given by the following equation:

$$\Delta p = \frac{4 b \sigma \cos \theta}{d}$$

**Equation 4. 1**

Where,  $\Delta p$  is Pressure Difference between Points A and B (Figure 4.13)

$b$  is Capillary Constant

$\sigma$  is Surface Tension of the Fluid

$d$  is Diameter of the Cylinder

$\theta$  is Contact Angle, dependent upon the surface tension between the solid and liquid

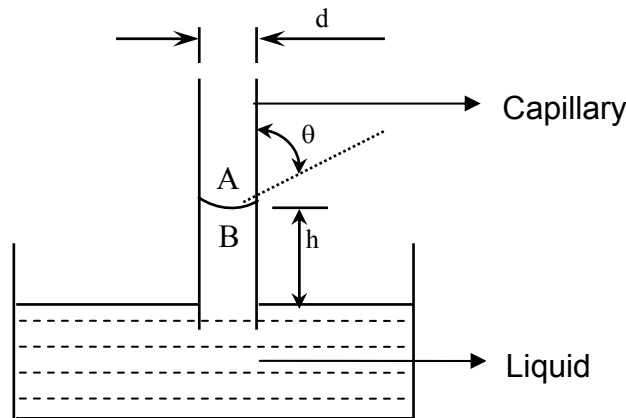


**Figure 4. 13: Principle of Capillary Flow**

For a given liquid of known surface tension, the diameter  $d$ , of the cylinder is inversely proportional to the pressure difference. During a test the pressure applied is incrementally increased, thus opening the pores of decreasing diameter. The first pore detected is called the 'bubble point' and has the largest diameter in the sample. Until the bubble point is reached there is no flow of gas/air through the material (solid).

The porometer consists of a sample chamber (Figure 4.14) in which the sample is mounted. Air under controlled and increasing pressure is forced through the

sample. The height of the sample chamber is fixed, hence to accommodate samples of various thicknesses; spacing inserts of different heights are used. The pore size of a sample can also be determined at known compression forces. To conduct this test, a known compression force is applied on the spacing insert, thereby transferring the force onto the sample.

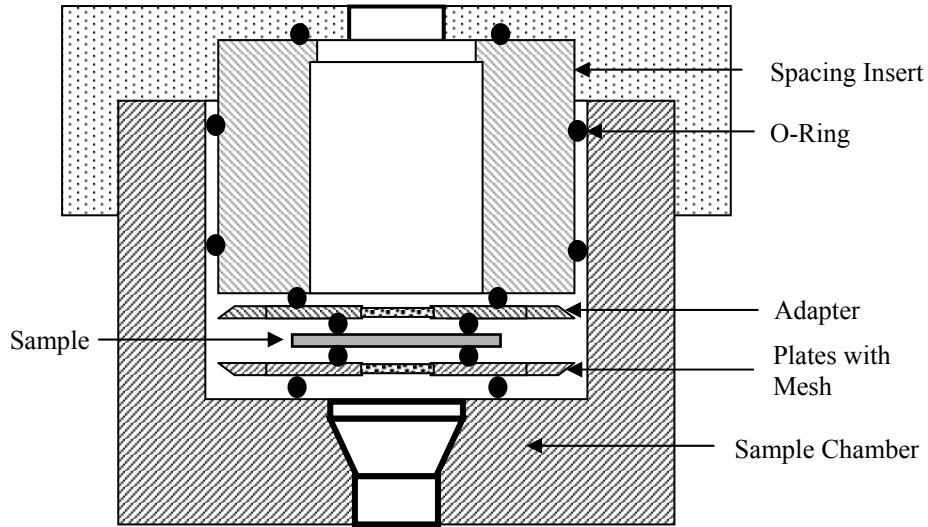


**Figure 4. 14: Essential Parts of Automated Perm Porometer [81]**

The porometer records the flow rate of the air through the sample for increasing pressures and the diameter is calculated based on the pressure difference between the dry sample and wet sample.

#### 4.5.3.2 Test Procedure

The type of capillary test that needs to be conducted on the electrospun sample is determined out of the four types that are available on the porometer. The four types of procedures that can be used are, a) Wet Up/Dry Down, b) Wet Up/Dry Up, c) Dry Up/Wet Up, and d) Wet Up/Linear Dry.

The test method is carried out by placing the sample in the chamber and sealing the chamber with the spacing insert and the threaded cover (Figure 4.14) and choosing the method of capillary test. Depending upon the type of capillary test that is conducted wet the sample with the liquid, with a known surface tension, until it is saturated with the liquid. In this work the test procedure that will be used is wet up/dry down type, wherein the sample is subjected to an increasing pressure when

the sample is saturated with the solution and decreasing pressure when the sample is completely dry.

The test is carried out by bubble point test with standard (automatic mode [82]. When the bubble point test begins, the program allows gas from the regulator to pass through valve **V1** (Figure 4.15), a fixed needle valve, a flow transducer and into the bottom of the sample chamber. As long as the pressure is below the bubble point, the sample seals the chamber and the pressure rises. The rate at which the gas enters the chamber is monitored using the flow transducer. When the flow rate falls to the user selected minimum, the regulator is incrementally increased and this increases the pressure at the fixed needle valve's inlet, increasing the flow through the valve, the flow transducer, and into the sample chamber. When the sample chamber pressure fails to rise while the flow through the flow transducer is maintained, the program takes the maximum pressure reached as the bubble point.

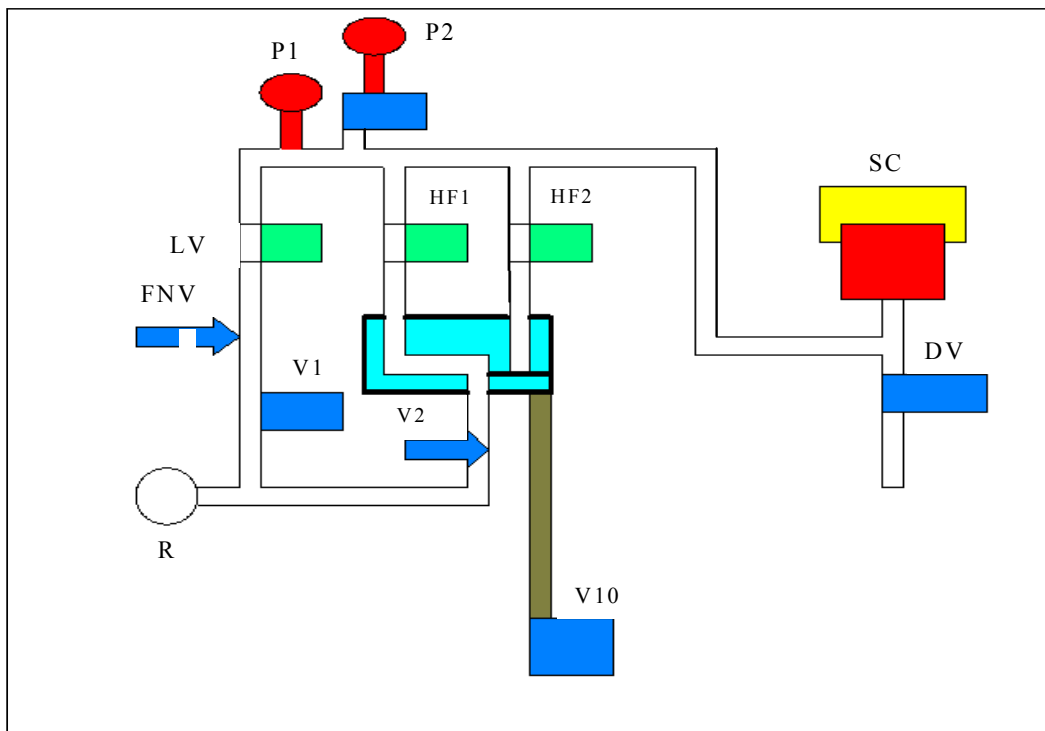


**Figure 4. 15: Diagrammatic representation of Bubble point test [82]** [H1 & H2 – High Flow 1 & 2, LV – low flow, FNV – fixed needle valve, R – regulator, SC – sample chamber, DV – drain valve]

#### 4.5.4 Differential Scanning Calorimetry

Thermal analysis for the electrospun web was carried out using Perkin Elmer Pyris DSC-7. This is a power compensated type of differential scanning calorimeter which has good resolution, fast heating/cooling capability and is more sensitive than the heat flux type of DSC. This has a temperature range of 720°C to -170°C, i.e., the maximum heating temperature of the instrument is 720°C. Numerous parameters can be obtained by this instrument namely, kinetics of reactions, purity of organic compounds, melting point ( $T_M$ ), glass transition temperature ( $T_G$ ), heat setting temperature/curing, phase changes and onset of oxidation.

The system uses aluminum pans for holding the sample/standard (left hot plate) and the reference (right hot plate) and these aluminum pans can either be volatile or non volatile. The equipment gives out the output in terms of the thermogram curves and the following information can be obtained from these thermograms. It essentially provides the melting point (endothermic peak upward), crystallization (exothermic peak downward) and glass transition temperature. The cooling options are ice water (0°C), intercooler (-60°C) or liquid nitrogen (-170°C).

The operation sequence of the equipment involves running the system base line to zero instrument, running the standard to calibrate temperature range and finally running the sample. In one of the pans, the sample is placed. The other pan is the reference pan, which is kept empty. Both the pans sit on the top of a heater. Now, the system is switched on where the computer turn on the heaters and it heats the two pans at a specific rate, usually 10°C per minute. The computer makes absolutely sure that the heating the rate stays exactly the same throughout the experiment.

But more importantly, it makes sure that the two separate pans, with their two separate heaters, heat at the same rate as each other. As the two pans are heated, the computer will plot the difference in heat output of the two heaters against temperature. That is, the heat absorbed by the polymer against temperature is plotted. As the heating of the polymer continues, there is more heat flow. There is an increase in the heat capacity of the polymer sample. This happens because the polymer has just gone through the glass transition. Above the glass transition, the

polymers have a lot of mobility. When they reach the right temperature, they will have gained enough energy to move into very ordered arrangements, in other terms called crystals. When polymers fall into these crystalline arrangements, they give off heat. There is a drop in the heat flow versus temperature curve. The temperature at the lowest point of the dip is usually considered to be the polymer's crystallization temperature, or  $T_c$ .

If the heating continues over its  $T_c$ , eventually it'll reach another thermal transition, called melting. When the polymer's melting temperature, or  $T_m$ , is reached, the polymer crystals begin to fall apart, that is they melt. The extra heat flow during melting shows up as a big peak on the DSC plot.

The thermal analysis was carried out on electrospun web using differential scanning calorimetry. The weight of the sample was 3.63 g, which was consistent with the weight of the standard sample, which is  $3.5 \pm 0.5$  g. For calibration, run the baseline to zero. The heating starts at room temperature and increment of  $25^\circ\text{C}$  can be given. Temperature should not exceed  $600^\circ\text{C}$ , since aluminum pans are being used. Care should be taken that the temperature should not go above  $20^\circ\text{C}$  to  $30^\circ\text{C}$ . Run a standard and in our case it was tin (3.84 g). The tin is calibrated by holding it for 4 minutes at  $150^\circ\text{C}$ , then heating from  $150^\circ\text{C}$  to  $260^\circ\text{C}$  at  $20^\circ\text{C}/\text{min}$ . For running the sample, heat it from  $25^\circ\text{C}$  to  $300^\circ\text{C}$  at  $20^\circ\text{C}/\text{min}$ .

#### 4.5.5 Basis Weight of Nanofiber webs

The electrospun fiberweb collected on the fiber glass screen was carefully removed from the collecting drum of the electrospinning apparatus. Fibers being very delicate, the fiberweb was handled with utmost care. The web was then carefully removed from the fiber glass screen without damaging the web sample. The specimen sample for weighing was then prepared by cutting the fiberweb of 5.08 cm x 5.08 cm dimension from different locations. These samples were then weighed. The data collected were reported in grams, and an accuracy of up to five decimal places was maintained. The data obtained were then used to calculate throughput in gram per hour and basis weight in  $\text{g}/\text{m}^2$ .

#### 4.6 Statistical analysis

The analysis was done using SAS, wherein the output was in the form of an Analysis of Variance (ANOVA) table. The column headings in an ANOVA table consists of SS, df, and MS, which stand for "Sum of Squares", "degrees of freedom", and "Mean Square", respectively. Since the regression included a constant, the total sum reflects the sum after removal of means, as does the sum of squares due to the model. The mean square error (MS) is defined as the residual sum of squares divided by the corresponding degrees of freedom. The  $F$  statistic tests the hypothesis that all coefficients excluding the constant are zero. The R-square value indicates that how well the model is fit for the given dependent variable. The value closer to one (1) means that the model is highly fitted. Note that the root mean square error is the square root of the mean square error reported for the residual in the ANOVA table.

To test for an interaction between concentration and electric field ( $x$ ), we compare the (reduced) model which allows for a quadratic dependence of width (fiber diameter) on  $x$  and possibly different intercepts for the four concentration levels with a (full) model which allows for four different quadratic dependencies on  $x$  for the four concentrations. Here, the concentration may not be considered as continuous variable and is taken as class variable. This is because, this study had only four distinct concentrations, whereas it had more distinct values of electric field in the design of the experiment. It is hard to say much about any polynomial association between the response and an experimental factor with only 4 distinct values. So the concentration is taken as class variable. Formally, the reduced and full models are written as,

##### Model 1: Reduced Model

$$\mu = \beta_0 + \beta_1 c_1 + \beta_2 c_2 + \beta_3 c_3 + \beta_4 x + \beta_8 x^2$$

Equation 4. 2



### Model 2: Full Model

$$\mu = \beta_0 + \beta_1 c_1 + \beta_2 c_2 + \beta_3 c_3 + (\beta_4 + \beta_5 c_1 + \beta_6 c_2 + \beta_7 c_3) * x + (\beta_8 + \beta_9 c_1 + \beta_{10} c_2 + \beta_{11} c_3) * x^2$$

**Equation 4. 3**

Where,

$\mu$  is response (Fiber Diameter, Anisotropy Ratio, or Basis Weight)

$c_1, c_2, c_3$  are indicator or dummy variables for concentrations 1, 2, and 3, and

$c_1 = 1$  if concentration 1, 0 else

$c_2 = 1$  if concentration 2, 0 else

$c_3 = 1$  if concentration 3, 0 else

$\beta_0, \beta_1, \beta_2, \beta_3$  = intercept

$\beta_4$  is slope

$\beta_5, \beta_6, \beta_7$  = linear coefficients

$\beta_8$  is curvature

$\beta_9, \beta_{10}, \beta_{11}$  = quadratic coefficients

Reduced model is a quadratic model with different intercepts that means there is no interaction between variables. In other words  $\beta_4$  and  $\beta_8$  are same for all the four levels of concentration. The full model is a quadratic model with different profiles for each concentration that means there is interaction. Here the model allows the profiles to vary. Profile may be defined as the combination of slope and curvature.

## 5 Results and Discussion

### 5.1 Fiber Diameter and its distribution

The images obtained from scanning electron microscope were studied for the effect of the polymer concentration and electric field on fiber diameter and its distribution. Figure 5.1 shows the effect of the electric field on the measured average fiber diameter of the fibers at four different concentrations of the polymer solution.

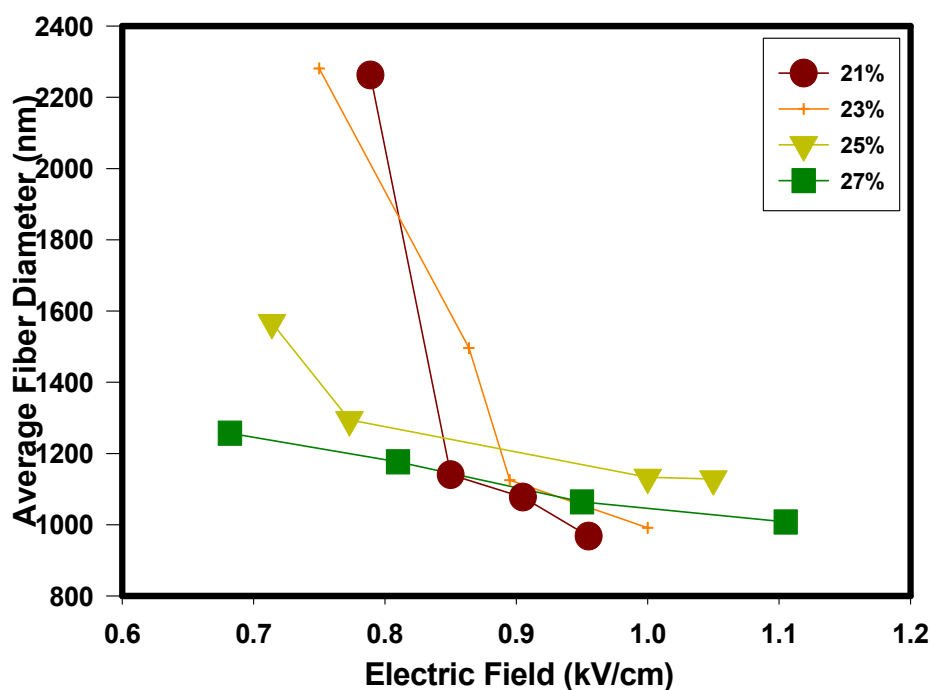


**Figure 5. 1: Influence of electric field and polymer concentration on the measured average diameter of electrospun fibers**

It is evident from the graph (and as expected) that as we increase the electric field at all concentrations, the average diameter of the electrospun fibers decreases. This plot indicates that diameter is decreasing in electric field at the concentrations considered in this experiment. Variability due to electric field also seems to reduce at the higher concentrations. But, clearer conclusions can only be obtained by doing more experimentation. Figures 5.2 and 5.3 are SEM pictures showing the diameter

of samples produced at 27 % polymer concentration and electric field of 1.105 kV/cm and 0.681 kV/cm respectively. These figures show the range of diameters for this concentration.

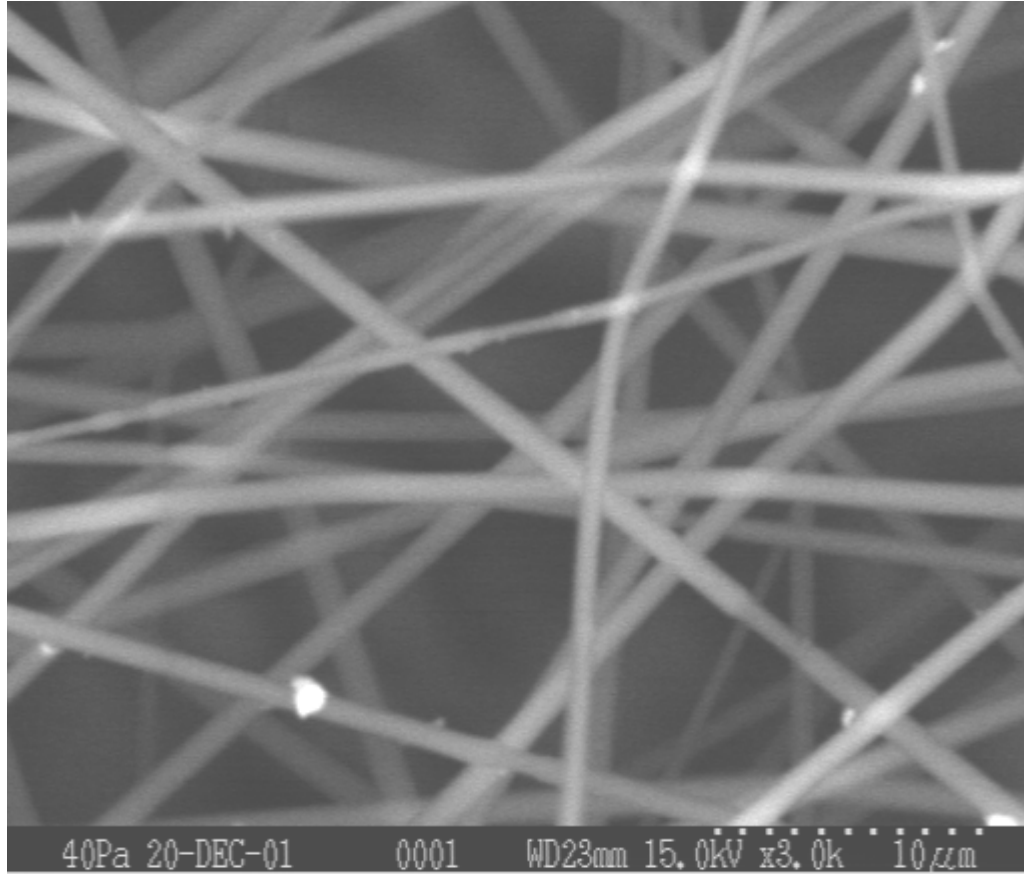


**Figure 5. 2: SEM image of electrospun web formed at Polymer Concentration 27 %, Voltage 21 kV, Distance 19 cm. (1.105 kV/cm)** [Measurement Environment: Hitachi ESEM S 3200, Air pressure 40 Pa, Magnification 3000x, Voltage 15 kV, Work distance 22 mm]

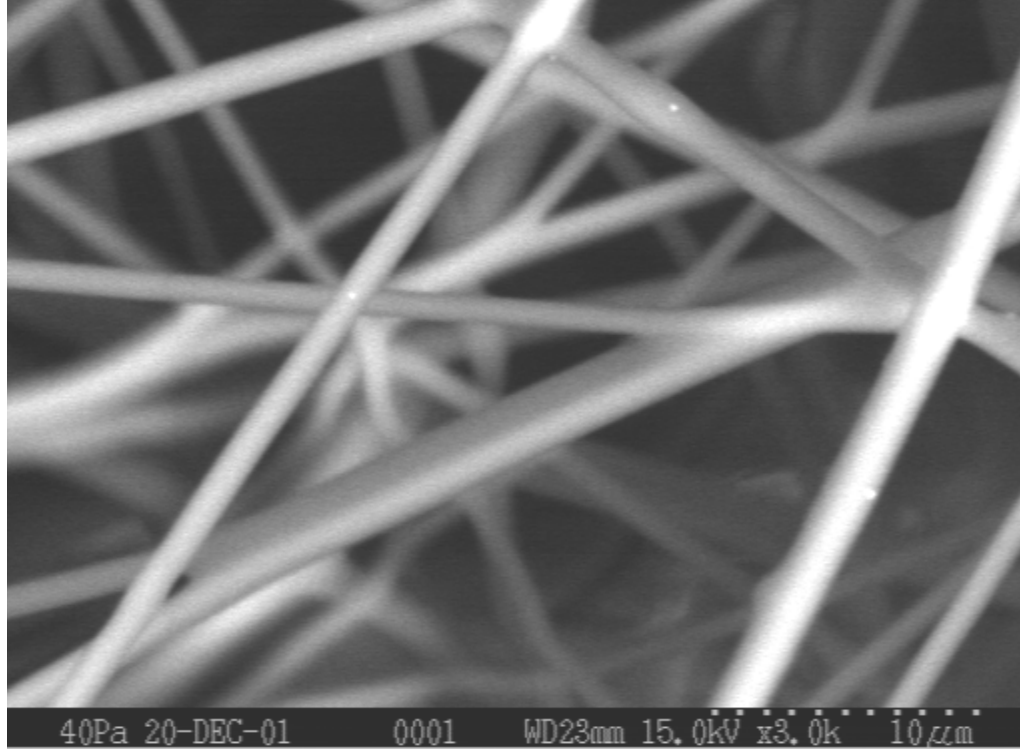


**Figure 5. 3: SEM image of electrospun web formed at Polymer Concentration 27 %, Voltage 15 kV, Distance 22 cm. (0.681 kV/cm)** [Measurement Environment: Hitachi ESEM S 3200, Air pressure 40 Pa, Magnification 3000x, Voltage 15 kV, Work distance 22 mm]

Statistical analysis was done for the average fiber diameter, emphasizing the effect of electric field on the average diameter of fibers under different polymeric concentrations of the solution. The statistical analysis software (SAS) by default takes the last entry as the baseline and here it is the data of 27 % polymer concentration. Therefore, the baseline quadratic regression function is,

$$\mu_4 = \beta_0 + \beta_4 x + \beta_8 x^2$$

and the remaining statements can be written as,

$$\mu_1 = \beta_0 + \beta_1 + (\beta_4 + \beta_5) * x + (\beta_8 + \beta_9) * x^2$$

$$\mu_2 = \beta_0 + \beta_2 + (\beta_4 + \beta_6) * x + (\beta_8 + \beta_{10}) * x^2$$

$$\mu_3 = \beta_0 + \beta_3 + (\beta_4 + \beta_7) * x + (\beta_8 + \beta_{11}) * x^2$$

**Equations 5. 1**

The test of interaction boils down to an F-test of

H0:  $\beta_5 = \beta_6 = \beta_7 = \beta_9 = \beta_{10} = \beta_{11} = 0$  (null hypothesis)

H1: not all 0 (research hypothesis)  
degrees of freedom (df)

On 6 and 4 numerator and denominator

There are 6 numerator degrees of freedom associated with the numerator, which is a difference of models involving 11 and 5 degrees of freedom and 4 denominator degrees of freedom associated with the full model.

$$F = \frac{[SSE(R) - SSE(F)]/6}{MSE(F)}$$

**Equation 5. 2**

Where,

SSE (R) – sum of squares of error for reduced model

SSE (F) – sum of squares of error for full model

MSE (F) – mean square error for full model

From the results obtained (section 8.2) for the reduced and full model, equation 5.2 can be written as,

$$F = \frac{[817430 - 67276]/6}{16819}$$

on 6, 4 degrees of freedom

$$F = 7.43$$

At 95 % confidence limit, the 'p' value at F = 7.43 is 0.0363. These values can also be checked for the values obtained from SAS in section 8.2. This F-ratio for concentration by electric field interaction is statistically significant. There is evidence that quadratic association between mean diameter and electric field varies by concentration (the model implied by H0 doesn't appear to fit).

The four fitted quadratic regressions, under the interaction model, are plotted in Figure 5.4. The general form of these fitted regressions appears as Equation 5.3.

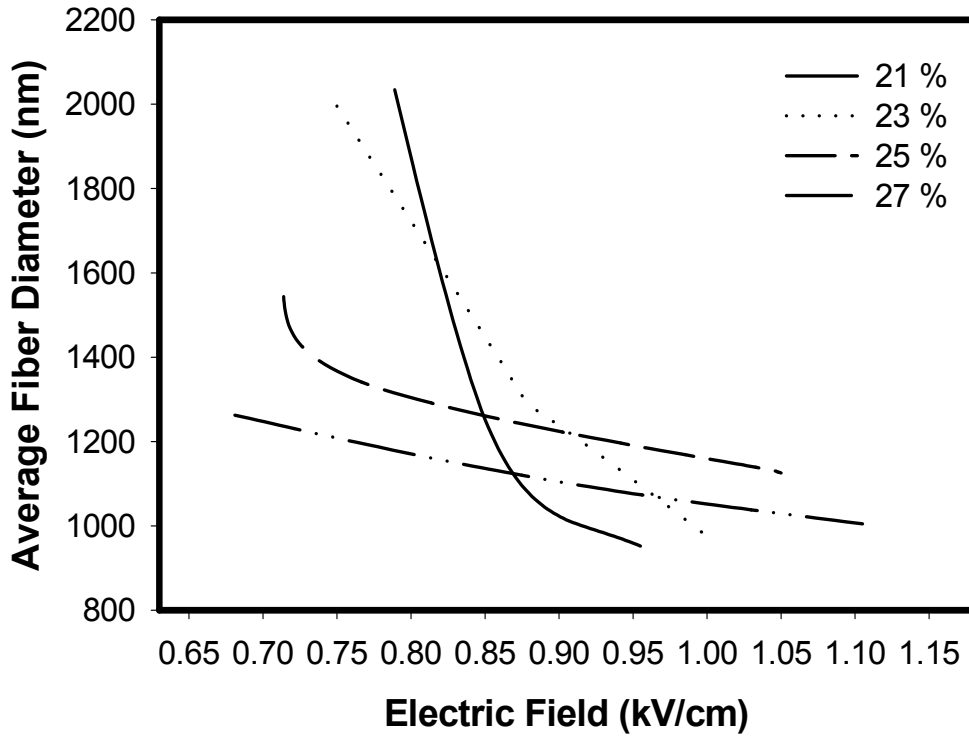


**Figure 5. 4: Influence of electric field and polymer concentration on the measured average diameter of electrospun fibers (plotted for regression equations**

The values of fiber diameter can be predicted by using the values obtained from SAS analysis (8.2). The model statement for the same is given in Equation 5.3.

$$\hat{Y} = \hat{\beta}_0 + \hat{\beta}_1(c1) + \hat{\beta}_2(c2) + \hat{\beta}_3(c3) + [\hat{\beta}_4 + \hat{\beta}_5(c1) + \hat{\beta}_6(c2) + \hat{\beta}_7(c3)] * X + [\hat{\beta}_8 + \hat{\beta}_9(c1) + \hat{\beta}_{10}(c2) + \hat{\beta}_{11}(c3)] * X^2$$

**Equation 5. 3**

So, for example, if we want to predict the fiber diameter at a given value of electric field (x) equal to 1.0 kV/cm and concentration 23 % under full model can be written as,

$$\hat{Y} = \hat{\beta}_0 + \hat{\beta}_1(0) + \hat{\beta}_2(1) + \hat{\beta}_3(0) + [\hat{\beta}_4 + \hat{\beta}_5(0) + \hat{\beta}_6(1) + \hat{\beta}_7(0)] * 1 + [\hat{\beta}_8 + \hat{\beta}_9(0) + \hat{\beta}_{10}(1) + \hat{\beta}_{11}(0)] * 1^2$$

The value of  $\hat{Y}$ , the predicted fiber diameter can be obtained if we plug in respective values (8.2) in the above equation.

$$\hat{Y} = 2087 + 10607 + [(-1582) + (-20320)] * 1 + [545 + 9638] * 1^2$$

$$\hat{Y} = 975 \text{ nm}$$

The predicted values can be written on the same way as of equation 5.3 and obtain the value of fiber diameters in nanometers. Figure 5.5 shows the relationship between observed fiber diameter and predicted fiber diameter.

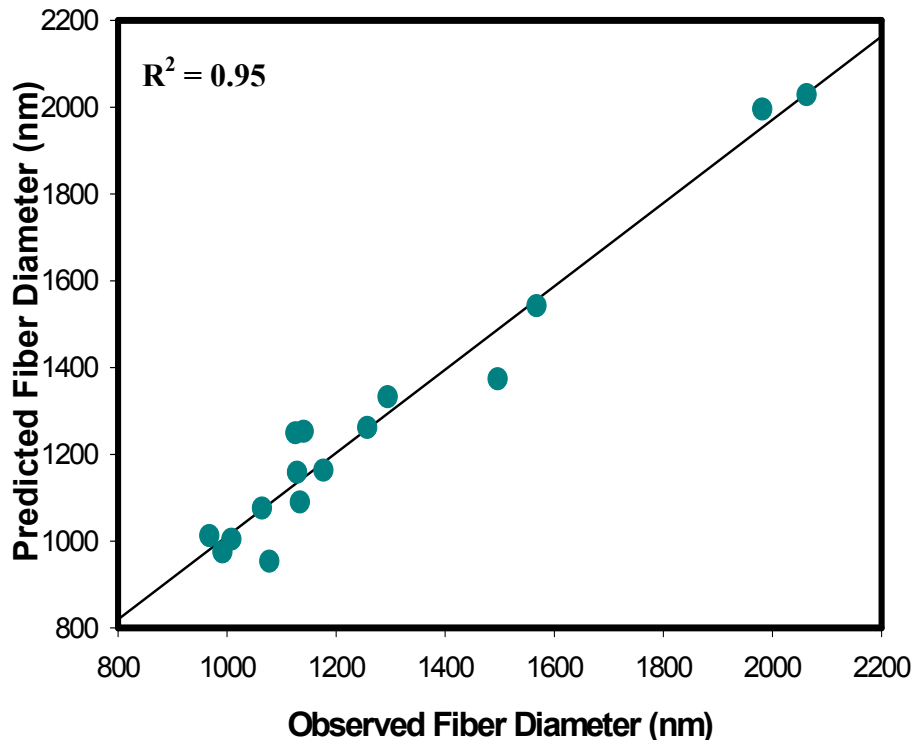


**Figure 5. 5: Plot showing the relationship between observed fiber diameter and predicted fiber diameter**

It can also be noted from Figure 5.1 that lower diameter fibers are obtained in the range of 0.85 kV/cm to 1.0 kV/cm, which agrees with results of previous work published [64]. Empirical cumulative distribution functions for fiber diameters at each combination of electric field and concentration are shown in Figures 5.6-5.9. These augment the analysis of the means in Figure 5.1 and provide more evidence that diameter decreases with electric field at each concentration.

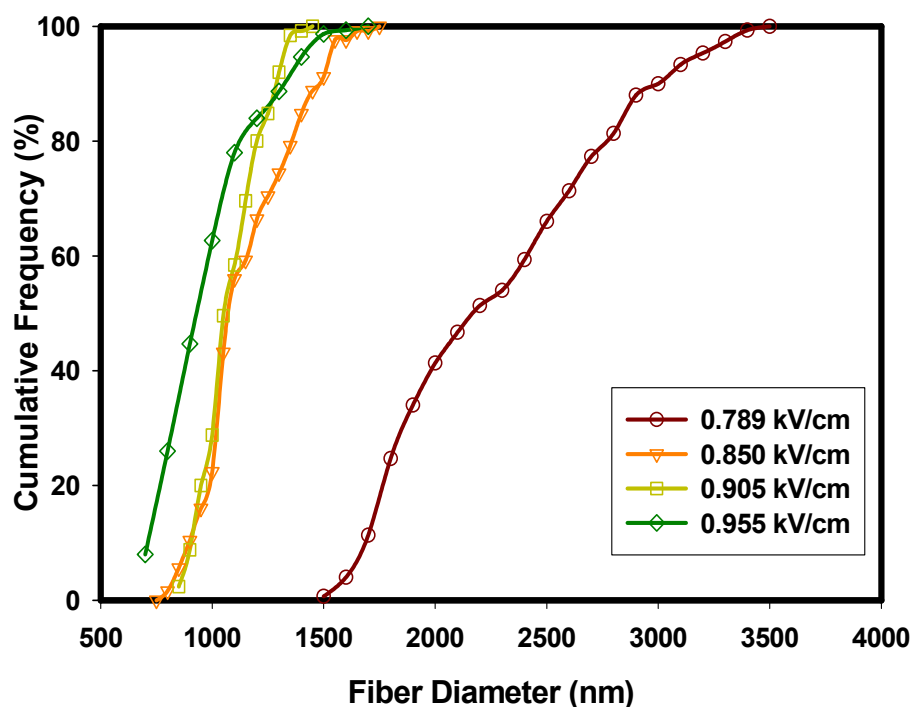


Figure 5. 6: Effect of varying electric field on the diameter distribution of the fibers at a constant concentration of 21%

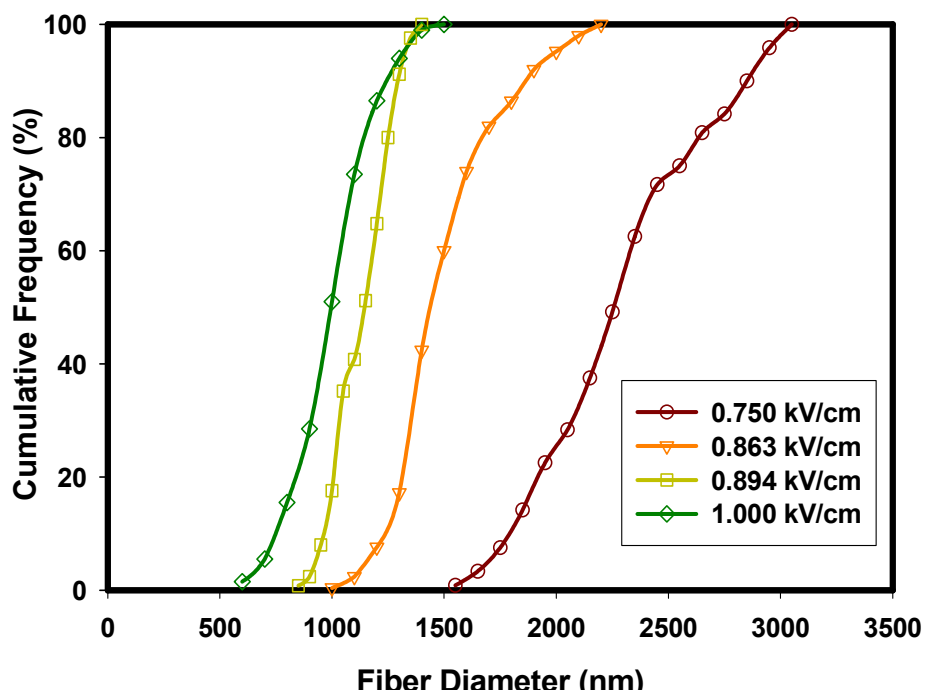


Figure 5. 7: Effect of varying electric field on the diameter distribution of the fibers at a constant concentration of 23%



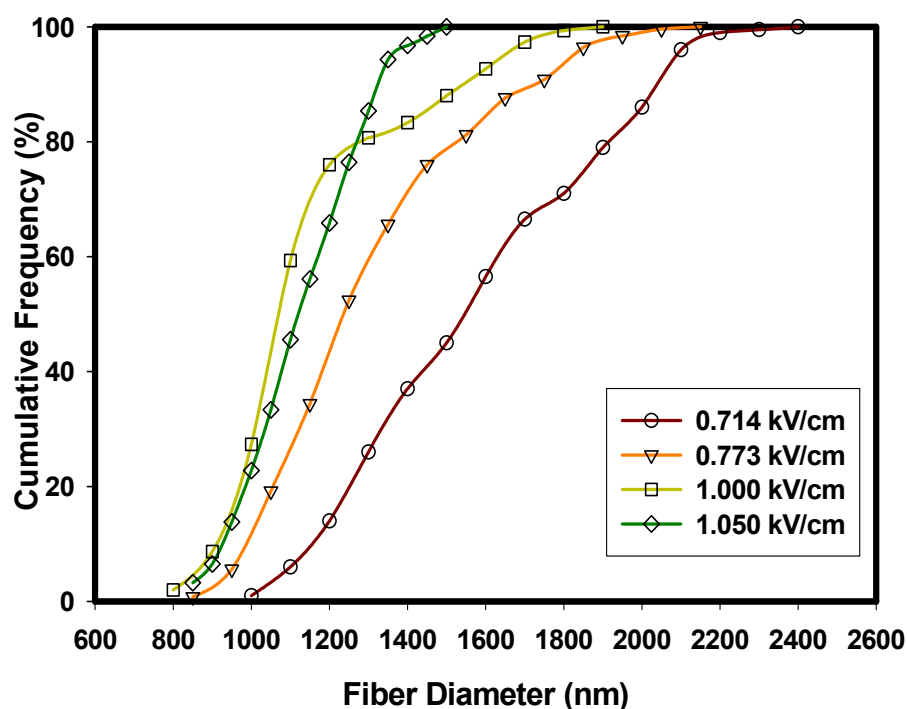


Figure 5. 8: Effect of varying electric field on the diameter distribution of the fibers at a constant concentration of 25%

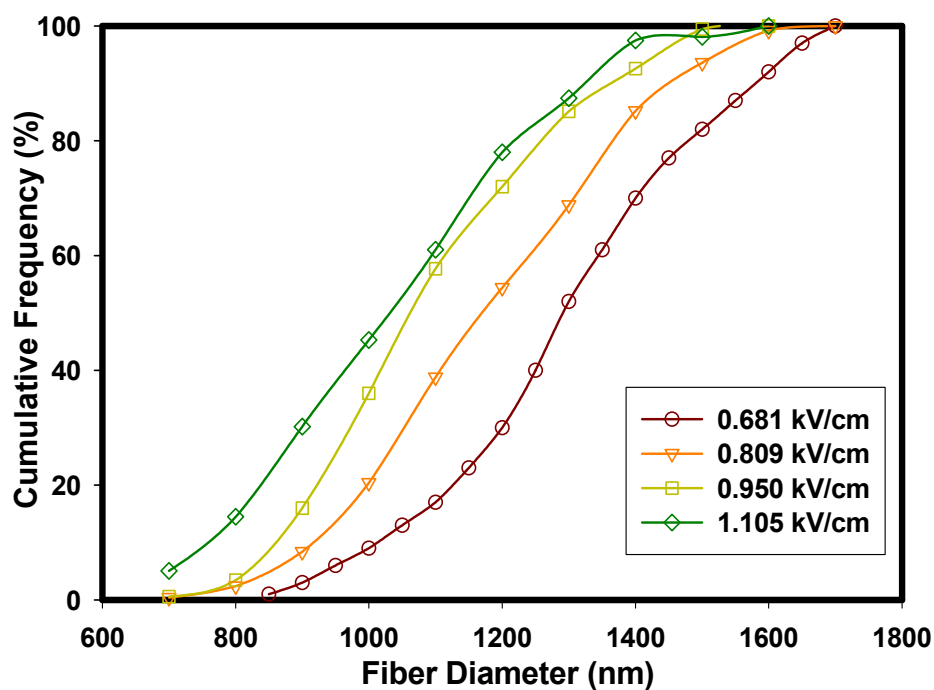
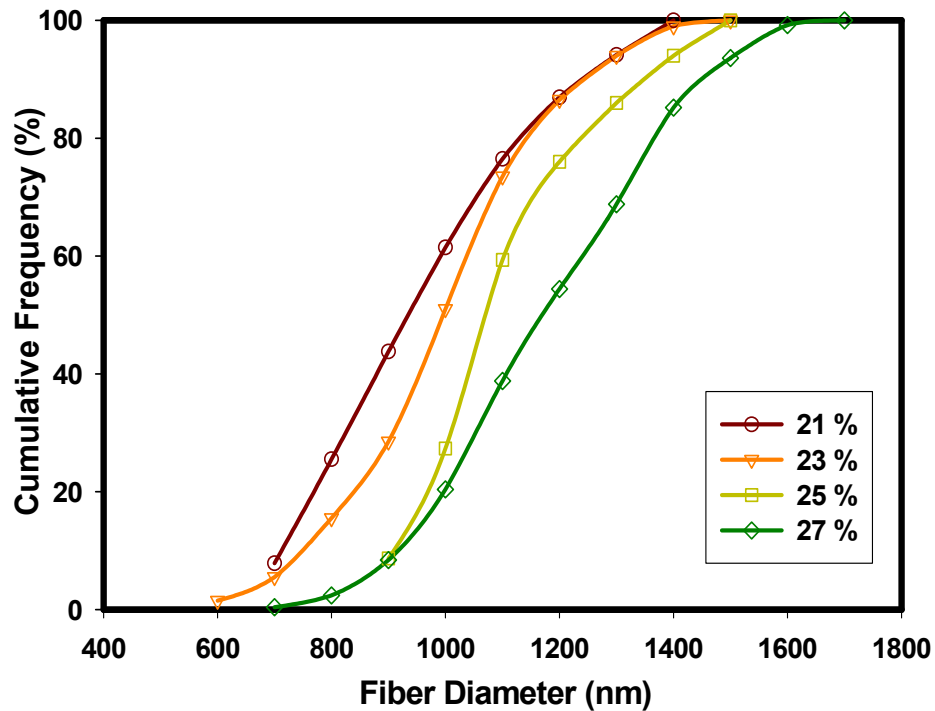


Figure 5. 9: Effect of varying electric field on the diameter distribution of the fibers at a constant concentration of 27%

As the concentration of the solution increases the fiber diameter increases and the diameter range is broadened (Figure 5.10). This behavior can be related to the fact that an increase in polymer concentration causes an increase in viscosity, which in turn causes the splay (formation) of thicker fibers. Higher polymer concentration means there is high viscous force within the solution and there are more molecules aggregated. Because of high aggregation of molecules it is difficult to split them. Lower viscous solutions are easy to split and they are much easier to splay to form fibers. Hence lower polymer solution concentration yields lower diameter fibers.



**Figure 5. 10: Effect of Concentration on the diameter distribution of fibers at an electric field of 1.0 kV/cm**

## 5.2 Throughput and Basis Weight

Figures 5.11 and 5.12 shows the effect of electric field on throughput and the basis weight at different polymer concentrations. It can be seen that as the electric field increases, the throughput and basis weight also increases. At higher polymer

concentrations, solution has high viscous force, which means the molecules are more aggregated and it is difficult to split them. As the electric field is increased, it becomes easy to split the aggregated molecules within the polymer solution. The solution, which now has more free molecules, tends to move easily out of the spinneret. That means there is higher draw force and more solution comes out of the spinneret. More solution coming out of the spinneret results in formation of more fibers which in turn causes higher weight of the sample. Also, higher concentration of polymer solution means lower electric charge per given surface area of the polymer in the solution coming out of the spinneret. This results in lower amount of fibers collected on the collecting screen, which means lower fiberweb weight.

This behavior can be observed for all four levels of concentration. It can also be observed that at increasing polymer concentrations, the throughput decreases. This may be explained by the fact that as the concentration of the polymer solution increases, the solution becomes more viscous with higher resistance to the drawing force created by the electric field. This means the amount of polymer solution coming out of the spinneret will be low, resulting in lower basis weight. Whereas low viscosity polymer solution will flow easier, and more solution is available for fiber formation, resulting in heavier fiberweb.

It can be observed from Figures 5.11 and 5.12 that the throughput and basis weight decreases at increasing polymer concentration, except for 21 % polymer concentration. It has been seen that at this particular concentration (21 %), the solution has a low viscosity and the amount of solution coming out of the spinneret is too high. The charge per given area is also high and the fibers formed are very fine. It has been observed that at this concentration the laying of fibers is wider than the length of the collecting drum. This results in some of the fibers getting lost and unavailable for weight measurement.

The throughput in g/hr was calculated as follows,

Given (known) parameters:

Collecting drum speed – 12 revolutions/hour

Number of layers collected – 4

Weight of the electrospun fiberweb of dimension 5.08 cm x 5.08 cm (2" x 2") –  
X grams

Collecting drum length – 35.56 cm (14")

Collecting drum diameter – 20.32 cm (8")

Therefore, to collect 4 layers of fiberweb, it took 20 minutes.

$$\text{Throughput (g/hr)} = \frac{60 * X * 35.56 * 20.32\pi}{20 * (5.08 * 5.08)}$$

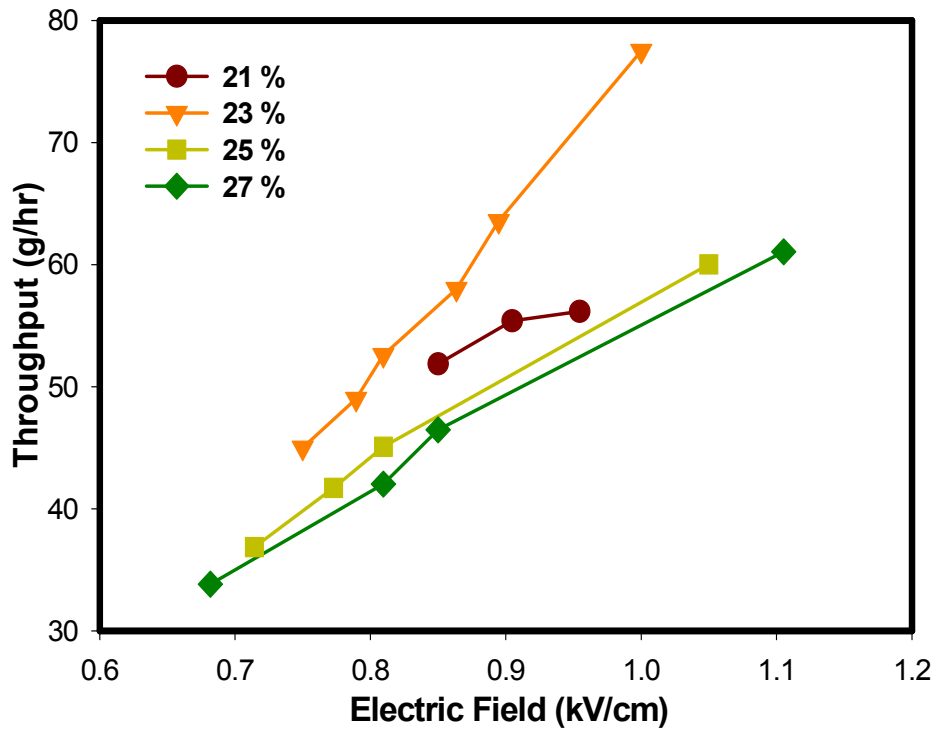


**Figure 5. 11: Influence of electric field on the throughput of an electrospun web produced at different polymeric concentrations.**

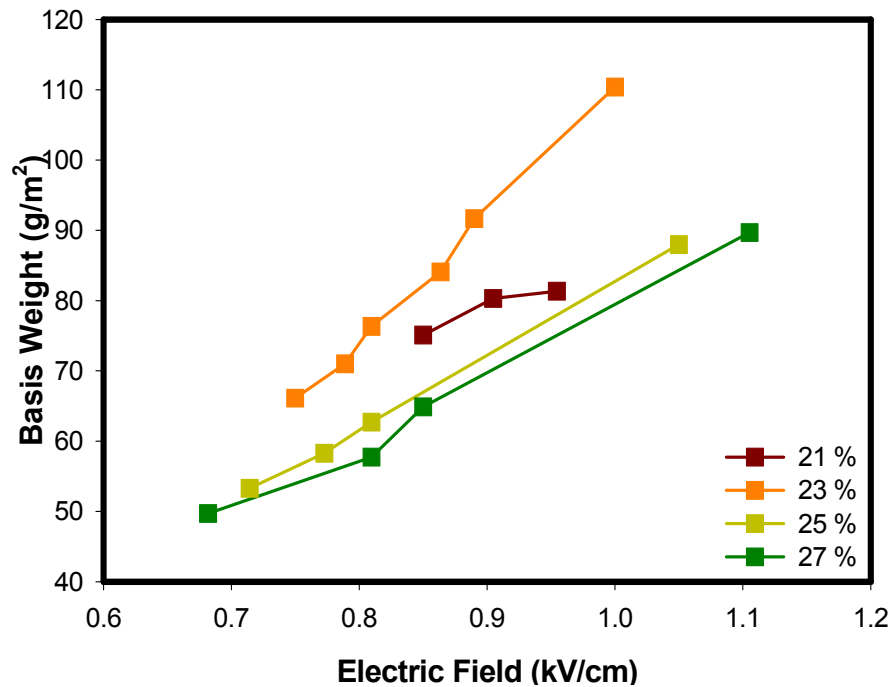


**Figure 5. 12: Influence of electric field on the basis weight of an electrospun web produced at different polymeric concentrations.**

Statistical analysis was done for the throughput, emphasizing the effect of electric field under different polymeric concentrations of the solution. The statistical analysis software (SAS) by default takes the last entry as the baseline and here it is the data of 27 % polymer concentration. Therefore, the baseline statement for the model will be,

$$\mu_4 = \beta_0 + \beta_4 x$$

And the remaining statements can be written as,

$$\mu_1 = \beta_0 + \beta_1 + (\beta_4 + \beta_5) * x$$

$$\mu_2 = \beta_0 + \beta_2 + (\beta_4 + \beta_6) * x$$

$$\mu_3 = \beta_0 + \beta_3 + (\beta_4 + \beta_7) * x$$

**Equations 5. 4**

The test of interaction boils down to an F-test of

H0:  $\beta_5 = \beta_6 = \beta_7 = 0$  (null hypothesis)

H1: not all 0 (research hypothesis)      On 3 and 9 numerator and denominator degrees of freedom (df)

The observed F-ratio for interaction is F=54.9, with a “p” value <0.0001 on 3 and 9 df. These values can be checked for the values obtained from SAS in section

8.3. The 'p' value obtained show significant values, indicating that the null hypothesis (H0) is valid as against the research hypothesis (H1). This means there is interaction between the two independent variables, namely the polymer concentration and the electric field on the throughput.

The model statement for determining the predicted throughput is given in equation 5.5. So, for example, if we want to predict the throughput at a given value of electric field (x) equal to 1.0 kV/cm and concentration 23 % under full model can be written as,

$$\hat{Y} = \hat{\beta}_0 + \hat{\beta}_1(c1) + \hat{\beta}_2(c2) + \hat{\beta}_3(c3) + [\hat{\beta}_4 + \hat{\beta}_5(c1) + \hat{\beta}_6(c2) + \hat{\beta}_7(c3)] * X$$

**Equation 5. 5**

$$\hat{Y} = \hat{\beta}_0 + \hat{\beta}_1(0) + \hat{\beta}_2(1) + \hat{\beta}_3(0) + [\hat{\beta}_4 + \hat{\beta}_5(0) + \hat{\beta}_6(1) + \hat{\beta}_7(0)] * 1$$

The value of  $\hat{Y}$ , the predicted throughput can be obtained if we plug in respective values (8.3) in the above equation. Figure 5.13 shows the relationship between observed throughput and predicted throughput.

$$\hat{Y} = -9.37 - 44.57 + 64.07 + 66.97 * 1 = 77.11 \text{ g/hr}$$

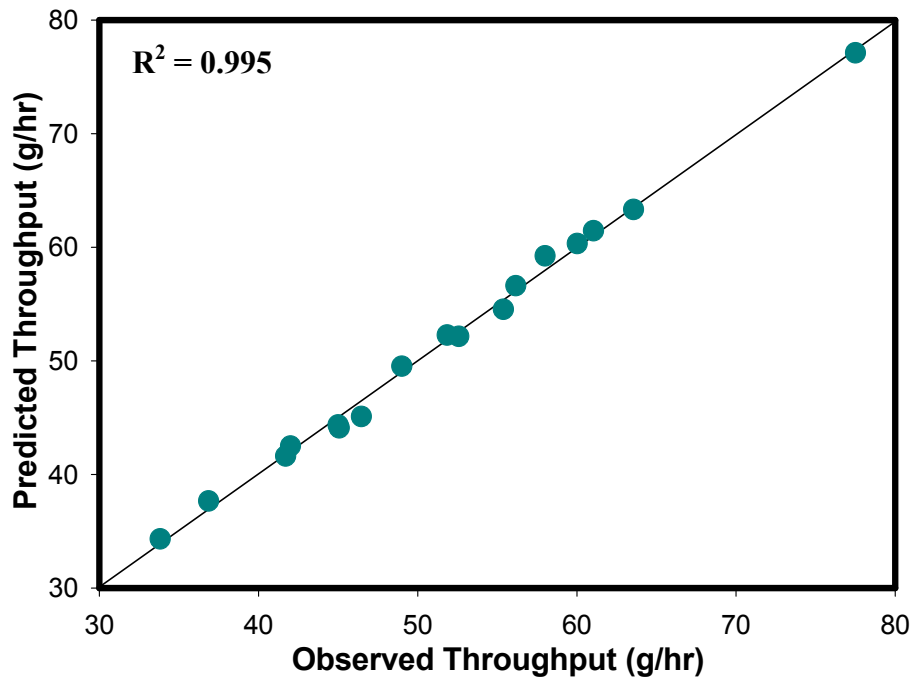


**Figure 5. 13: Plot showing the relationship between observed throughput and predicted throughput**

### 5.3 Fiber Orientation Distribution

Figures 5.14 – 5.17 show the results of fiber orientation distribution as impacted by the electric field and concentration. The figures indicate that as we increase the electric field by keeping polymeric concentration constant, the fibers are more oriented towards the machine direction. Measured or generated data can be grouped into bins, i.e., discretized by classifying into groups each characterized by a range of values in characteristic variables. The resulting graphical representation shows the distribution of fibers in percentage in terms of fiber orientation angle.

In general, because of the movement of the drum, the fibers tend to orient themselves in the machine direction. But in the case of electrospinning, one more factor comes into picture i.e., the draw force. As we increase the electric field, more molecules are split and it is easier for the polymer solution to flow through the spinneret. Higher electric field means higher draw force resulting from the drum surface. Thus the fibers are forced to flow in the direction of rotation of the drum.

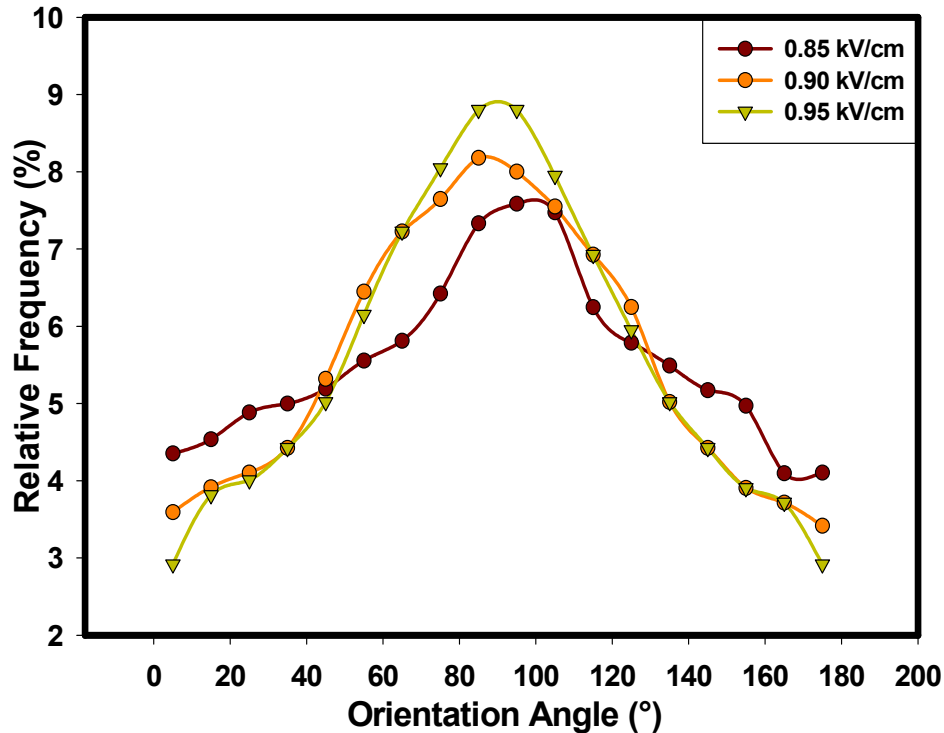
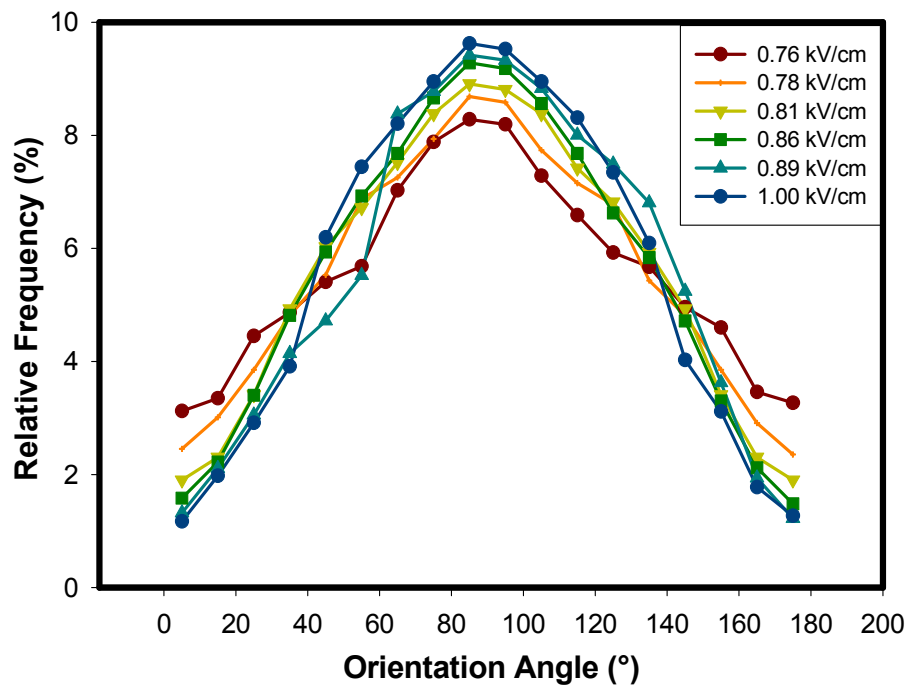
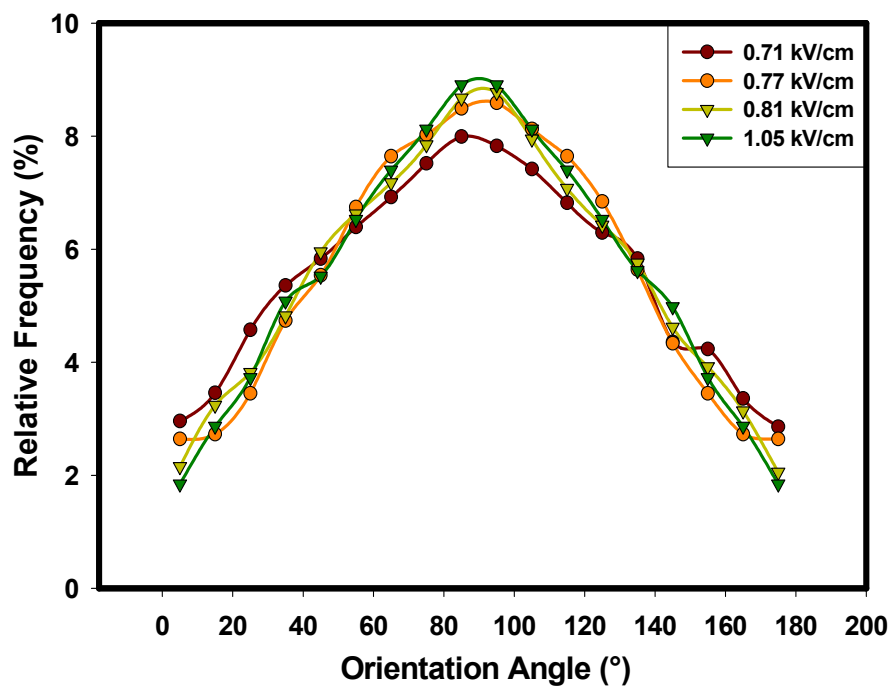


Figure 5. 14: Orientation distribution function of an electrospun sample at a constant concentration of 21% with varying electric fields



**Figure 5. 15: Orientation distribution function of an electrospun sample at a constant concentration of 23% with varying electric fields**



**Figure 5. 16: Orientation distribution function of an electrospun sample at a constant concentration of 25% with varying electric fields**



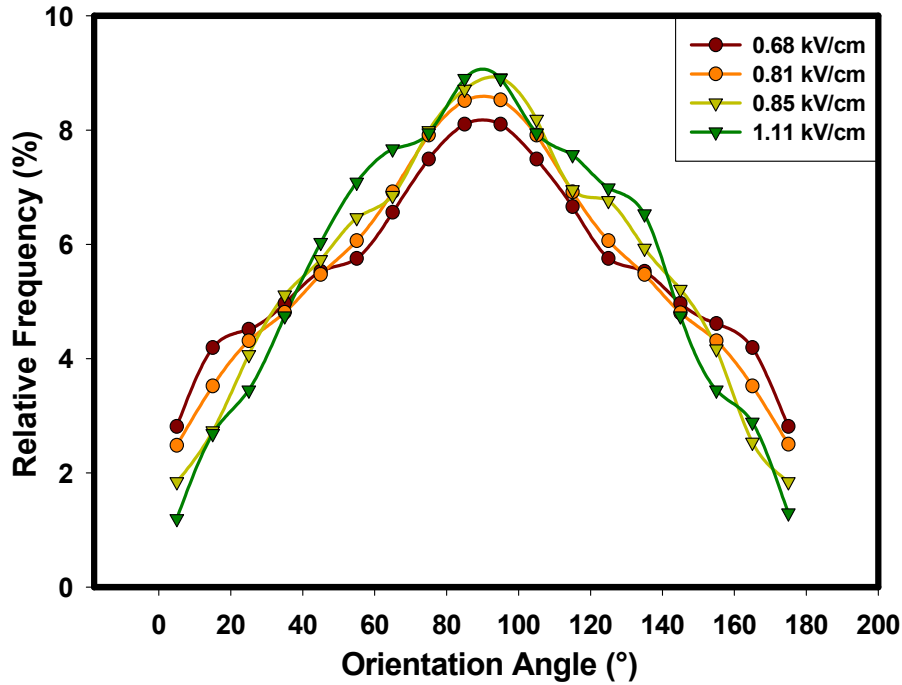


**Figure 5. 17: Orientation distribution function of an electrospun sample at a constant concentration of 27% with varying electric fields**

It can be said that if the target was stationary, the orientation of the fibers would have been completely random. But in this case since we have a source to carry the fibers splayed, the fibers tend to orient in the direction in which the target turns/rotates. The effect of orientation of fibers towards the machine direction at increased electric field can be seen from the SEM images of Figures 5.18 and 5.19. These are the SEM pictures of 25 % concentration at 0.714 kV/cm and 0.809 kV/cm respectively, and there is a considerable difference in the orientation of fibers. Although the fibers at 0.714 kV/cm electric field are oriented towards machine direction, it is more oriented towards machine direction at 0.809 kV/cm.

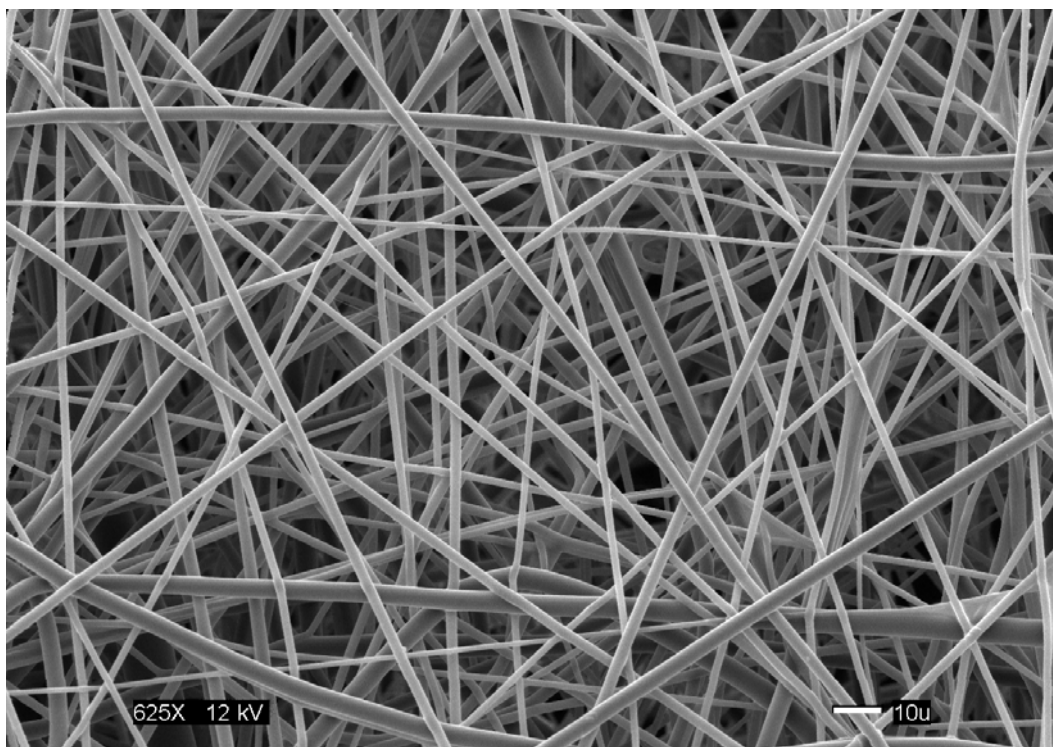


**Figure 5. 18: SEM image of electrospun web formed at Polymer Concentration 25 %, Voltage 15 kV, Distance 21 cm. (0.714 kV/cm) [Measurement Environment: Philips 505 T, Magnification 625x, Voltage 12 kV]**

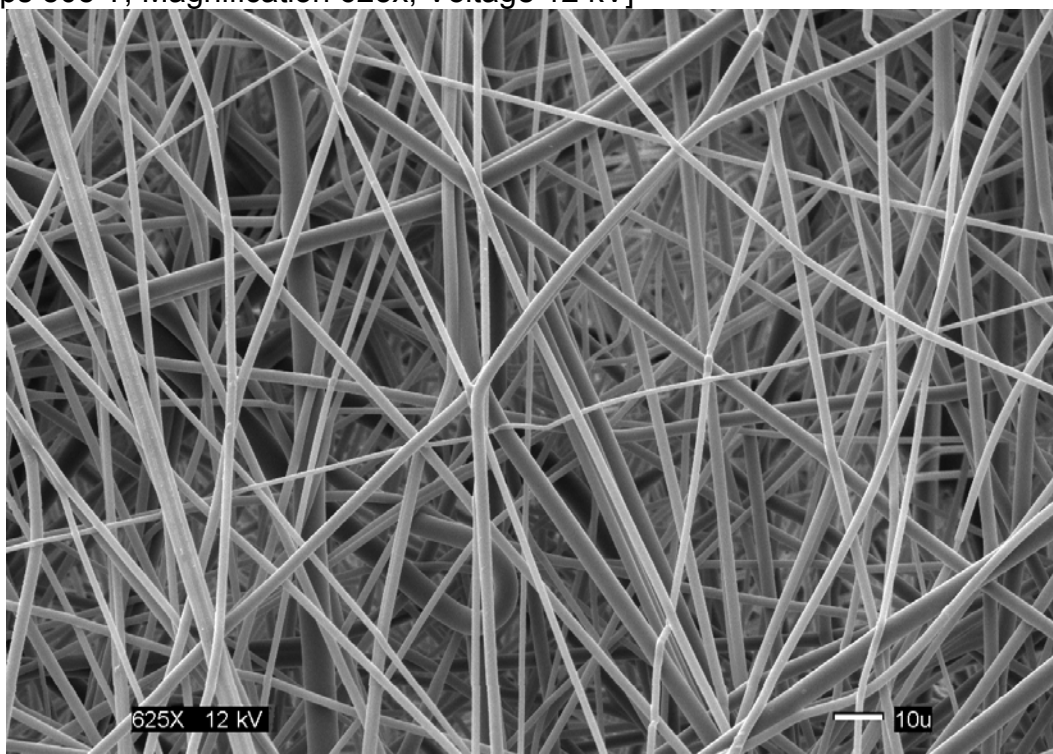


**Figure 5. 19: SEM image of electrospun web formed at Polymer Concentration 25 %, Voltage 17 kV, Distance 21 cm. (0.809 kV/cm) [Measurement Environment: Philips 505 T, Magnification 625x, Voltage 12 kV]**

### 5.3.1 Anisotropy Ratio

Anisotropy ratio may be defined as the ratio of a parameter measured in machine direction to the parameter measured in the cross direction. In this case it is defined as the ratio of relative frequency of fibers in machine direction to the relative frequency of fibers in the cross direction [52]. The anisotropy value of 1 or near 1 indicates that the orientation of fibers is random (or bimodal). Anisotropy values above 1 indicate that the orientation of fibers in machine direction is more than that of cross direction.

The anisotropy data (Figure 5.20) indicates that as the electric field is increased by keeping a constant concentration of the polymer solution there is a considerable increase in the anisotropy level. This indicates that at lower electric field, the fibers are laid somewhat random, whereas at higher electric fields, the fibers are laid more parallel and they are oriented towards the machine direction.

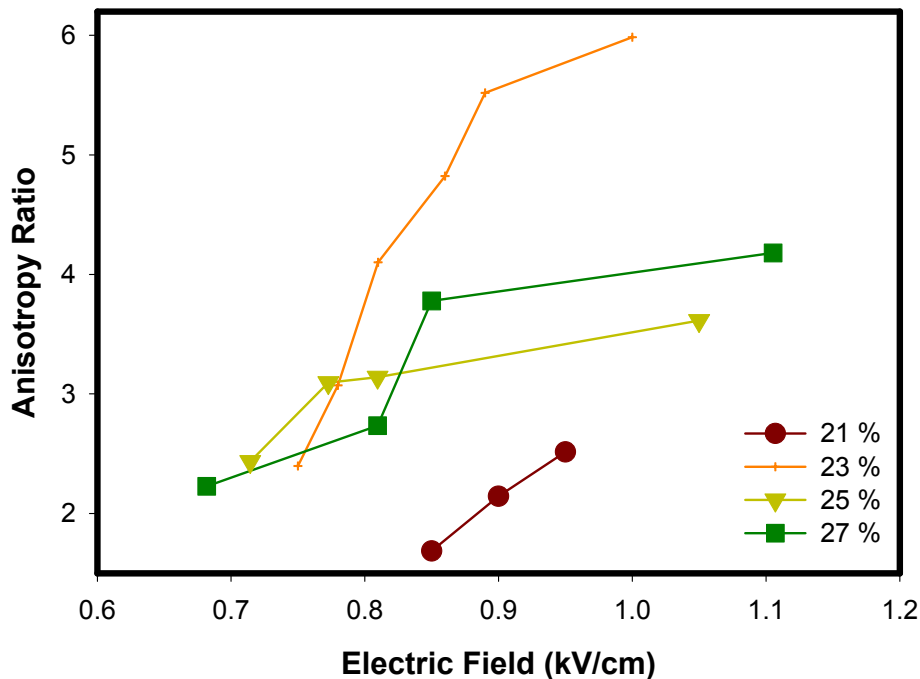


**Figure 5. 20: Effect of electric field and concentration on the anisotropy ratio of an electrospun fiberweb**

Statistical analysis was done for the anisotropy ratio, emphasizing the effect of electric field under different polymeric concentrations of the solution. The

statistical analysis software (SAS) by default takes the last entry as the baseline and here it is the data of 27 % polymer concentration. Therefore, the baseline statement for the model will be,

$$\mu_4 = \beta_0 + \beta_4 x$$

And the remaining statements can be written as,

$$\mu_1 = \beta_0 + \beta_1 + (\beta_4 + \beta_5) * x$$

$$\mu_2 = \beta_0 + \beta_2 + (\beta_4 + \beta_6) * x$$

$$\mu_3 = \beta_0 + \beta_3 + (\beta_4 + \beta_7) * x$$

#### Equation 5. 6

The test of interaction boils down to an F-test of

H0:  $\beta_5 = \beta_6 = \beta_7 = 0$  (null hypothesis)

H1: not all 0 (research hypothesis) On 3 and 9 degrees of freedom (df)

At 95 % confidence limit, the 'p' value at  $F = 15.55$  is 0.0002. These values can be checked for the values obtained from SAS in section 8.4. The 'p' value obtained show significant values, indicating that the null hypothesis (H0) is valid as against the research hypothesis (H1). This means there is interaction between the two independent variables, namely the polymer concentration and the electric field on the anisotropy level.

The model statement for determining the predicted anisotropy ratio is given in equation 5.7. So, for example, if we want to predict the anisotropy ratio at a given value of electric field (x) equal to 1.0 kV/cm and concentration 23 % under full model can be written as,

$$\hat{Y} = \hat{\beta}_0 + \hat{\beta}_1(c1) + \hat{\beta}_2(c2) + \hat{\beta}_3(c3) + [\hat{\beta}_4 + \hat{\beta}_5(c1) + \hat{\beta}_6(c2) + \hat{\beta}_7(c3)] * X$$

#### Equation 5. 7

$$\hat{Y} = \hat{\beta}_0 + \hat{\beta}_1(0) + \hat{\beta}_2(1) + \hat{\beta}_3(0) + [\hat{\beta}_4 + \hat{\beta}_5(0) + \hat{\beta}_6(1) + \hat{\beta}_7(0)] * 1$$

The value of  $\hat{Y}$ , the predicted anisotropy ratio can be obtained if we plug in respective values (8.4) in the above equation. Figure 5.21 shows the relationship between observed anisotropy and predicted anisotropy ratio.

$$\hat{Y} = -0.637 - 7.366 + 4.48 + 10.04 * 1 = 6.519$$

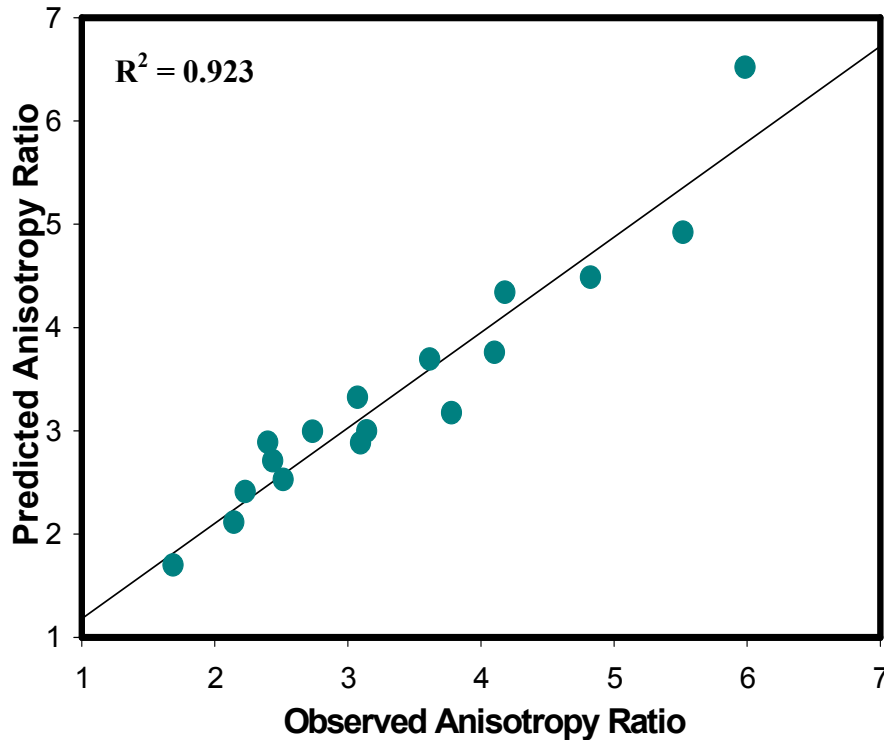


**Figure 5. 21: Plot showing the relationship between observed anisotropy ratio and predicted anisotropy ratio**

#### **5.4 Pore Size and its distribution**

The control of the pore of electrospun web is of prime importance in the fabrics that are being produced for the purposes of fluid flow and filtration.

##### **5.4.1 Mean Flow Pore Size**

As mentioned in the experimental chapter that a saturated sample will pass air when the applied pressure exceeds the capillary attraction of the fluid in the pores. Smaller pores have a higher capillary attraction than larger pores and hence open at higher pressures. By increasing pressure in small steps, it is possible to determine by the flow contribution of very small pore size increments. The pressure at which wet flow is one-half the dry flow is used to calculate the mean flow pore size.

Average pore diameter and basis weights are plotted together against electric field in Figures 5.22 - 5.24. The figures show that increased electric field results in

decreased average pore diameter and increased basis weight. It can also be observed that the samples produced at increased concentration of the polymer solution and by maintaining the range of electric fields specified the average pore diameter also increases. The analyzed samples of concentrations 23% (average pore diameter – 14.25  $\mu\text{m}$ ), 25% (average pore diameter – 15.72  $\mu\text{m}$ ) and 27% (average pore diameter – 17.02  $\mu\text{m}$ ) explains the above property. As has been explained earlier, the weight of the sample is more at higher electric fields. This is because there is higher draw force of the solution at higher electric field, which actually splits the aggregated molecules within the solution. Higher polymer solution coming out of the spinneret causes higher formation of electrospun fibers, which results in increased fiberweb weight. Since there are more fibers at higher electric field the fiber coverage is more in the fiberweb. Increased coverage means that there is high resistance for any fluid to pass through this web, which tells that the average pore diameter is less. This behavior as expected is observed for all polymer concentrations.

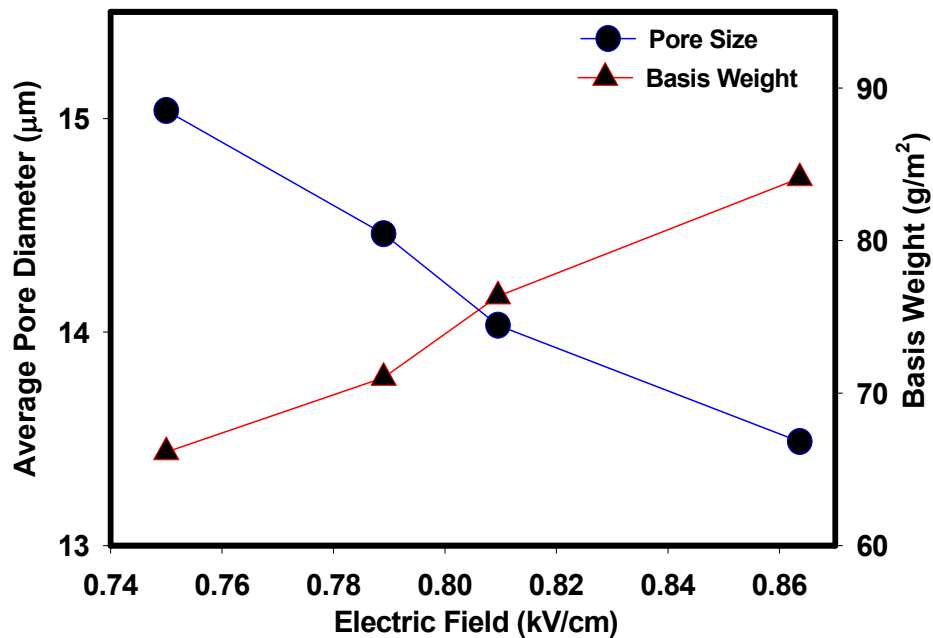


**Figure 5. 22: Effect of average pore diameter and basis weight with varying electric field at constant concentration 23%**

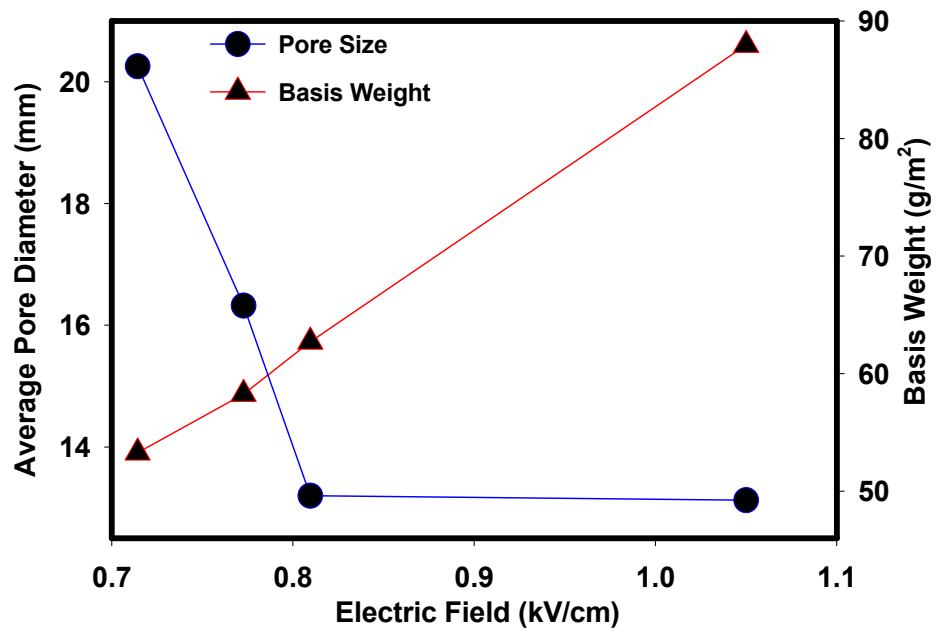


Figure 5. 23: Effect of average pore diameter and basis weight with varying electric field at constant concentration 25%

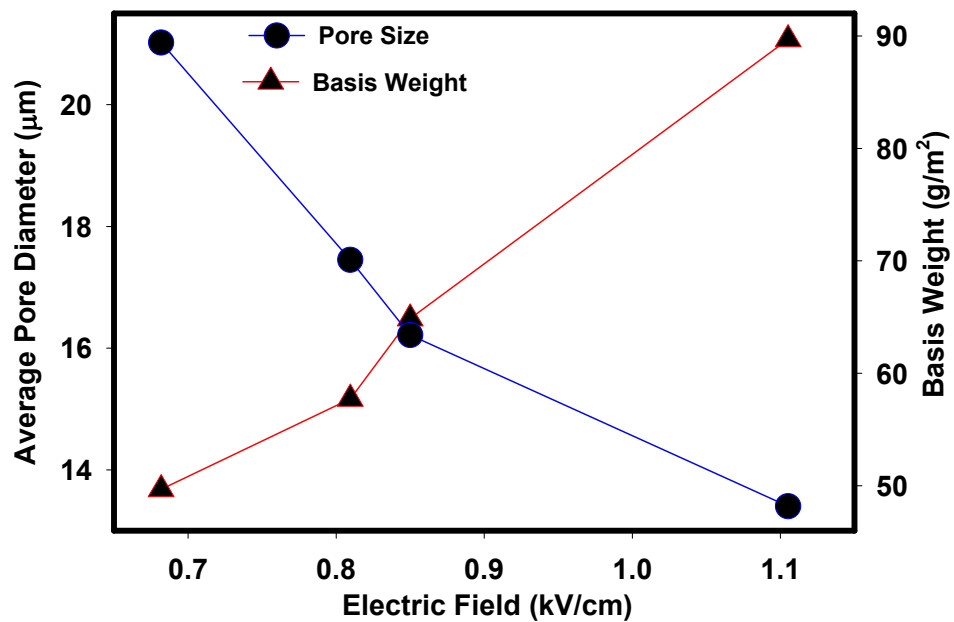
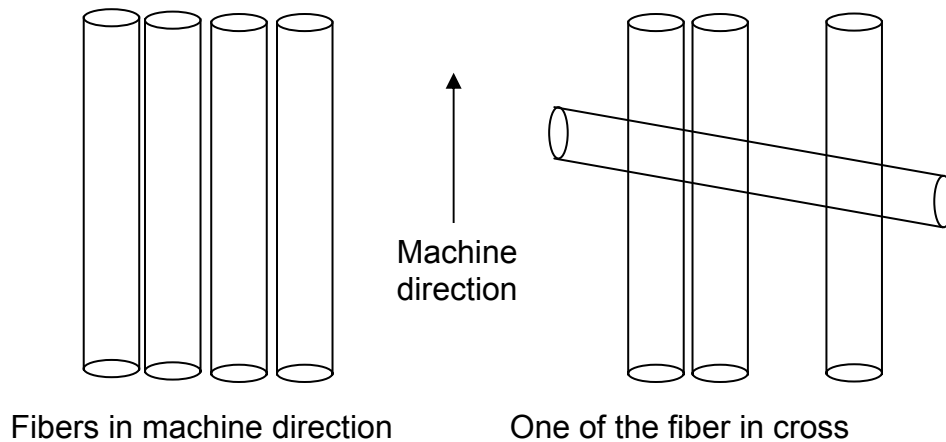


Figure 5. 24: Effect of average pore diameter and basis weight with varying electric field at constant concentration 27%

To understand the pore size, analyzing basis weight does not give full information. It may so happen that bigger diameter fibers are the cause for higher basis weight, in which case the average pore diameter should increase at higher electric field. So, to know the pore size better, orientation of fibers and fiber diameter should be explained.

Orientation of fibers in a fiberweb affects largely on the pore size distribution. Fibers splayed at lower electric field are more random, whereas at higher electric fields, the fibers are splayed in a preferential direction. That means at higher level of electric field, the fibers are laid more parallel and they are oriented towards the machine direction. Understanding the fiber orientation distribution will help in characterizing the pore size measurement. Fiberweb sample having more fibers oriented towards the machine direction will have more cover. From Figure 5.25, it can be observed that, web with fibers perfectly oriented in the machine direction have more cover than web with fibers oriented in the machine direction and other direction. So it becomes extremely important for understanding and analyzing the fiber orientation in an electrospun fabric.



**Figure 5. 25: Pictorial of fibers arranged in an electrospun web**

Figures 5.26 – 5.28 show the effect of anisotropy and average pore diameter on varying electric field, and as expected, the anisotropy level increases at increased electric field indicating that the fibers are oriented towards the preferential direction i.e., the machine direction. This effect can be seen from Figures 5.29 and 5.30. It shows random orientation has more pores than machine oriented fibers in a fiberweb.



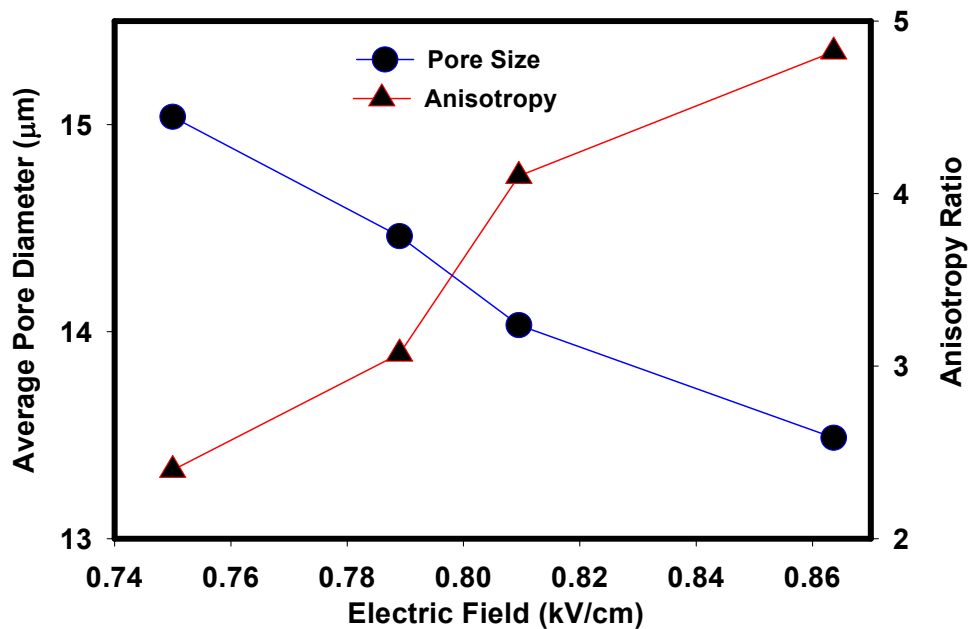


Figure 5. 26: Effect of average pore diameter and anisotropy on a four-layered sample with varying electric field at constant concentration 23%

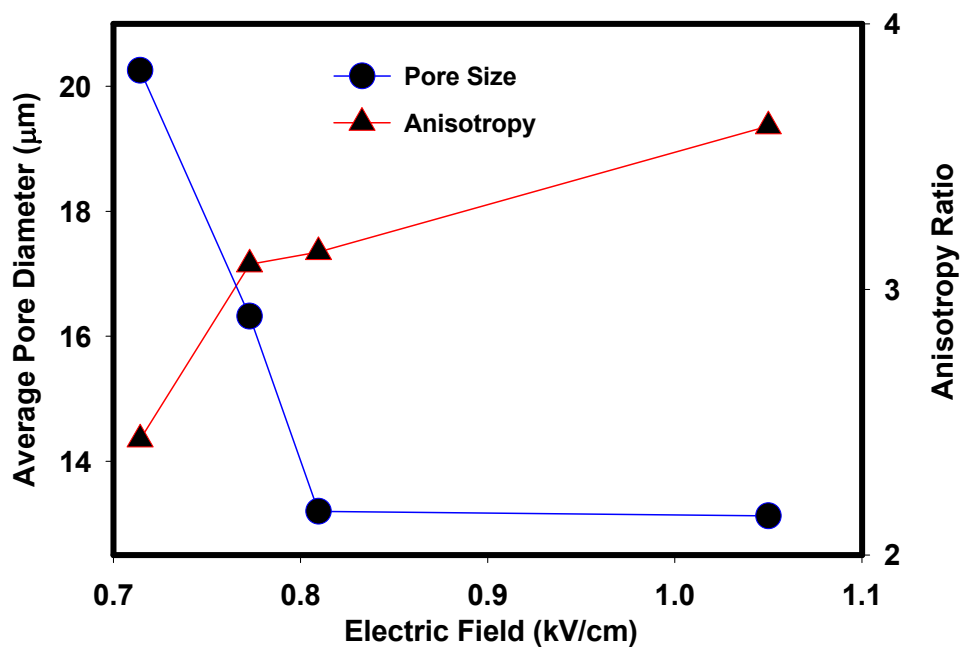
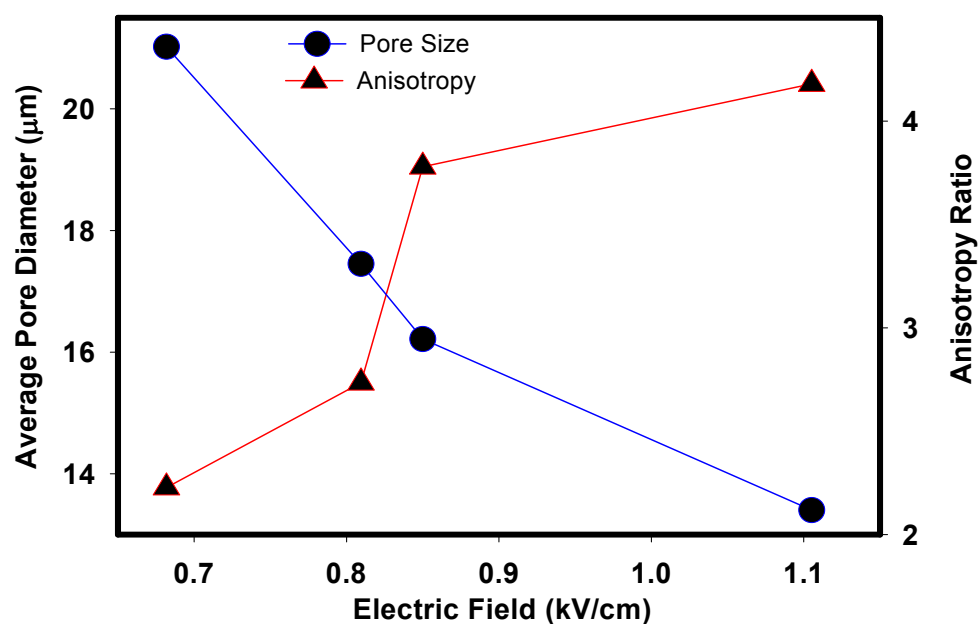
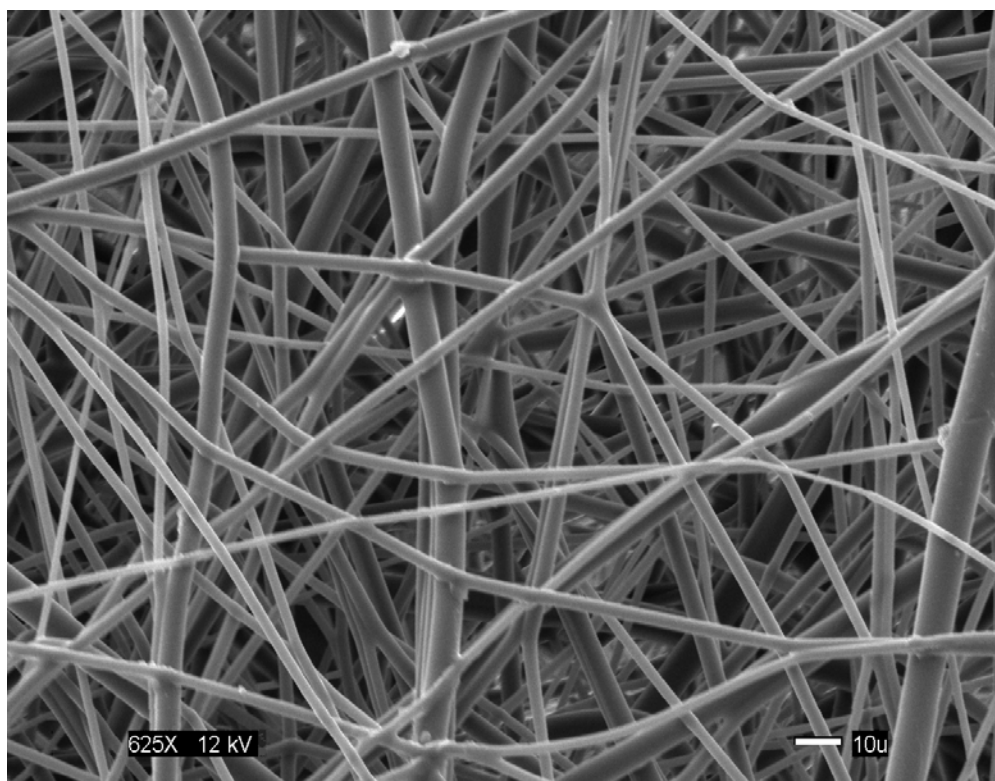


Figure 5. 27: Effect of average pore diameter and anisotropy on a four-layered sample with varying electric field at constant concentration 25%



**Figure 5. 28: Effect of average pore diameter and anisotropy on a four-layered sample with varying electric field at constant concentration 27%**



**Figure 5. 29: SEM image of electrospun web formed at Polymer Concentration 23 %, Voltage 15 kV, Distance 20 cm. (0.75 kV/cm) [Measurement Environment: Philips 505 T, Magnification 625x, Voltage 12 kV]**

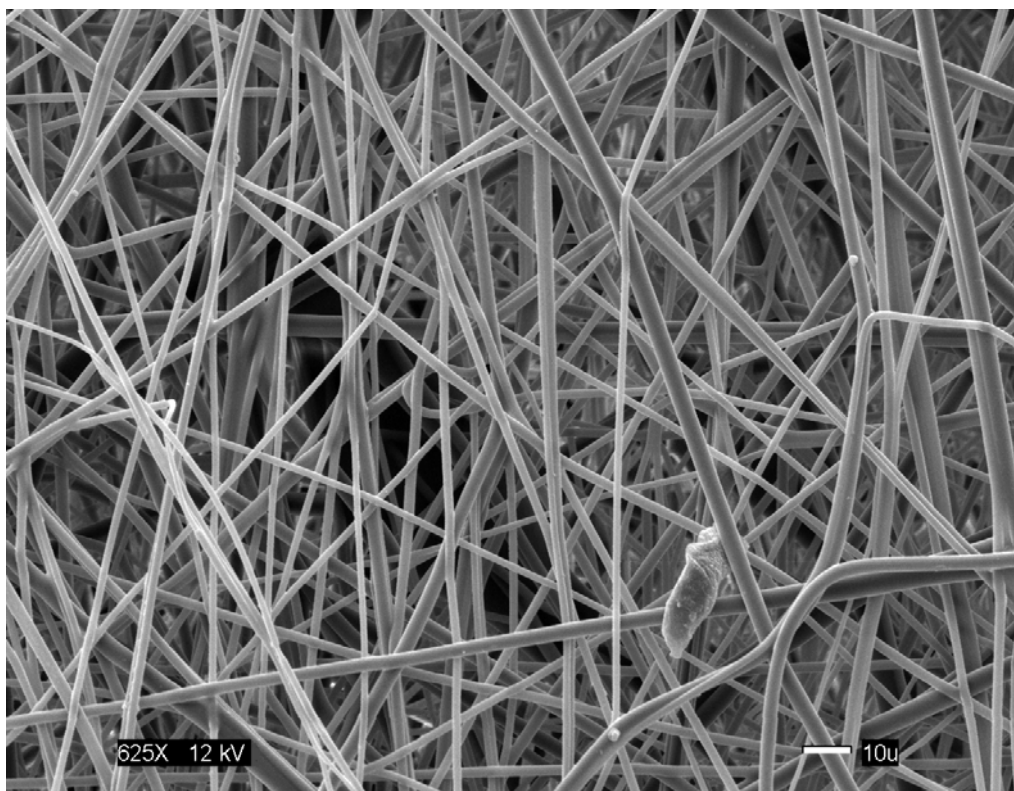


**Figure 5. 30: SEM image of electrospun web formed at Polymer Concentration 23 %, Voltage 19 kV, Distance 22 cm. (0.863 kV/cm) [Measurement Environment: Philips 505 T, Magnification 625x, Voltage 12 kV]**

It has been observed from Figures 5.5 – 5.8 that as the electric field increase, the average diameter of the fibers decrease, thus the surface area or coverage increases which results in having lower mean flow pore diameter. This can be explained with a logical reasoning that bigger the pore diameter, lesser mean flow pressure is required, that is the webs have a higher mean flow pore diameter. Figures 5.31 – 5.33 are plotted for constant polymer concentration with varying electric field against average pore diameter and average fiber diameter. If the diameter of the fibers decreases, the number of fibers in a given area will be more, because of more polymer solution coming out of the spinneret due to higher draw force. This will increase the cover of the fiberweb, resulting in decrease in average pore diameter. Figures 5.34 and 5.35 show this effect, showing SEM pictures of 27 % polymer concentration and 0.681 kV/cm and 1.105 kV/cm electric field respectively. These explain our discussion that both pore diameter and fiber diameter decrease at increasing electric field.

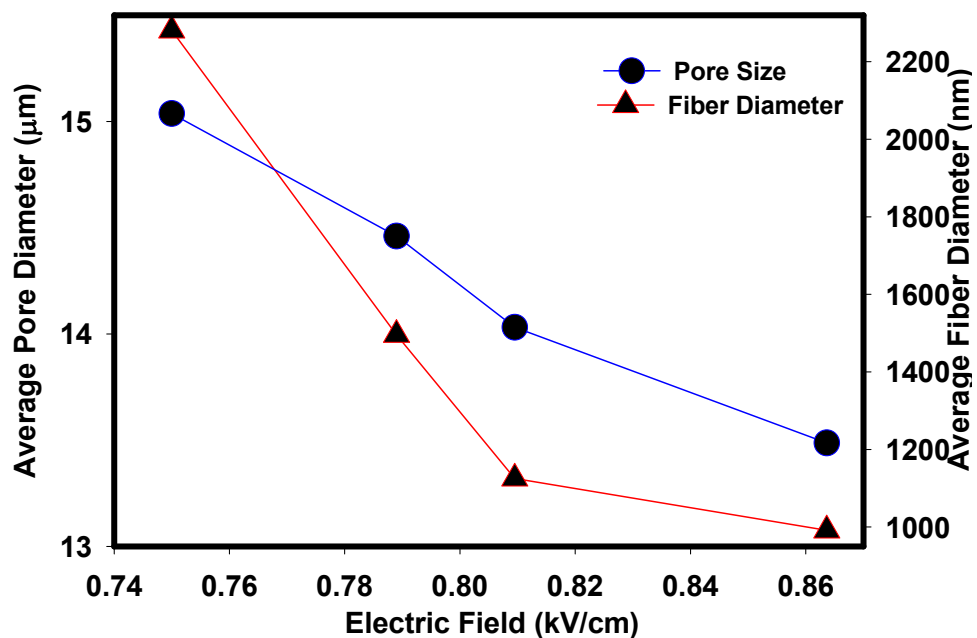


Figure 5. 31: Effect of average pore diameter and fiber diameter with varying electric field at constant concentration 23%

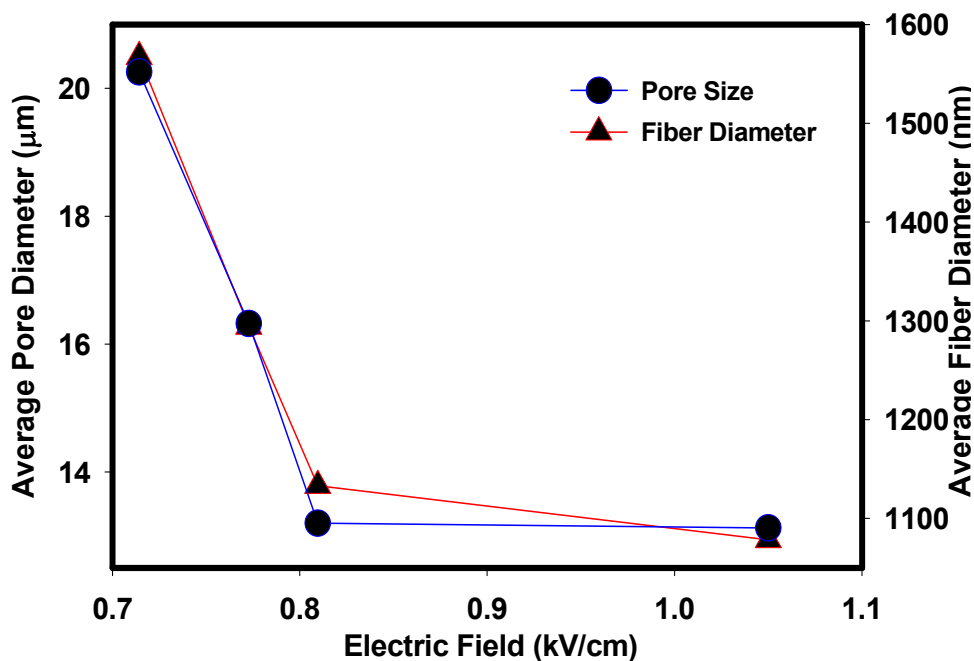


Figure 5. 32: Effect of average pore diameter and fiber diameter with varying electric field at constant concentration 25%

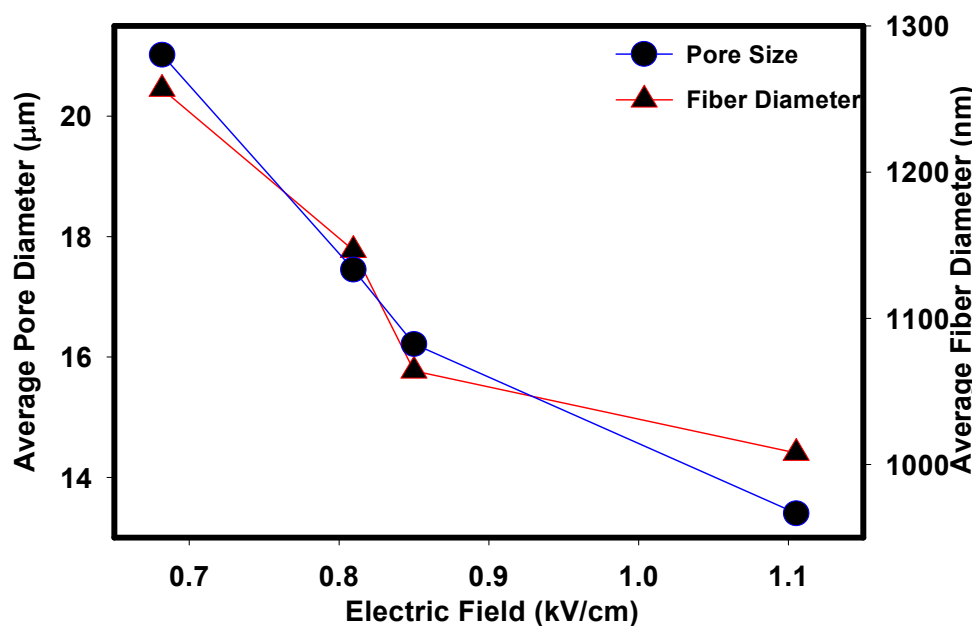


Figure 5. 33: Effect of average pore diameter and fiber diameter with varying electric field at constant concentration 27%

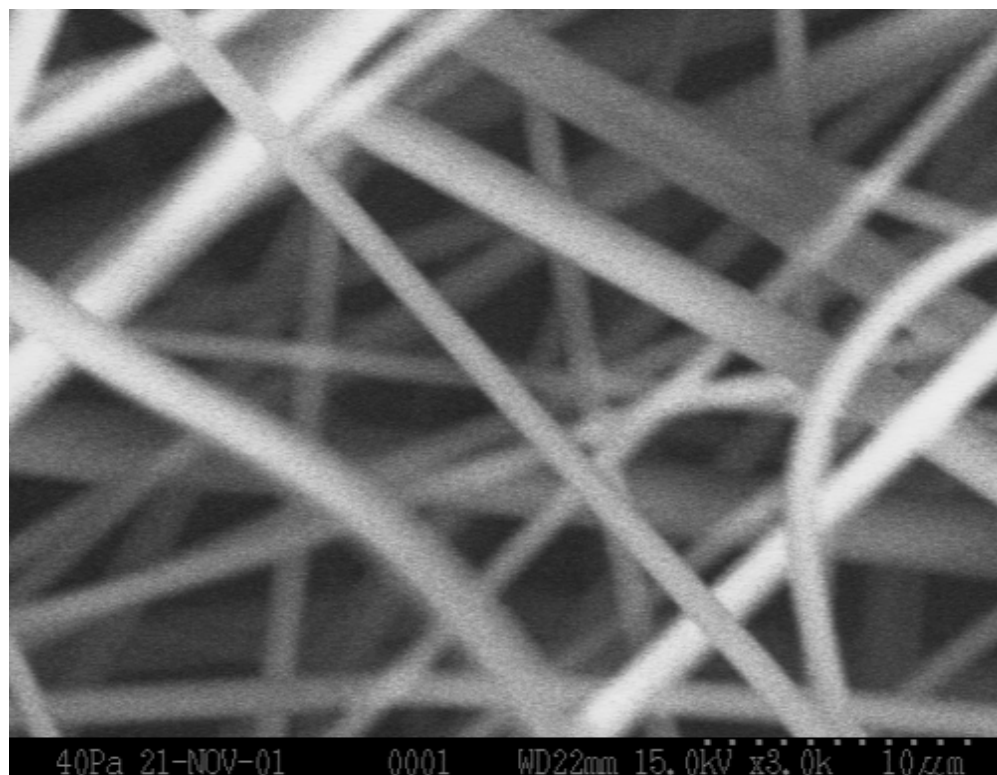
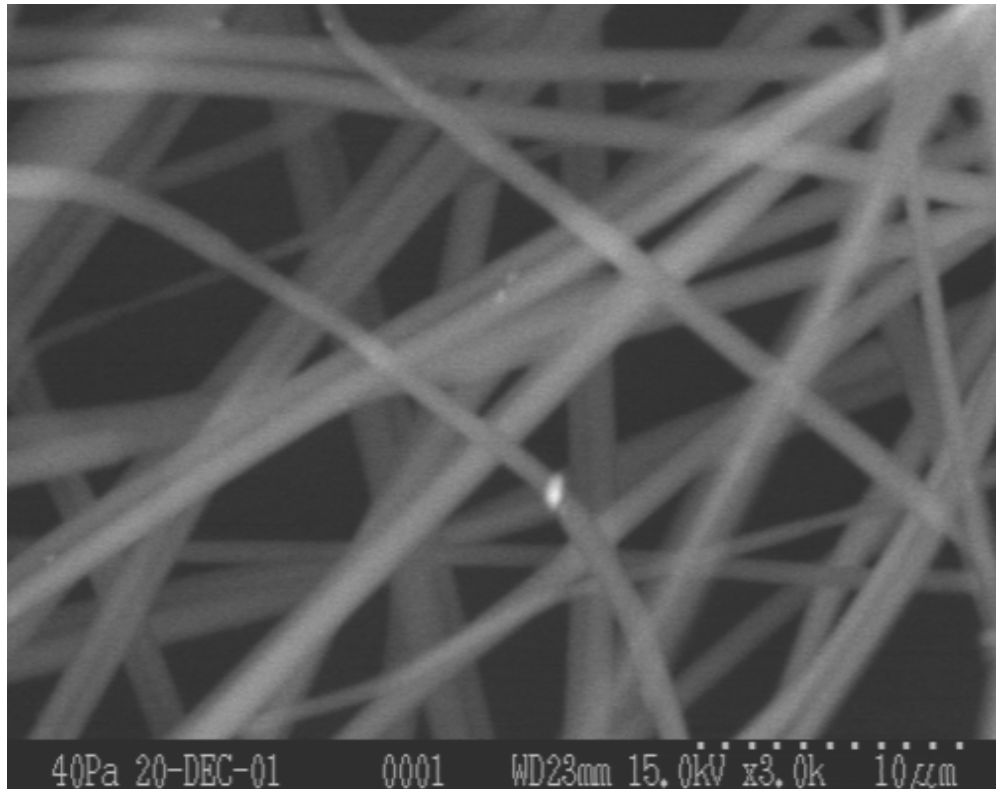


Figure 5. 34: SEM image of electrospun web formed at Polymer Concentration 27 %, Voltage 17 kV, Distance 20 cm. (0.85 kV/cm) [Measurement Environment: Hitachi ESEM S 3200, Air pressure 40 Pa, Magnification 3000x, Voltage 15 kV, Work distance 22 mm]



**Figure 5. 35: SEM image of electrospun web formed at Polymer Concentration 27 %, Voltage 21 kV, Distance 19 cm. (1.105 kV/cm)** [Measurement Environment: Hitachi ESEM S 3200, Air pressure 40 Pa, Magnification 3000x, Voltage 15 kV, Work distance 23 mm]

The statistical analysis investigates associations between average pore diameter, average fiber diameter, anisotropy ratio and the process parameters electric field and polymer concentration. Previous analyses indicated quadratic and linear dependencies of average fiber diameter on electric field, depending on the level of concentrations. Associations can also be seen for the other two responses, average pore diameter and anisotropy ratio, in the plot below.

The plots indicate that average pore diameter (Figure 5.36) and average fiber diameter (Figure 5.1) are decreasing in electric field, while anisotropy ratio (Figure 5.20) is increasing in electric field. For average pore diameter, a test of a single quadratic profile with different intercepts (reduced model) against an interaction model, with different quadratic profiles for the three concentrations (full model) is statistically significant ( $F = 14.49$ ;  $p = 0.0265$ ;  $df = 4; 3$ ). The full model, based on observations at four electric fields for each of three concentrations, explains more than 99% of the observed variation.

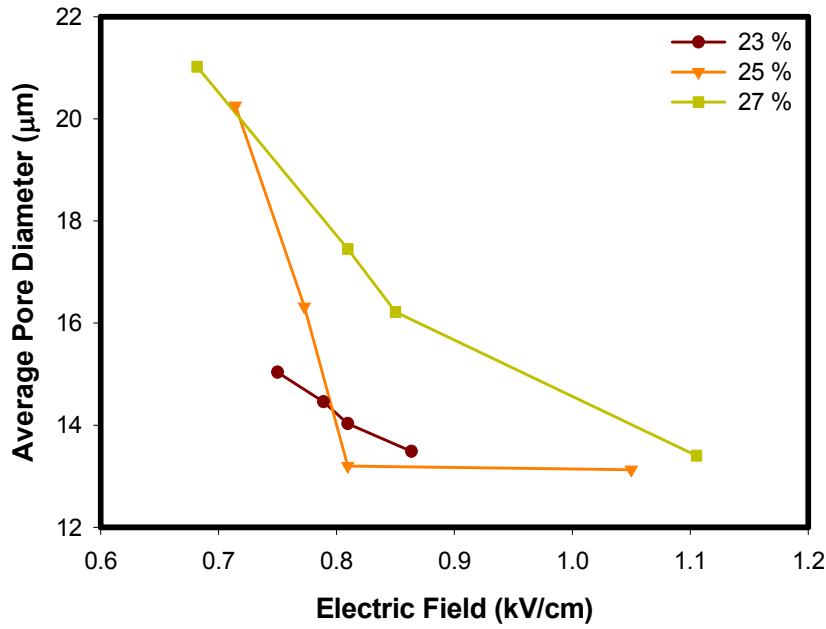


**Figure 5. 36: Effect of electric field and concentration on the average pore diameter of an electrospun fiberweb**

The general linear model procedure used to obtain the ANOVA table by considering average pore diameter as the dependent variable can be seen from output in section 8.5. The 'p' value of 0.0034 indicates that the research hypothesis is significant.

The associations between the response anisotropy ratio and the process parameters electric field and concentration is more difficult to model, as the anisotropy ratio profile in electric field appears s-shaped for fixed concentration. A quadratic model doesn't fit well, but a linear model with electric field and concentration interaction captures much of the variability in anisotropy ratio  $r^2 = 0.88$ . The output of this has been reported in section 8.6.

Partial correlation coefficients can be used to describe linear associations between pairs of response variables after accounting for effects due to electric field and concentration. The squared partial correlation between average pore diameter (APD) and average fiber diameter (AFD) after accounting for electric field and concentration is  $r^2_{\{APD, AFD; \text{model}\}} = (0.46)^2 = 0.207$ . The squared partial correlation between average pore diameter and anisotropy ratio (AR) after accounting for electric field and concentration is  $r^2_{\{APD, AR; \text{model}\}} = (-0.11)^2 = 0.0127$ . Neither of these correlations are statistically significant. Though there is some evidence of marginal negative association between average pore diameter

and anisotropy ratio,  $r = -0.70$ ;  $p = 0.012$ , the linear association goes away after dependence on electric field and concentration are accounted for in the model. Partial correlations can be obtained in SAS using either the PCORR1 option within PROC REG or by generating the necessary residuals from the appropriate models and then using PROC CORR to get correlations. The outputs from both procedures are given in section 8.7.

#### 5.4.2 Pore Size Distribution

The distribution can be calculated by determining the wet and dry flows at the pressure limits from the wet and dry flow curves [83].

$$Q = \frac{WetFlow_h}{DryFlow_h} - \frac{WetFlow_l}{DryFlow_l} \times 100$$

**Equation 5. 8**

Where,

Q - filter flow percentage

l - lower pressure limit

h - higher pressure limit

$$D = \frac{Q - Q_L}{d_L - d}$$

**Equation 5. 9**

Where,

D - pore size distribution

Q - filter flow percentage

d - maximum pore diameter

L - previous value

It is evident that as the electric field is increased, the average pore diameter decreases and this is true for all concentrations of the polymer solution. All the samples produced were collected at a constant drum speed. The Pore size distribution depends largely on the basis weight (the number of layers in the



sample), orientation of fibers, and fiber diameter of the electrospun sample. It was observed that basis weight of the sample played a major role in the pore size distribution of the sample, wherein an increase in basis weight resulted in decrease of average pore diameter and decrease in basis weight resulted in increased average pore diameter. An analysis made on the sample produced at 23% concentration shows that samples with three layers (lower basis weight) had an average (weighted) pore diameter of 17.56  $\mu\text{m}$ , whereas samples with four layers (higher basis weight) had an average pore diameter of 14.6  $\mu\text{m}$ .

Increase in the layer of the fiberweb decreases the average pore size. Figure 5.37 plotted for average pore size against electric field for a constant polymer concentration of 23 %, shows the influence of two different layers namely three and four layers. Although the graph has been plotted for different electric fields, it can be observed that increase in fiberweb layer affects largely on the average pore diameter. It can be seen that at 0.809 kV/cm, the average pore diameter of a three-layered web has a pore diameter of 18.83  $\mu\text{m}$ , whereas it is 14.03  $\mu\text{m}$  for a four-layered web.

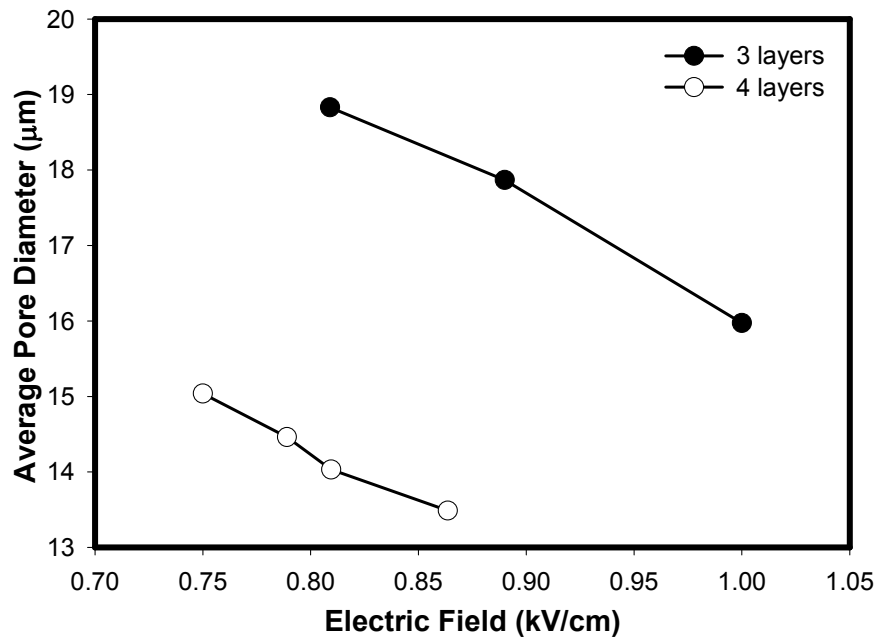


**Figure 5. 37: Influence of fiberweb layers on the average pore diameter at a constant concentration of 23 %**

Figures 5.38 – 5.42 show that there is a decrease in average pore diameter plotted against the cumulative filter flow percentage at increasing electric fields. The effect of decreased filter flow percentage at increasing electric field can be observed for all layers and all concentrations. Higher electric field, as explained earlier results in higher drawing force of the polymer solution, which in turn results in higher formation of fibers. Higher number of fibers means higher coverage in the web, which automatically results in lower average pore diameter and hence the filter flow. The cumulative filter flow measures the volume of air passed through the electrospun fabric sample at increased air pressures. All the cumulative filter flow graphs give the probability of the size of the particle that can pass through the web.

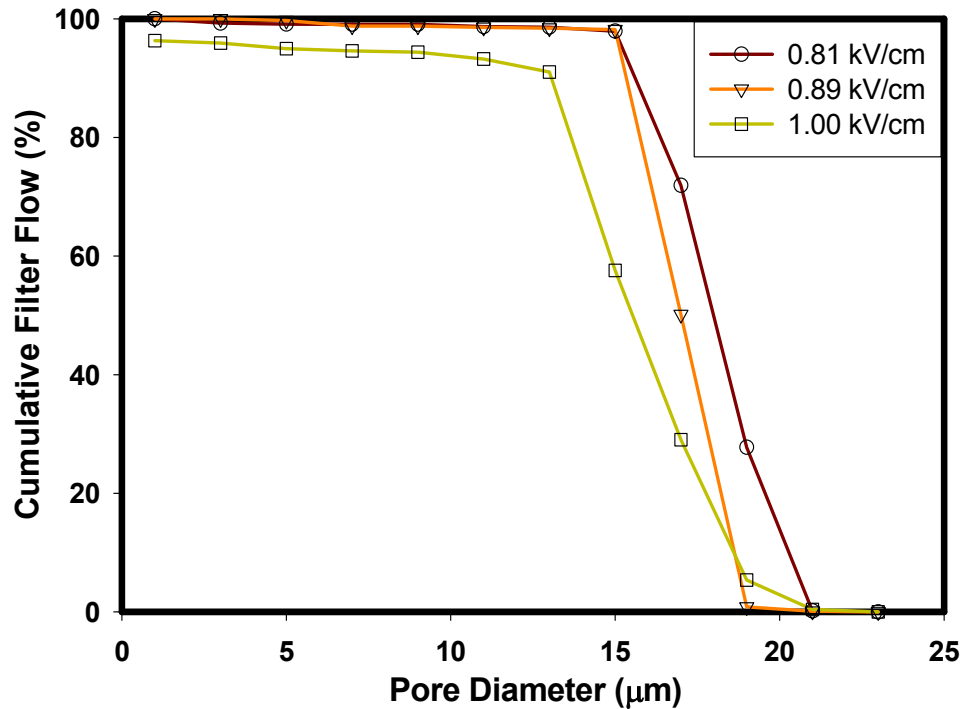


**Figure 5. 38: Effect of varying electric field on the cumulative filter flow at a constant concentration of 21% (3 layers)**

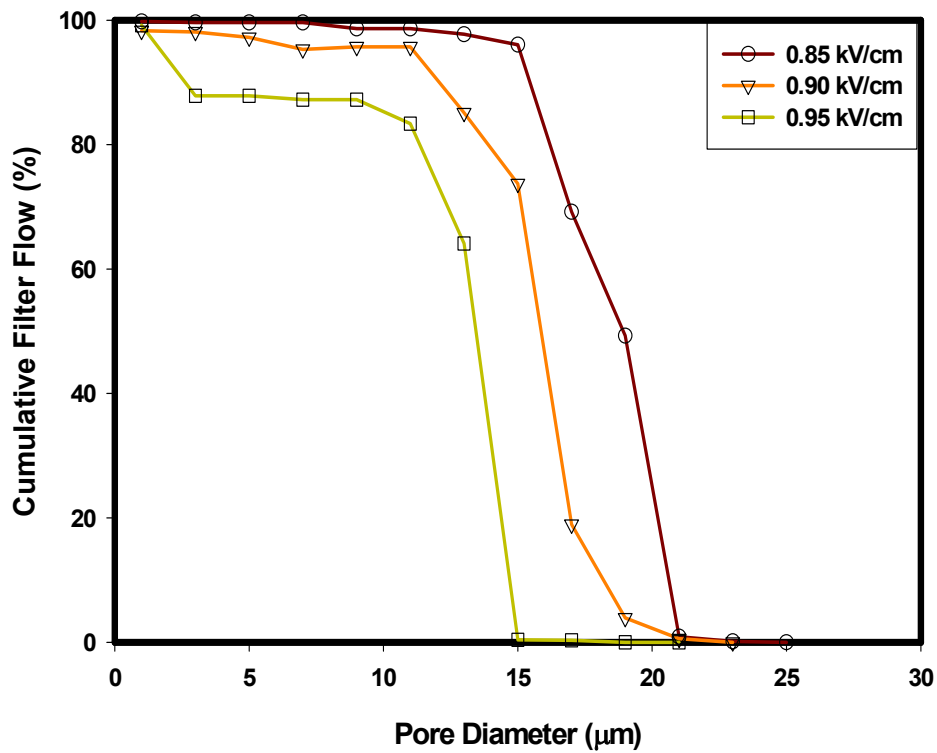


Figure 5. 39: Effect of varying electric field on the cumulative filter flow at a constant concentration of 23% (3 layers)

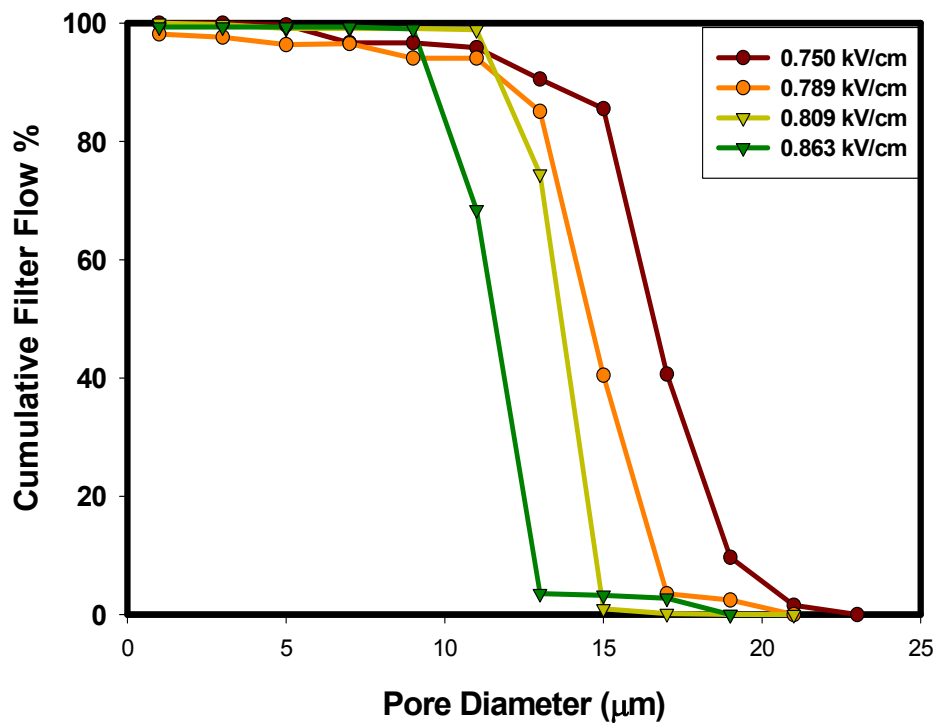


Figure 5. 40: Effect of varying electric field on the cumulative filter flow at a constant concentration of 23% (4 layers)

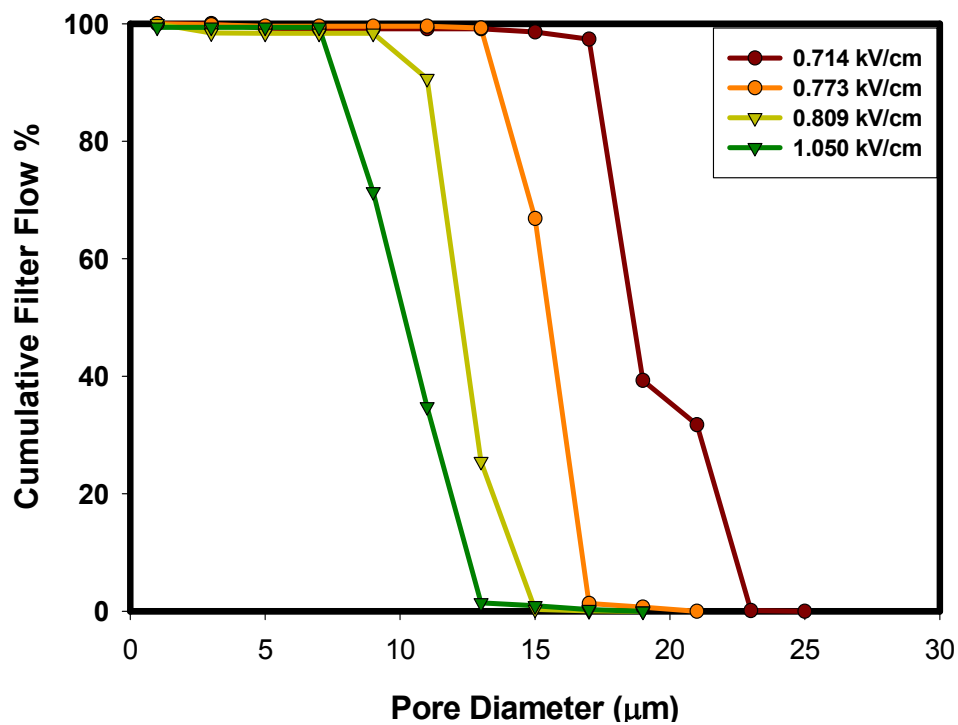


Figure 5. 41: Effect of varying electric field on the cumulative filter flow at a constant concentration of 25% (4 layers)

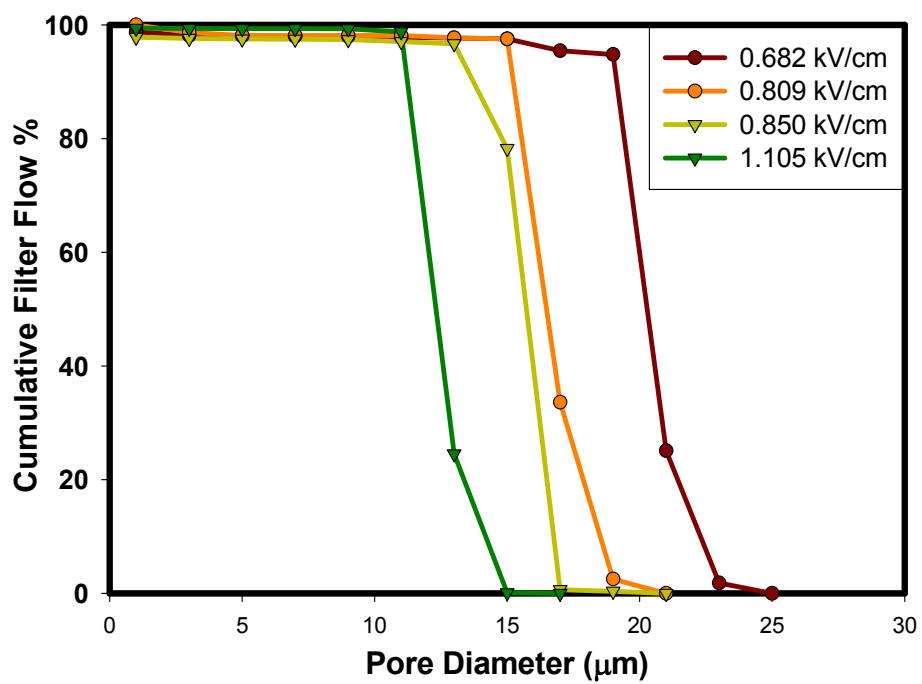
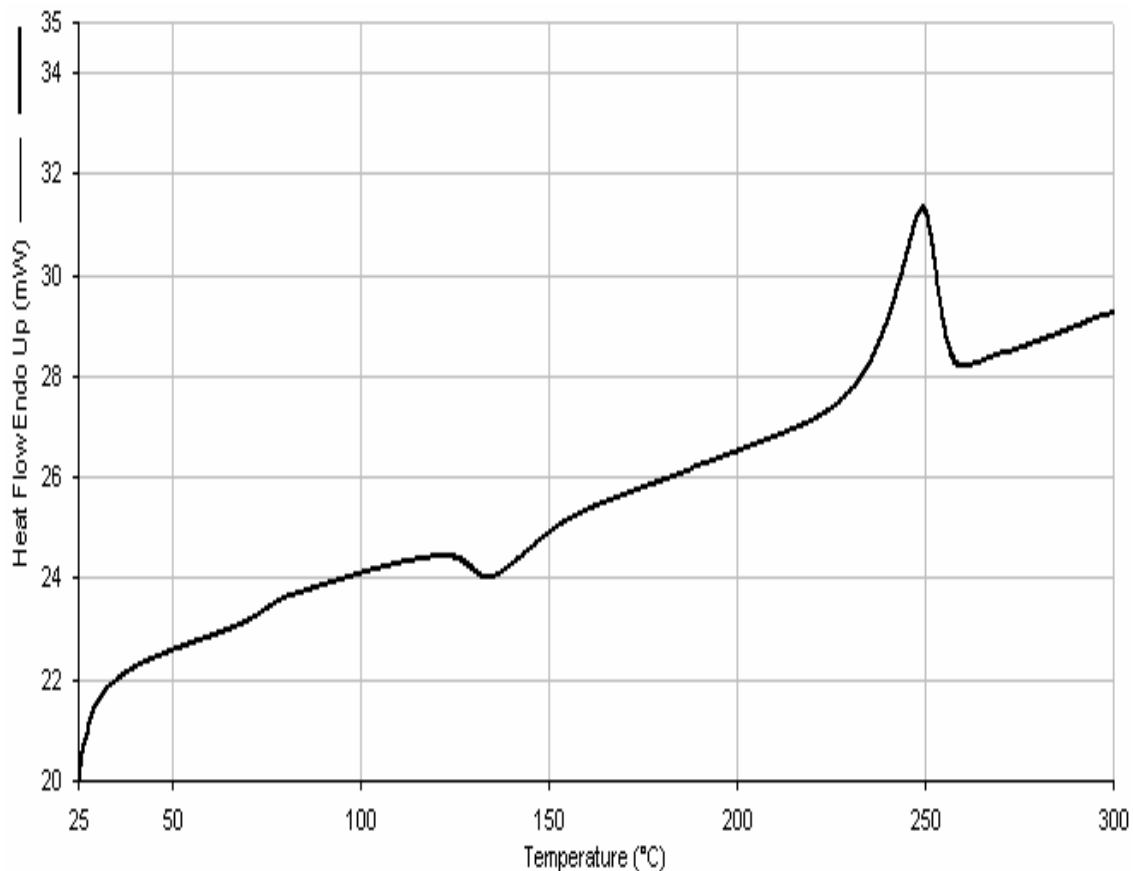


Figure 5. 42: Effect of varying electric field on the cumulative filter flow at a constant concentration of 27% (4 layers)

The effect showing the decreased pore distribution on increasing the electric field can also be explained by the graphs of pore diameter plotted against the normalized pore distribution. The analysis clearly indicates that as we increase the electric field, by keeping the concentration of the polymer solution constant the average pore diameter decreases. More fibers at given square area results in decreased pore size, thus increasing the filtration efficiency of the fabric sample.

### 5.5 Thermal Analysis by DSC

All the graphs were plotted for temperature °C (X-axis) against the heat flow, mW (Y-axis), except for the Crystallinity curve wherein it is plotted for time against the heat flow. The melting point, crystallization and glass transition temperature (Figure 5.43) indicates that the characteristic property of polyester is not hampered even after dissolving in methylene chloride and trifluoroacetic acid and even when processed at high voltage.



**Figure 5. 43: DSC Curve for Polyester**

The glass transition temperature was achieved at an onset temperature of 70.686°C. The glass transition temperature for the electrospun polyester sample can be seen in Figure 5.44. The inflection point is 75.40°C and the end point is 78.787°C.

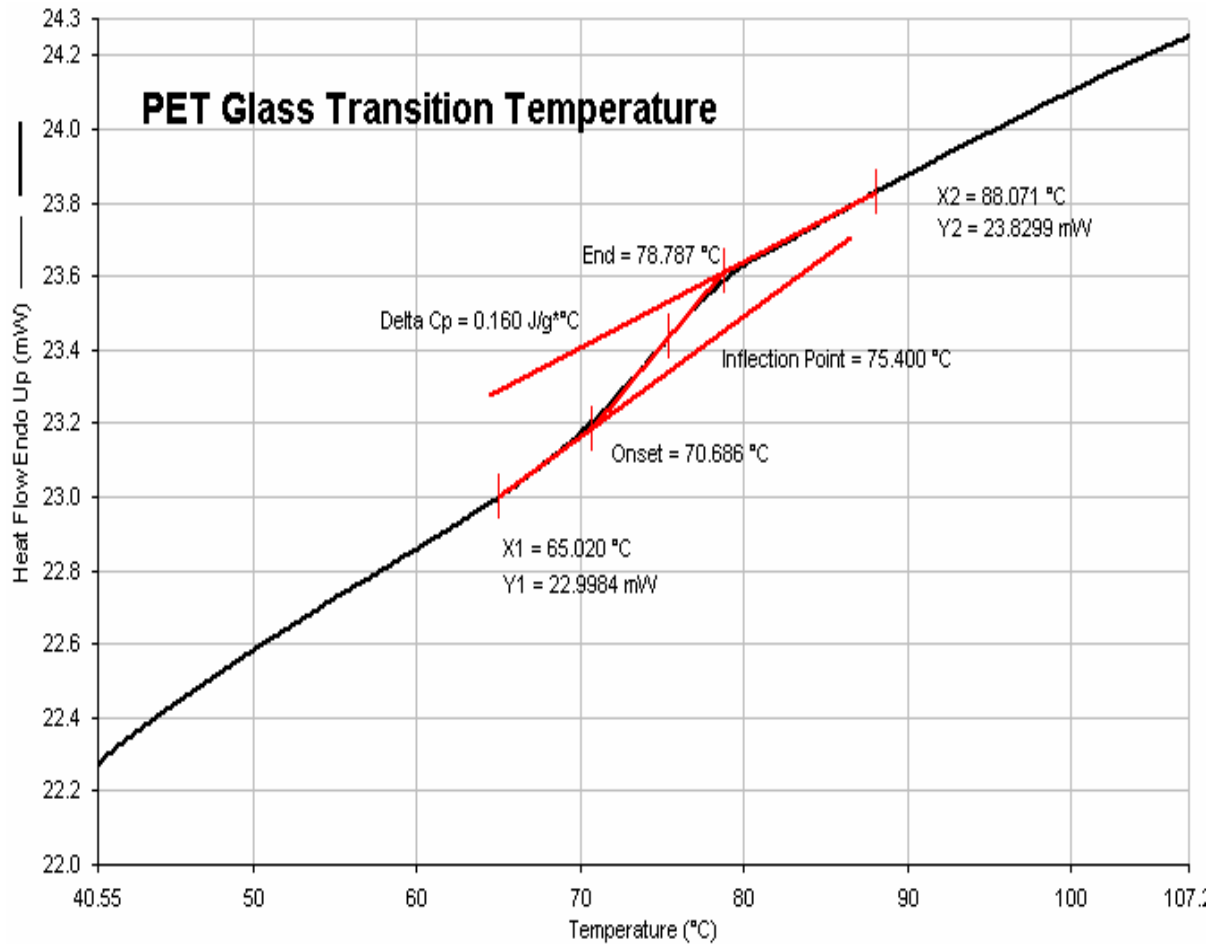


**Figure 5. 44: Glass Transition Temperature of Polyester**

The crystallization (Figure 5.45) occurred at an onset temperature of 124.035°C (slope uncorrected) or 123.620°C (slope corrected). The peak temperatures for the crystallization were 134.733°C (uncorrected slope) or 134.870°C (corrected slope).

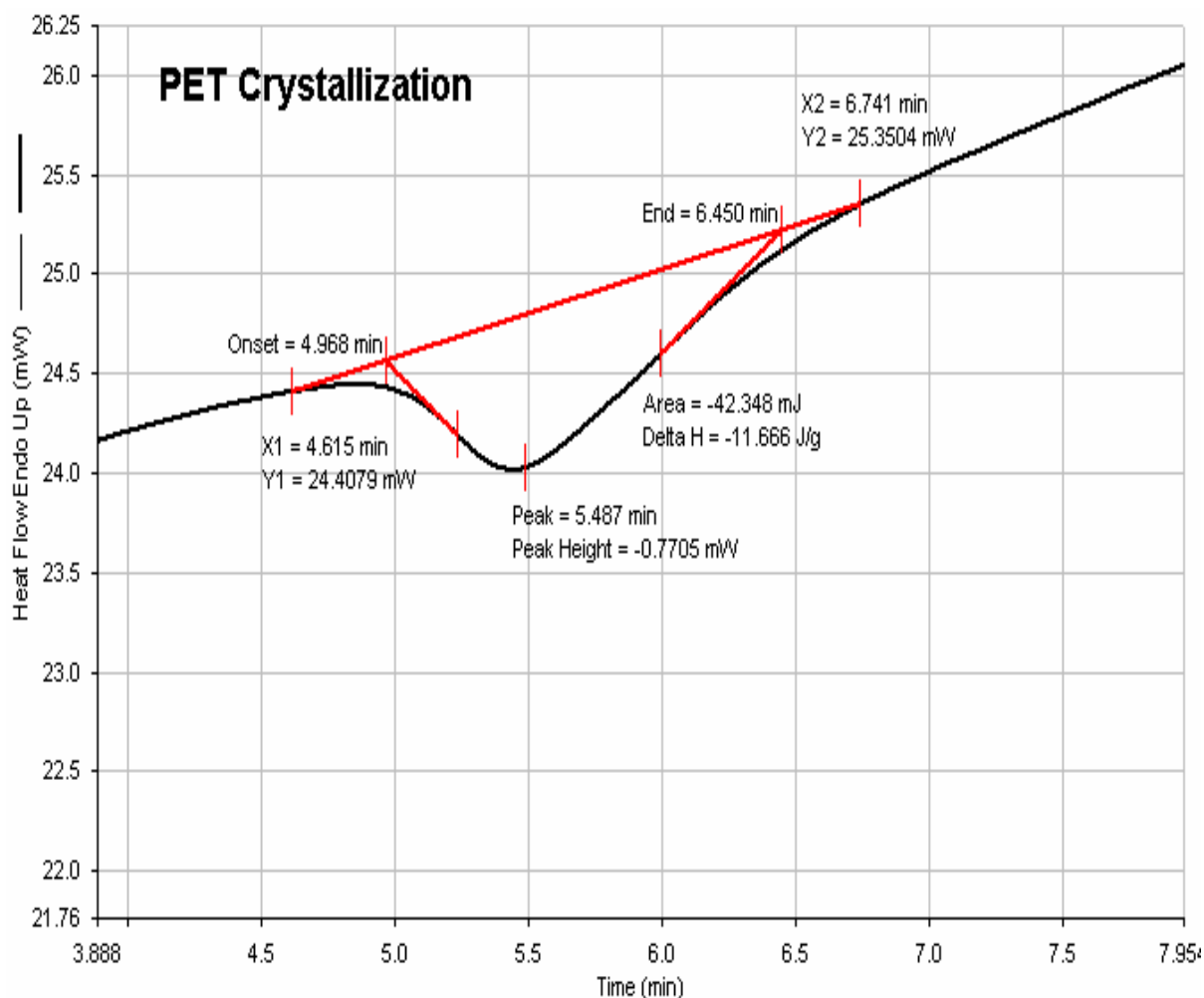


**Figure 5. 45: Crystallinity of Polyester**

The melting point occurred at an onset temperature of 235.328°C (uncorrected slope) and 235.181°C (corrected slope). The peak temperatures of melting were 249.133°C for both uncorrected and corrected slopes. The melting point curve can be seen in Figure 5.46.

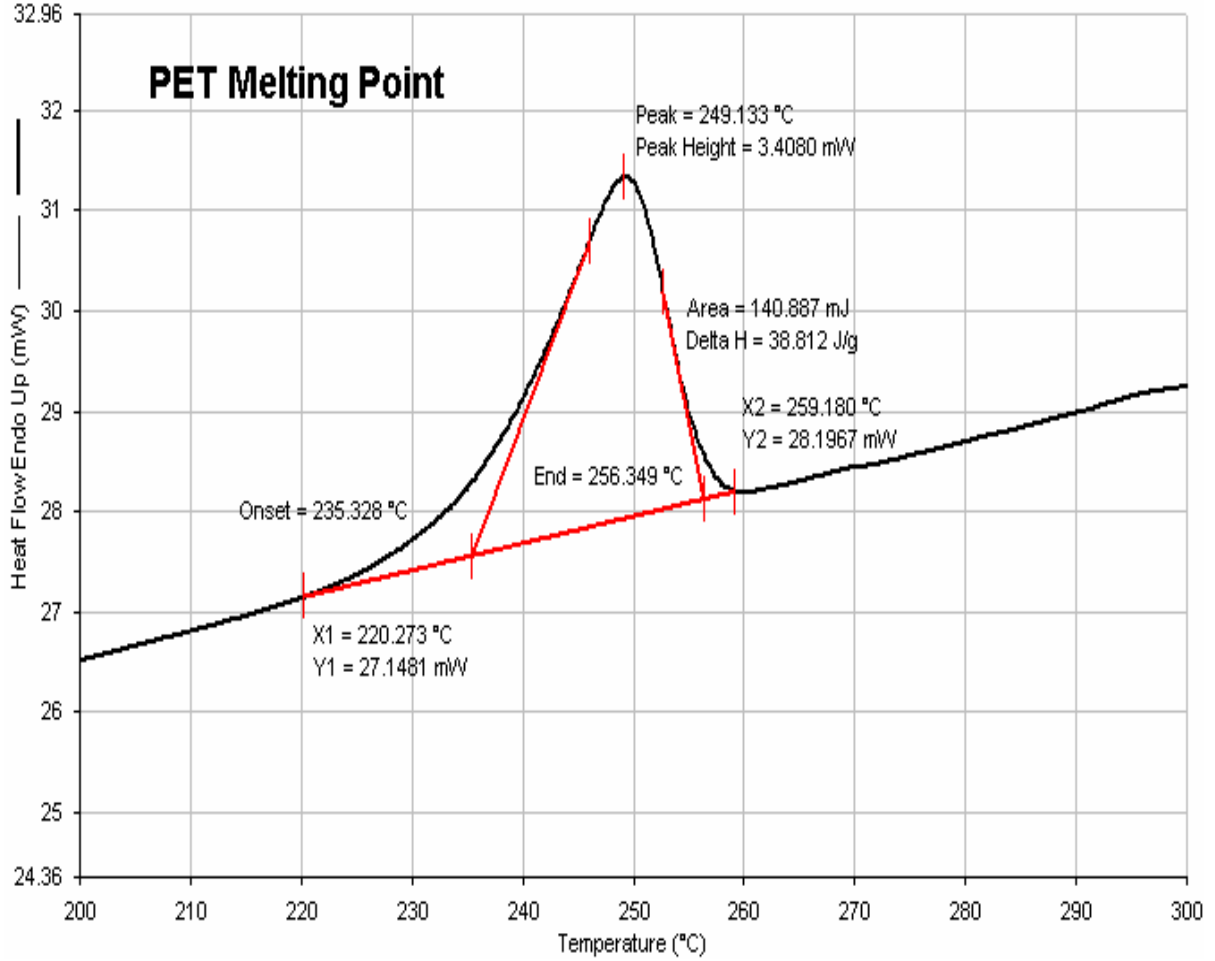


**Figure 5. 46: Melting Point of Polyester**

The crystallization temperature and the melting temperature of the electrospun sample is almost the same as that of a normal polyester fiber. This means that dissolving the polymer in the two solvents and then splaying the fibers through electrospinning process does not hamper the thermal property of the fiber.

The degree of crystallinity can be calculated by [84],

$$\text{Degree of Crystallinity} = \frac{\Delta H_m - \Delta H_c}{\Delta H_{m(100\%)}}$$

**Equation 5. 10**

Where,

$\Delta H_{m(100\%)} = 140 \text{ J/g}$  for 100% crystalline polyester [85]



$\Delta H_m$  = Measured enthalpy of melting

$\Delta H_c$  = Measured enthalpy of crystallization

So, for the electrospun web sample, the degree of crystallinity is,

$$\text{Degree of Crystallinity} * 100 = \frac{38.812 + 11.666}{140} * 100 -$$
$$= 36.056 \%$$

The degree of crystallinity of poly (ethylene terephthalate) obtained from an electrospun sample of 36.056 % is well within the range of crystallinity for polyester (35-45 %). This indicates that there is not much degradation of the polymer material when dissolved in the solvent.

## 6 Conclusion

The process of electrospinning using polymer solution was successfully carried out using polyester as the polymer and trifluoroacetic acid and methylene chloride as the solvents. A successful design of experiment and equipment was made to produce fibers. The process of electrospinning from the solution yielded very fine fibers with diameters in the nanometer range. The equipment for this process is relatively simple and small. Small amount of polymers can be processed into fiberweb.

The fibers were spun using various polymer concentrations, voltages and collecting distances. An experimental design was proposed involving all the three parameters. The morphology of the fibers shows that a wide variety of shapes and sizes can be produced. Process performance also depends on the ambient factors such as air velocity in the electrospinning hood and temperature and on the properties of the solution like the viscosity and surface tension. It was observed that the fibers spun below or above the proposed range yielded fiber shots in the web. Considerable steps were undertaken in the design and the experimental procedure to prevent the formation of shots. The electrospun web produced under the known process parameters and factors was appreciably characterized for structure and morphology using different techniques.

The process yielded very fine fibers ranging from a few hundred nanometers to a few microns. The diameters of the fibers produced by electrospinning are one or two orders of magnitude smaller than the conventional fiber and because of the smaller fiber diameter it provides a large surface area to mass ratio. The results show that an increase in the electric field results in the decrease of the average diameter of the electrospun fibers. It has also been observed that there is interaction between the concentration and the electric field. This has been supported by statistical analysis. It can also be noted that lower diameter fibers are obtained in the electrical field range of 0.85 kV/cm to 1.0 kV/cm. As the concentration of the solution increases the fiber diameter increases and the diameter range broadened. This

behavior can be related to the fact that an increase in polymer concentration causes an increase in viscosity, which in turn causes the splay of thicker fibers.

As we increase the electric field by keeping polymeric concentration constant, the fibers are more oriented towards the machine direction. Since the fibers are fine and there is higher degree of draw force at higher electric fields, fibers tend to move easily along the drum or in other words the machine direction. The analysis of anisotropy indicates that by keeping a constant concentration of the polymer solution and as the electric field is increased, there is a considerable increase in the anisotropy level. This indicates that at lower electric field, the fibers are laid more random, whereas at higher electric fields, the fibers are splayed in a preferential direction.

It was observed that as the electric field is increased, the average pore diameter decreases. All the analysis were carried out by plotting pore diameter against the cumulative filter flow, which measures the volume of air passed through the electrospun fabric sample at increased air pressures. It was also observed that the samples produced at increased concentration of the polymer solution and by maintaining the range of electric fields specified, the average pore diameter also increases. The decrease in average pore size at increased level of electric fields is due to more number of fine fibers (due to higher drag force) within the same area. The decrease in average pore size at increased electric field has been explained in terms of web structural parameters (basis weight and orientation) and fiber diameter.

## **6.1 Recommendations**

In this work, the collecting drum speed was kept constant at 12 revolutions per hour speed. Varying the collection speed will be an added independent variable parameter, which can be studied in detail for the production of electrospun fibers.

Not much work has been carried out on electrospun fibers in terms of characterization of the web. Characterization of fibers should be analyzed for polymers and composites involving electrospinning process in terms of diameter distribution, pore size distribution, and orientation distribution function. A further step to these techniques is the characterization methods for the mechanical properties of

electrospun fibers like strength, modulus, toughness, elongation etc. and physical properties of the web like tensile, elastic and time dependant behavior. The other properties, which can also be considered, are chemical, thermal, frictional, fiber structure and structure-property relationship. To determine all these properties of the electrospun nanofiber web, various methods and techniques need to be developed and could be compared to the properties of fibers produced by conventional processes.

The various fiber characterization techniques will help in knowing the electrospun nanofiber web better, thus fiberweb from nanofibers can be engineered to meet certain requirements.

## 7 Bibliography

1. Koombhongse S, Liu W, Reneker DH. Flat Polymer Ribbons and Other Shapes by Electrospinning. *Journal of Polymer Science: Part B: Polymer Physics*, Vol 39, 2598-2606 (2001)
2. Jaeger R, Schonherr H, Vancso J. Chain packing in electrospun poly (ethylene oxide) visualized by atomic force microscopy. *Macromolecules* 1996; 29 (23): 7634-7636
3. Jaeger R, Bergshoef MM, Battle CM, Schonherr H, Vancso GJ. Electrospinning of ultra-thin polymer fibers. *Macromolecular Symposium* 1998; 127: 141-150
4. Yarin AL. *Free liquid jets and films: hydrodynamics and rheology*. New York: Wiley, 1993
5. Entov VM, Shmaryan LE. Numerical modeling of the capillary breakup of jets of polymer liquids. *Fluid Dynamics* 1997; 32 (5): 696-703
6. Fong H, Chun I, Reneker DH. Beaded nanofibers formed during electrospinning. *Polymer* 40 (1999) 4585-4592
7. Fang X, Reneker DH. DNA fibers by electrospinning. *Journal of Macromolecular Science- Physics*, B36 (2), 169-173 (1997)
8. Bergshoef MM, Vancso GJ. Transparent Nanocomposites with Ultrathin Electrospun nylon-4, 6 Fiber Reinforcement. *Advanced Materials*. 1999, 11, No. 16, 1362-1365
9. Kim J-S, Reneker DH. Polybenzimidazole nanofibers produced by electrospinning. *Polymer engineering and science*, May 1999, Vol. 39, No. 5, 849-854
10. Norris ID, Shaker MM, Ko FK, MacDiarmid AG. Electrostatic fabrication of Ultrafine conducting fibers: polyaniline/polyethylene oxide blends. *Synthetic Metals* 114 (2000) 109-114
11. Zarkoob S, Reneker DH, Eby RK, Hudson SD, Ertley D, Adams WW. Structure and Morphology of Nano Electrospun Silk fibers. *Polymer preprint*, Division of Polymer chemistry, ACS, Vol.39, No.2, Aug 1998, 244-245

12. Srinivasan G, Reneker DH. Structure and Morphology of Small diameter Electrospun Aramid fibers. *Polymer international* 36 (1995) 195-201
13. Kim J-S, Reneker DH. Mechanical Properties of Composites Using Ultrafine Electrospun Fibers. *Polymer Composites*, Feb 1999, Vol.20, No.1, 124-131
14. Kim J-S, Lee DS. Thermal Properties of Electrospun Polyesters. *Polymer Journal*, Vol.32, No.7, 616-618 (2000)
15. Buer A, Ugbohue SC, Warner SB. Electrospinning and Properties of Some Nanofibers. *Textile Research Journal*. 71 (4), 323-328 (2001)
16. Fong H. The study of electrospinning and the physical properties of electrospun nanofibers. Doctoral Dissertation. University of Akron. 1999
17. Koombhongse S. The formation of nanofibers from electrospinning process. Doctoral Dissertation. University of Akron. 2001
18. Reneker DH, Yarin AL, Fong H, Koombhongse S. *Journal of Applied Physics*, 87, 4531 (2000)
19. Shin YM, Hohman MM, Brenner MP, Rutledge GC. Electrospinning: A whipping fluid jet generates submicron polymer fibers. *Applied Physics Letters*. Vol. 78, No.8, 1149-1151, 19 February 2001
20. Yarin AL, Koombhongse S, Reneker DH. Bending instability in electrospinning of nanofibers. *Journal of Applied Physics*. Vol. 89, No.5, 3018-3026, 1 March 2001
21. Hohman MM, Shin M, Rutledge G, Brenner MP. Electrospinning and electrically forced jets. I. Stability theory. *Physics of Fluids*. Vol. 13, No.8. August 2001
22. Hohman MM, Shin M, Rutledge G, Brenner MP. Electrospinning and electrically forced jets. II. Applications. *Physics of Fluids*. Vol. 13, No.8. August 2001
23. Shin YM, Hohman MM, Brenner MP, Rutledge GC. Experimental characterization of electrospinning: the electrically forced jet and instabilities. *Polymer*, 42 (2001) 9955-9967
24. Spivak AF, Dzenis YA, Reneker DH. A Model of Steady State Jet in the Electrospinning Process. *Mechanics Research Communications* (Pergamon), Vol. 27, No.1, 37-42, 2000
25. Deitzel JM, Kleinmeyer JD, Hirvonen JK, Beck Tan NC. Controlled deposition of electrospun poly (ethylene oxide) fibers. *Polymer*, 42 (2001) 8163-8170

26. Taylor GI. Electrically Driven Jets. Proceedings of the Royal Society of London Series A Mathematical and Physical Sciences. Vol. 313, 453-475, 1969
27. Taylor GI. Disintegration of Water Drops in an Electric Field. Proceedings of the Royal Society of London Series A Mathematical and Physical Sciences. Vol. 280, 383, 1964
28. Taylor GI. The Force Exerted by an Electric Field on a Long Cylindrical Conductor. Proceedings of the Royal Society of London Series A Mathematical and Physical Sciences. Vol. 291, 145, 1966
29. Taylor GI. Studies in Electrohydrodynamics. I. The Circulation Produced in a Drop by Electrical Field. Proceedings of the Royal Society of London Series A Mathematical and Physical Sciences. Vol. 291, 159, 1966
30. Zeleny J. Physical Review, Vol. 3, 69 (1914)
31. Zeleny J. Proceedings of the Cambridge Phil Society. Vol. 18, 71 (1915)
32. Zeleny J. Physical Review, Vol. 10, 1 (1917)
33. Zeleny J. Journal of the Franklin Institute. 219, 659 (1935)
34. Rayleigh FRS. Philosophical Magazine, 14, 184 (1882)
35. Bailey AG. Electrostatic Spraying of Liquids. Research Studies Press, New York: Wiley 1988
36. Blanchard D C, (1963), Progress in Oceanography. Ed. M Sears. Pergamon Press. Vol.1, 71 et seq.
37. Holme I, McIntyre JE, Shen ZJ. Electrostatic Charging of Textiles. Textile Progress. Vol. 28, Number 1, 1998.
38. Malkan SR and Wadsworth LC. Process-Structure-Property Relationships in Melt Blowing of Different Molecular Weight Polypropylene Resins part I – Physical Properties. INDA Journal, 3 (2), 21-34, 1991
39. Dullien FAL. Porous Media: Fluid Transport and Pore Structure, 24, Second edition, Academic press, New York, 1992
40. Xu B. Measurement of Pore Characteristics in Nonwoven fabrics Using Image Analysis. Clothing and Textiles Research Journal, Vol. 14, No.1, 81-88 (1996)
41. Bear J, Buchlin J-M. Modelling and applications of transport phenomena in porous media. Dordrecht, Boston, 1991

42. Bear J. Dynamics of fluids in porous media. Environmental Science Series, 1972.
43. Bhatia SK, Smith JL, Christopher BR. Geotextile Characterization and Pore Size Distribution: Part III. Comparison of methods and application to design. Geosynthetics International, Vol. 3 No.3, 301-328, 1996
44. Bhatia SK, Smith JL. Comparative Study of Bubble Point Method and Mercury Intrusion Porosimetry Techniques for Characterizing the Pore-Size distribution of Geotextiles. Geotextiles and Geomembranes, 13 (1994) 679-702
45. Huang X, Bresee RR. Characterizing Nonwoven Web Structure Using Image Analysis Techniques. Part I: Pore Analysis in Thin Webs. INDA Journal of Nonwovens Research, Vol. 5, No.1, 13-21
46. Pourdeyhimi B, Xu B. Pore Characterization in Nonwoven Fabrics: Shape Considerations. INDA Journal of Nonwovens Research, Vol. 6, No.1, 26-30
47. Huang X, Bresee RR. Characterizing Nonwoven Web Structure Using Image Analysis Techniques. Part II: Fiber Orientation Analysis in Thin Webs. INDA Journal of Nonwovens Research, Vol. 5, No.2, 14-21
48. Pourdeyhimi B, Ramanathan R, Dent R. Measuring Fiber Orientation in Nonwovens. Part I: Simulation. Textile Research Journal. 66 (11), 713-722 (1996)
49. Pourdeyhimi B, Ramanathan R, Dent R. Measuring Fiber Orientation in Nonwovens. Part II: Direct Tracking. Textile Research Journal. 66 (12), 747-753 (1996)
50. Pourdeyhimi B, Dent R, Davis H. Measuring Fiber Orientation in Nonwovens. Part III: Fourier Transform. Textile Research Journal. 67 (2), 143-151 (1997)
51. Pourdeyhimi B, Dent R. Measuring Fiber Orientation in Nonwovens. Part IV: Flow Field Analysis. Textile Research Journal. 67 (3), 181-187 (1997)
52. Pourdeyhimi B, Dent R, Jerbi A, Tanaka S, Deshpande A. Measuring Fiber Orientation in Nonwovens. Part V: Real Webs. Textile Research Journal. 69 (3), 185-192 (1999)
53. Pourdeyhimi B, Dent R. Measuring Fiber Diameter Distribution in Nonwovens. Textile Research Journal. 69 (4), 233-236 (1999)



54. Xu B, Yu L. Determining Fiber Orientation distribution in Nonwovens with Hough Transform Techniques. *Textile Research Journal*. 67 (8), 563-571 (1997)
55. Gong RH, Newton A. Image-analysis Techniques. Part II: The Measurement of Fiber Orientation in Nonwoven Fabrics. *Journal of Textile Institute*. 87, Part 1, No.2, 371-388, 1996
56. Baumgarten PK. Electrostatic Spinning of Acrylic Microfibers. *Journal of Colloid and Interface Science*, Vol. 36, No.1, 71-79, May 1971
57. Larrondo L, Manley RS. *Journal of Polymer Science: Polymer Physics Edition*, 19, 909, 1981
58. Larrondo L, Manley RS. *Journal of Polymer Science: Polymer Physics Edition*, 19, 921, 1981
59. Larrondo L, Manley RS. *Journal of Polymer Science: Polymer Physics Edition*, 19, 933, 1981
60. Doshi J, Reneker DH. Electrospinning Process and Applications of Electrospun fibers. *Journal of Electrostatics*. 35, 151-160, 1995
61. Doshi J. The electrospinning process and applications of electrospun fibers. Doctoral Dissertation, The University of Akron. 1994
62. Reneker DH, Chun I. Nanometre diameter fibers of polymer, produced by electrospinning. *Nanotechnology*, 7, 216-223, 1996
63. Chun I. Fine fibers spun by electrospinning process from polymer solutions and polymer melts in air and vacuum: Characterization of structure and morphology on electrospun fibers and developing a new process model. Doctoral Dissertation, The University of Akron. 1995
64. Srinivasan G. Structure and morphology of Electrospun Polymer Fibers. Doctoral Dissertation, The University of Akron. 1994
65. Formhals A, USPat. (1934), 1,975,504
66. Simons HL, USPat. (1966), 3,280,229
67. Martin GE, Cockshott ID, and Fildes JT, USPat. (1977), 4,044,404
68. Talbott JW, Logan JD, USPat. (1978), 4,113,812
69. Simm W, Gosling C, Bonart R, VON Falkai B, USPat. (1978), 4,069,026
70. Simm W, Gosling C, Bonart R, VON Falkai B, USPat. (1979), 4,143,196

71. Fine J, De Tora SA, USPat. (1980), 4,223,101
72. Bornat A, USPat. (1982), 4,323,525
73. Bornat A, USPat. (1987), 4,689,186
74. How TV, USPat. (1985), 4,552, 707
75. Middleton I, Paprotny J, USPat. (1989), 4,798,607
76. Berry JP, USPat. (1991), 5,024,789
77. [www.fibersource.com](http://www.fibersource.com)
78. Schreuder-Gibson, H.L, Gibson, P. Transport Properties of Electrospun Nonwoven Membranes. International Nonwovens Journal, 21-26, Summer 2002.
79. Gibson, P, Schreuder-Gibson, H.L, Rivin, D. Transport properties of porous membranes based on electrospun nanofibers.
80. Backer S, Petterson DR. Some Principles of Nonwoven Fabrics. Textile Research Journal, Vol. 30, 709, 1960.
81. Yogeshwar Velu. Structure and Formation of Meltblown 3D Fabrics Using Robotic Fiber Assembly and Control System (RFACS). Doctoral Dissertation, North Carolina State University. 2002.
82. PMI Manual
83. Schreuder-Gibson H.L, Gibson, P. Electrospinning.  
<http://www.sbcom.army.mil/products/cie/Electrospinning.htm>
84. Bullions TA, Wei M, Porbeni FE, Gerber MJ, Peet J, Balik M, White JL, Tonelli. Reorganization of the structures, morphologies and conformations of bulk polymers via coalescence from polymer-cyclodextrin inclusion compounds. Journal of Polymer Science. Part B: Polymer Physics. Vol. 40, 992-1012, 2002.
85. Mehta A, Gaur U, Wunderlich B. Equilibrium melting parameters of poly (ethylene terephthalate). Journal of Polymer Physics. Vol. 16, 289-296, 1978.
86. Class Notes MB 705 Spring 2002 NCSU
87. Class Notes TMS 763 Spring 2002 NCSU
88. Ding B, Kim H-K, Lee S-C, Lee D-R, Choi K-J. Preparation and Characterization of Nanoscaled Poly (vinyl alcohol) Fibers via Electrospinning. Fibers and Polymers Vol.3, No. 2, 73 – 79, 2002

## 8 Appendices

The process of electrospinning involves usage of highly toxic and corrosive chemicals, as well as very high voltage equipment. The personnel using this equipment should practice extreme measures for their safety. A list of procedures for chemical and electrical safety has been listed below. All persons using this equipment/process should follow these safety measures.

### ***8.1 Safety procedures for the electrospinning set up***

#### 8.1.1 General description of the apparatus

- ❑ The electrospinning apparatus consists of a glass sprayer filled with polymer solution, a collecting device, a high voltage instrument whose positive is terminated at the glass pipette and the other end to the collecting drum, and the system has an external motor to give motion to the collecting device.
- ❑ The glass sprayer is held by a support system, which is made up of Garolite, a woven glass fabric coated with epoxy.
- ❑ The collecting device is a PVC pipe cylindrical drum, which is attached with a metal plate, a bush and a wire terminating from it so as to complete the electrical connection.
- ❑ A foil of aluminum is wound over this non-conducting drum to maintain the same electric field throughout the surface of the drum.
- ❑ A sheet of fiberglass screen is wound over the foil to assist in removing the electrospun sample without any damage to the sample.

#### 8.1.2 Chemical Safety

- ❑ Always wear eye protection, hand protection and protective clothing.
- ❑ Handle the chemicals listed above with care and store them at proper/regular places.
- ❑ Make sure the solution is prepared inside the hood and the fumes emerging from the chemicals should be properly ventilated.

- ❑ Clean beakers and bottles should be used for transferring of chemicals and preparing of solution.
- ❑ Close the bottles of methylene chloride and trifluoroacetic acid immediately after use and also close the glass lid of the bottle containing the prepared solution.
- ❑ The polymer chips added to the solution to dissolve can be assisted using a magnetic stirrer and an external source for stirring.
- ❑ Spills and wastes are removed and discarded as mentioned above. Dispose of all contaminated materials properly.
- ❑ Keep spilled materials out of drains and water supplies.
- ❑ Get medical help immediately if someone is overexposed to chemicals.

### 8.1.3 Electrical Safety

The electrospinning system itself uses electrical power for its operation. Any of these smaller pieces of equipment may produce a potentially damaging or lethal shock or serve to ignite flammable materials. Although such shocks and fires may result from defective equipment, most often they may result from the unsafe practices of the user.

- ❑ Proper care should be taken while terminating the end at the glass pipette containing polymer solution, have to make sure that the wire is completely immersed in the solution and it has been fixed properly to the pipette.
- ❑ The other end from the high voltage instrument is connected to the collecting device and make sure that the end is properly fixed. Soldering is the best option.
- ❑ The collecting device can be rotated by an external motor drive, which can drive the drum from 0 to 100 revolutions per hour.
- ❑ Set the drum speed to 12 revolutions per hour, which is the minimum speed required to rotate the drum.
- ❑ Check again the feed and the return paths are correctly fixed.
- ❑ Make sure that the line side and high voltage sides are grounded.

- ❑ Make sure that there are no metal parts near the set up or as a matter of fact in the hood.
- ❑ Check that the wires coming from high voltage instrument, collecting device and the external motor do not cross over.
- ❑ Close the sash of the hood to at least 18 inches.
- ❑ If the above lines are OK, start the experiment with switching on the power switch and slowly increasing the voltage through regulator.
- ❑ The high voltage instrument has variable output from, 0 to 40 kilovolts; the range being used for the electrospinning process is 15 to 25 kilovolts.
- ❑ To turn down the system, slowly decrease the voltage, turn the power switch off and then take out the power supply plug.
- ❑ Turn the system down when the polymer level is near the ending stage and polymer is near the vicinity of the submerged wire or when the polymer is still around 5 ml in the glass pipette.
- ❑ Open the sash, take out the positive end from the pipette, remove the remaining solution to a container, and stop the external drive.
- ❑ The fiberglass mesh containing electrospun fibers can now be removed from the drum for analysis.
- ❑ Use the power supply controls to cut off the power in an emergency. These are the ONLY controls for the emergency power off.

## **8.2 ANOVA Model for Diameter Distribution of electrospun fibers**

The REG Procedure  
Model: MODEL1  
Dependent Variable: diameter  
Analysis of Variance

Source	DF	Sum of Squares	Mean Square	F Value	Pr > F
Model	11	1607591	146145	8.69	0.0255
Error	4	67276	16819		
Corrected Total	15	1674866			

Root MSE            129.68788   R-Square    0.9598  
 Dependent Mean   1279.34688   Adj R-Sq    0.8494  
 Coeff Var            10.13704

#### Parameter Estimates

Variable	DF	Parameter Estimate	Standard Error	t value	Pr >  t
Intercept	1	2086.71536	2555.89519	0.82	0.4601
conc1	1	52828	16434	3.21	0.0324
conc2	1	10607	6904.61649	1.54	0.1993
conc3	1	6876.46283	6938.28576	0.99	0.3777
ef	1	-1581.65045	5848.39351	-0.27	0.8002
ef2	1	544.93172	3259.48222	0.17	0.8753
conc1xef	1	-115724	37853	-3.06	0.0378
conc2xef	1	-20320	15890	-1.28	0.2701
conc3xef	1	-15098	16082	-0.94	0.4010
conc1xef2	1	63188	21695	2.91	0.0436
conc2xef2	1	9637.93245	9048.97713	1.07	0.3469
conc3xef2	1	8261.67840	9083.58726	0.91	0.4145

#### The REG Procedure

Model: MODEL1

Test 1 Results for Dependent Variable diameter

Source	DF	Mean Square	F value	Pr > F
Numerator	6	125026	7.43	<b>0.0363</b>
Denominator	4	16819		

#### Full Model

The GLM Procedure

Dependent Variable: diameter

Source	DF	Sum of Squares	Mean Square	F Value	Pr > F
Model	11	1607590.660	146144.605	8.69	0.0255
Error	4	<b>67275.784</b>	<b>16818.946</b>		
Corrected Total	15	1674866.445			

R-Square    Coeff Var    Root MSE    diameter Mean  
 0.959832    10.13704    129.6879    1279.347

Source	DF	Type I SS	Mean Square	F value	Pr > F
ef	1	642072.3650	642072.3650	38.18	0.0035
ef*conc	3	84511.2320	28170.4107	1.67	0.3083
ef*ef	1	51054.9057	51054.9057	3.04	0.1564
ef*ef*conc	3	618605.7829	206201.9276	12.26	0.0174
conc	3	211346.3745	70448.7915	4.19	0.1001

Source	DF	Type III SS	Mean Square	F value	Pr > F
ef	1	222357.3478	222357.3478	13.22	0.0220
ef*conc	3	184443.8866	61481.2955	3.66	0.1213
ef*ef	1	189984.4694	189984.4694	11.30	0.0283
ef*ef*conc	3	163538.2044	54512.7348	3.24	0.1429
conc	3	211346.3745	70448.7915	4.19	0.1001

Parameter		Estimate	Standard Error	t Value	Pr >  t
Intercept		2086.7154 B	2555.89519	0.82	0.4601
ef		-1581.6505 B	5848.39351	-0.27	0.8002
ef*conc	21	-115723.7679 B	37852.89396	-3.06	0.0378
ef*conc	23	-20319.7910 B	15890.03422	-1.28	0.2701
ef*conc	25	-15098.2604 B	16082.49982	-0.94	0.4010
ef*conc	27	0.0000 B	-	-	-
ef*ef		544.9317 B	3259.48222	0.17	0.8753
ef*ef*conc	21	63188.3463 B	21694.75667	2.91	0.0436
ef*ef*conc	23	9637.9324 B	9048.97713	1.07	0.3469
ef*ef*conc	25	8261.6784 B	9083.58726	0.91	0.4145
ef*ef*conc	27	0.0000 B	-	-	-

**Reduced Model**  
The GLM Procedure  
Dependent Variable: diameter

Source	DF	Sum of Squares	Mean Square	F Value	Pr > F
Model	5	857436.309	171487.262	2.10	0.1492
Error	10	<b>817430.135</b>	81743.014		
Corrected Total	15	1674866.445			

R-Square    Coeff Var    Root MSE    diameter Mean

0.511943    22.34791    285.9074    1279.347

Source	DF	Type I SS	Mean Square	F Value	Pr > F
ef	1	642072.3650	642072.3650	7.85	0.0187
ef* ef	1	3587.2431	3587.2431	0.04	0.8383
conc	3	211776.7012	70592.2337	0.86	0.4914

Source	DF	Type III SS	Mean Square	F Value	Pr > F
ef	1	106046.5345	106046.5345	1.30	0.2813
ef* ef	1	80046.2287	80046.2287	0.04	0.3457
conc	3	211776.7012	70592.2337	0.98	0.4914

### 8.3 ANOVA Model for Throughput of electrospun fibers

Obs	j	conc	x (electric field)	Y (throughput)	conc1	conc2	conc3
1	1	21	-	-	1	0	0
2	1	21	-	-	1	0	0
3	1	21	-	-	1	0	0
4	1	21	0.8500	51.8587	1	0	0
5	1	21	0.9048	55.3861	1	0	0
6	1	21	0.9546	56.1668	1	0	0
7	2	23	0.7500	45.0093	0	1	0
8	2	23	0.7895	49.0092	0	1	0
9	2	23	0.8095	52.5866	0	1	0
10	2	23	0.8636	58.0035	0	1	0
11	2	23	0.8947	63.5675	0	1	0
12	2	23	1.0000	77.5015	0	1	0
13	3	25	-	-	0	0	1
14	3	25	-	-	0	0	1
15	3	25	0.7143	36.8671	0	0	1
16	3	25	0.7727	41.7018	0	0	1
17	3	25	0.8095	45.0726	0	0	1
18	3	25	1.0500	60.0252	0	0	1
19	4	27	-	-	0	0	0
20	4	27	-	-	0	0	0
21	4	27	0.6818	33.8246	0	0	0
22	4	27	0.8095	42.0156	0	0	0
23	4	27	0.8500	46.4692	0	0	0
24	4	27	1.1053	61.0499	0	0	0



The GLM Procedure  
Dependent Variable: y (throughput)

Source	DF	Sum of Squares	Mean Square	F Value	Pr > F
Model	7	1885.5631	269.3662	305.49	<0.0001
Error	9	7.9357	0.8817		
Corrected Total	16	1893.4988			

R-Square    Coeff Var    Root MSE    y Mean  
0.995809    1.822046    0.939013    51.53619

Source	DF	Type I SS	Mean Square	F Value	Pr > F
conc	3	503.5033	167.8344	190.34	<0.0001
x	1	1236.8104	1236.8104	1402.68	<0.0001
x*conc	3	145.2494	48.4165	54.91	<0.0001

Source	DF	Type III SS	Mean Square	F Value	Pr > F
conc	3	93.0039	31.0013	35.16	<0.0001
x	1	395.9987	395.9987	449.11	<0.0001
x*conc	3	145.2494	48.4165	54.91	<0.0001

Parameter	Estimate	Standard Error	t Value	Pr >  t
Intercept	-9.3747	2.6730	-3.51	0.0066
conc 21	26.2823	11.7870	2.23	0.0527
conc 23	-44.5694	4.8241	-9.24	<0.0001
conc 25	-1.1952	4.1006	-0.29	0.7773
conc 27	0.0000 B	-	-	-
x	64.07996	3.0539	20.98	<0.0001
x*conc 21	-22.4867	13.0596	-1.72	0.1192
x*conc 23	66.9743	5.6019	11.96	<0.0001
x*conc 25	3.4366	4.7778	0.72	0.4902
x*conc 27	0.0000 B	-	-	-

#### 8.4 ANOVA Model for Anisotropy ratio of electrospun fibers

Obs	j	conc	x (electric field)	y (anisotropy ratio)	conc1	conc2	conc3
1	1	21	-	-	1	0	0
2	1	21	-	-	1	0	0
3	1	21	-	-	1	0	0
4	1	21	0.8500	1.6859	1	0	0
5	1	21	0.9048	2.1435	1	0	0
6	1	21	0.9546	2.5142	1	0	0
7	2	23	0.7500	2.3977	0	1	0
8	2	23	0.7895	3.0715	0	1	0
9	2	23	0.8095	4.1015	0	1	0
10	2	23	0.8636	4.8224	0	1	0
11	2	23	0.8947	5.5178	0	1	0
12	2	23	1.0000	5.9839	0	1	0
13	3	25	-	-	0	0	1
14	3	25	-	-	0	0	1
15	3	25	0.7143	2.4349	0	0	1
16	3	25	0.7727	3.0945	0	0	1
17	3	25	0.8095	3.1408	0	0	1
18	3	25	1.0500	3.6143	0	0	1
19	4	27	-	-	0	0	0
20	4	27	-	-	0	0	0
21	4	27	0.6818	2.2277	0	0	0
22	4	27	0.8095	2.7345	0	0	0
23	4	27	0.8500	3.7786	0	0	0
24	4	27	1.1053	4.1796	0	0	0

The GLM Procedure  
Dependent Variable: y (anisotropy ratio)

Source	DF	Sum of Squares	Mean Square	F Value	Pr > F
Model	7	21.9727	3.1386	15.55	0.0002
Error	9	1.8169	0.2019		
Corrected Total	16	23.7897			

R-Square	Coeff Var	Root MSE	y Mean
0.923623	13.29732	0.449319	3.379018

Source	DF	Type I SS	Mean Square	F Value	Pr > F
conc	3	10.5300	3.5100	17.39	0.0004
x	1	7.5941	7.5941	37.62	0.0002
x*conc	3	3.8486	1.2829	6.35	0.0133

Source	DF	Type III SS	Mean Square	F Value	Pr > F
conc	3	2.9672	0.9891	4.90	0.0275
x	1	3.6469	3.6469	18.06	0.0021
x*conc	3	3.8486	1.2829	6.35	0.0133

Parameter	Estimate	Standard Error	t Value	Pr >  t
Intercept	-0.6376	1.2614	-0.51	0.6254
conc 21	-4.7026	5.8621	-0.80	0.4431
conc 23	-7.3669	2.2795	-3.23	0.0103
conc 25	1.2915	1.9370	0.67	0.5215
conc 27	0.0000 B	-	-	-
x	4.4842	1.4391	3.12	0.0124
x*conc 21	3.7988	6.5153	0.58	0.5742
x*conc 23	10.0388	2.6521	3.79	0.0043
x*conc 25	-1.5899	2.2579	-0.70	0.4991
x*conc 27	0.0000 B	-	-	-

### 8.5 ANOVA Model for Average Pore Diameter of electrospun fibers

The GLM Procedure  
Dependent Variable: average pore diameter (apd)

Source	DF	Sum of Squares	Mean Square	F Value	Pr > F
Model	8	80.078336	10.00979	56.93	0.0034
Error	3	0.5274852	0.175828		
Corrected Total	11	80.605822			

R-Square	Coeff Var	Root MSE	apd Mean
0.993456	2.676431	0.419319	15.66710

Source	DF	Type I SS	Mean Square	F Value	Pr > F
ef	1	34.8704	34.8704	198.32	0.0008
ef*ef	1	21.3158	21.3158	121.69	0.0016
conc	2	13.6212	6.81060	38.73	0.0072
ef*conc	2	1.6738	0.83689	4.76	0.1173
ef*ef*conc	2	8.5171	4.24856	24.22	0.0141

Parameter	Estimate	Standard Error	t Value	Pr >  t
Intercept	62.3490	8.4924	7.34	0.0052
ef	-86.7892	19.1949	-4.52	0.0202
ef*ef	38.4489	10.5595	3.64	0.0357
conc 23	-9.9427	89.6761	-0.11	0.9187
conc 25	129.8865	19.2274	6.76	0.0066
conc 27	0.0000	-	-	-
ef*conc 23	5.7621	222.1241	0.03	0.9809
ef*conc 25	-302.5350	43.8583	-6.90	0.0062
ef*conc 27	0.0000	-	-	-
ef*ef*conc 23	3.1799	137.2575	0.02	0.9830
ef*ef*conc 25	169.8651	24.4173	6.96	0.0061
ef*ef*conc 27	0.0000	-	-	-

### 8.6 ANOVA Model for Anisotropy ratio (dependent variable) on Average Pore Diameter of electrospun fibers

The GLM Procedure  
Dependent Variable: Anisotropy ratio

Source	DF	Sum of Squares	Mean Square	F Value	Pr > F
Model	5	6.38497	1.27699	9.25	0.0087
Error	6	0.82870	0.13811		
Corrected Total	11	7.21367			

R-Square    Coeff Var    Root MSE    AR Mean  
0.885121    11.26235    0.371641    3.299852

Source	DF	Type I SS	Mean Square	F Value	Pr > F
conc	2	0.58495	0.29247	2.12	0.2015
ef	1	3.55826	3.55826	25.76	0.0023
ef*conc	2	2.24175	1.12088	8.12	0.0197

Source	DF	Type III SS	Mean Square	F Value	Pr > F
conc	2	2.03859	1.01929	7.38	0.0241
ef	1	5.0045	5.0045	36.23	0.0009
ef*conc	2	2.24175	1.12088	8.12	0.0197

Parameter	Estimate	Standard Error	t Value	Pr >  t
Intercept	-0.6982	1.0579	-0.66	0.5338
conc 23	-13.4398	3.7964	-3.54	0.0122
conc 25	1.3309	1.6229	0.82	0.4435
conc 27	0.0000	-	-	-
ef	4.5590	1.2087	3.77	0.0093
ef *conc 23	17.5274	4.6905	3.74	0.0097
ef *conc 25	-1.6445	1.8909	-0.87	0.4179
ef *conc 27	0.0000 B	-	-	-

### 8.7 Partial Correlation Coefficients to describe linear associations between pair of response variables

The CORR Procedure  
 Pearson Correlation Coefficients, N = 12  
 Prob > |r| under H0 : Rho = 0

	rapd	rafd	rar
rapd	1.0000	0.4555 0.1368	-0.113 0.7274
rafd	0.4555 0.1368	1.0000	-0.805 0.0016
rar	-0.113 0.7274	-0.805 0.0016	1.0000

[apd – average pore diameter, afd – average fiber diameter, ar – anisotropy ratio]

The REG Procedure  
 Model : MODEL 1  
 Dependent Variable: apd

Source	DF	Sum of Squares	Mean Square	F Value	Pr > F
Model	9	80.1878	8.9098	42.62	0.0231
Error	2	0.4181	0.2090		
Corrected Total	11	80.6058			

Root MSE                      0.45720   R-Square      0.9948

**Parameter Estimates**

Variable	DF	Parameter Estimate	Standard Error	t value	Pr >  t	Squared Partial Corr Type I
Intercept	1	49.69153	19.7932	2.51	0.1287	-
c1	1	-422.0649	577.918	-0.73	0.5412	0.14872
c2	1	90.74602	58.0226	1.56	0.2583	0.04896
ef	1	-71.18927	30.0477	-2.37	0.1413	0.71358
ef2	1	31.16268	15.2959	2.04	0.1785	0.42656
c1ef	1	981.07269	1369.54	0.72	0.5481	0.13877
c2ef	1	-216.41334	128.274	-1.69	0.2336	0.02019
c1ef2	1	-573.05651	810.345	-0.71	0.5528	0.00084
c2ef2	1	123.06821	69.9422	1.76	0.2206	0.94163
afd	1	0.00429	0.00593	0.72	0.5445	0.20746

Model : MODEL 2  
Dependent Variable: apd  
Analysis of Variance

Source	DF	Sum of Squares	Mean Square	F Value	Pr > F
Model	9	80.0850	8.89834	34.17	0.0287
Error	2	0.52079	0.26039		
Corrected Total	11	80.6058			

Root MSE                      0.51029   R-Square      0.9935

**Parameter Estimates**

Variable	DF	Parameter Estimate	Standard Error	t value	Pr >  t	Squared Partial Corr Type I
Intercept	1	61.33551	12.11415	5.06	0.0369	-
c1	1	-14.77128	113.20858	-0.13	0.9081	0.14872
c2	1	129.29021	23.69240	5.46	0.0320	0.04896
ef	1	-84.14014	28.60990	-2.94	0.0988	0.71358
ef2	1	37.27680	14.78347	2.52	0.1278	0.42656
c1ef	1	16.11406	277.91377	0.06	0.9590	0.13877
c2ef	1	-300.99367	54.23176	-5.55	0.0310	0.02019
c1ef2	1	-2.12043	170.27354	-0.01	0.9912	0.00084
c2ef2	1	168.88285	30.33924	5.57	0.0308	0.94163
ar	1	-0.11490	0.71647	-0.16	0.8873	0.01270